Stony Brook University

Poly(diiododiacetylene): A Potential Precursor for New All-Carbon Materials

A Dissertation Presented

by

Daniel Joseph Resch

to

The Graduate School

in Partial Fulfillment of the

Requirements

for the Degree of

Doctor of Philosophy

in

Chemistry

Stony Brook University

August 2013

Stony Brook University

The Graduate School

Daniel Joseph Resch

We, the dissertation committee for the above candidate for the

Doctor of Philosophy degree, hereby recommend

acceptance of this dissertation.

Nancy S. Goroff – Dissertation Advisor
Associate Professor, Department of Chemistry

Kathlyn A. Parker - Chairperson of Defense
Professor, Department of Chemistry

Robert B. Grubbs – Third Member of Defense
Associate Professor, Department of Chemistry

Nicholas J. Ramer – Outside Member of Defense
Associate Professor, Department of Chemistry, LIU Post

This dissertation is accepted by the Graduate School

Charles Taber
Interim Dean of the Graduate School

Abstract of the Dissertation

Poly(diiododiacetylene): A Potential Precursor for New All-Carbon Materials

by

Daniel Joseph Resch

Doctor of Philosophy

in

Chemistry

Stony Brook University

2013

Poly(diiododiacetylene) (PIDA) is a polymer consisting entirely of carbon and iodine. The polymer is prepared by cocrystallizing a bis(nitrile) oxalamide host with the monomer diiodobutadiyne. These compounds are held together by a halogen bond and an ordered 1,4-topochemical polymerization occurs in the solid state. The formation of the monomer cocrystals was found to be highly solvent dependent. Acetonitrile was found to greatly improve the yield of cocrystals over solvents used in the past. Cocrystals could not be obtained from other solvents such as dimethoxyethane and acetone. THF did give some cocrystal but the yield was poor. The use of acetonitrile as a solvent now allows for PIDA cocrystals to be reliably prepared in excellent yield for detailed studies.

The weak C-I bonds in PIDA can be broken under mild conditions with simple Lewis bases like pyrrolidine and iodide ion. Studies with small molecule models show that the mechanism of elimination is E2-like and highly solvent dependent. Polar aprotic solvents favor the reaction while non-polar solvents disfavor it. Reaction occurs in protic solvents, but the rate is much slower. Iodide was found to carry out the reaction in 1 hour d_5-$PhNO_2$ while reaction with pyrrolidine did not reach completion in 15 hours.

When PIDA is subjected to deiodination the product is an amorphous graphite-like material that contains non-carbon atoms. Depending on the reaction conditions, it is possible to incorporate sulfur or

phosphorus into the final product. The source of these elements is the reducing agent that is typically added to sequester molecular iodine. Sequestering the iodine prevents it from reacting with the carbon species. New insights into the deiodination reaction have made PIDA more promising as a precursor to prepare all-carbon materials or heteroatom-functionalized carbon under mild conditions.

Dedication Page

I would like to dedicate this dissertation to my parents, Edward and Anne; maternal grandparents, Salvatore and Dolores; paternal grandparents, Edward and Dorothy; brother, Paul; and fiancée, Alexandra. Your love, laughs, exquisite cooking, and encouragement helped make all this possible. I would also like to dedicate this work to my soon-to-be in-laws Stephan, DeeAnn, Alyssa, and Taylor. You have created an invaluable home away from home for me. I am very fortunate to have all of you in my life.

A special dedication also goes to past professor, Dr. Joan E. Shields, who passed away before I graduated from C.W. Post. She was instrumental in encouraging me to pursue a graduate career in chemistry.

Table of Contents

List of Figures

List of Schemes

List of Tables

List of Abbreviations

Poly(aniline) (PANI)
Organic Field Effect Transistor (OFET)
Nonlinear Optics (NLO)
Linear Optics (LO)
Dye Sensitized Solar Cells (DSSC)
Organic Light Emitting Diode (OLED)
Highest Occupied Molecular Oribital (HOMO)
Lowest Unoccupied Molecular Orbital (LUMO)
Poly(2,5-thienylene vinylene) (PTV)
Real-time polymerase chain reaction (RT-PCR)
Microwave amplification by stimulated emission (MASER)
Langmuir-Blodgett (LB)
Poly(diacetylene toluene sulfonate) (PTS)
Chemical vapor deposition (CVD)
Poly(diiododiacetylene) (PIDA)
Poly(diactylene) (PDA)
Tetrabutylammonium iodide (TBAI)
Tetrabutylammonium bromide (TBABr)
Tetrabutylammonium chloride (TBACl)
Tetrabutylammonium fluoride (TBAF)
Tetrahydrofuran (THF)
Standard operating procedures (SOPs)
Amorphous graphite-like carbon (AGLC)

Acknowledgments

I would like to acknowledge my dissertation advisor Dr. Nancy S. Goroff, for her patience, direction, advice, and generosity throughout my time as a student in her research group. She has challenged me to be the best I can be. I would also like to acknowledge my chair, Dr. Kathlyn A. Parker, for sharing her expertise in organic synthesis with me. My third member, Dr. Robert Grubbs Jr., has also provided me with great advice and guidance over the years. His encouragement to run the small molecule model studies is a key aspect of this project. I also extend a special thank you to Dr. Nicholas J. Ramer of the Chemistry Department at LIU Post, for serving as the outside member of my committee.

I would also like to recognize the members of the Goroff group, both past and present. Christopher Wilhelm and Liang Luo first introduced me to the world of chemistry in the Goroff group. My former officemate, Dr. Racquel C. DeCicco, was always there to give a fresh perspective on my work. I would also like to acknowledge the current members Dr. David Connors, Allison Black, Honjian Jin, Xiuzhu Ang, and Matthew Freitag for their years of support and advice. A special acknowledgement goes out to former undergraduate students Chang H. Lee and Siew Yoong Tan. These students made great contributions to my project and mentoring them was an honor.

I am also deeply thankful for those who contributed to my work via collaborative efforts. Professor Gary Halada and Christopher Young were fundamental in obtaining all of the Raman data in my dissertation. Dr. James Quinn conducted the SEM/EDS work, as well as great insight into other areas of science. I thank Dr. James Marecek and Francis Picart for training me on the NMR instruments and teaching me how to collect kinetic data.

I greatly thank the entire Main Office staff of the Chemistry Department for their tireless efforts to keep the program in excellent shape. I especially thank Katherine Hughes for helping me with administrative matters. A special thanks also goes to the NSF for funding.

Description for a General Audience

Carbon is a very interesting and versatile element on the periodic table. Atoms of carbon can bond with each other in different ways to give different materials with different properties. Diamond and graphite are examples of materials made entirely of carbon. Despite being made of the same element, these materials have very different properties. For example, diamond is very hard, whereas graphite is very brittle. By visual inspection, graphite is black and opaque, while pure diamond is colorless and translucent. At the atomic level, diamond looks much like a 3D matrix of carbon atoms, while graphite looks like stacked layers of honeycombs in a beehive. While these are the most well-known forms of carbon, other forms exist as well. Carbon also forms tube and soccer ball-shaped structures. At the atomic level, however, tube-like and soccer ball-like carbons are discrete molecules and only nanometers in size.

My research focuses on making new compounds that consist entirely of carbon atoms from a material called poly(diiododiacetylene) (PIDA). PIDA is a compound made up of entirely carbon and iodine atoms. The chemical bonds that hold the iodine and carbon atoms together are very weak. These weak bonds can be broken under mild conditions to make a compound that has a higher ratio of carbon atoms to iodine atoms. Making carbon and carbon-rich materials often requires high temperatures and/or specialized equipment. PIDA, however, offers a potential route towards these compounds under conditions that can be employed in any lab.

One such material that may be made from PIDA is called carbyne. Carbyne is a form of carbon where all the carbon atoms are in a line. Preparing carbyne would allow us to discover its properties, and see how they compare to other forms of carbon. The preparation of carbyne is challenging, because it is expected to be highly unstable. Models of carbyne called polyynes

have been prepared and showed that stability is an issue that requires special attention. One must protect the carbon rod from other carbon rods since they can react with each other. This is why iodine-capped carbon rods are used to make PIDA. The iodine groups protect the carbon rod from other molecules.

PIDA is made from iodine-capped rigid carbon rods that have been helped to align in crystals in a specific orientation. The iodine-capped carbon rods react with each other in the presence of light and heat. As a random solid, the rods explode when heated to 90°C to make a black powder! In a solution, the iodine-capped carbon rods can decompose to give off iodine if exposed to light. In the crystals we study, the molecules used to align the iodine-capped carbon rods are called host molecules. The iodine-capped carbon rods are called guests. A solution of the host and guest is allowed to evaporate to form cocrystals. In the cocrystals, the hosts make the iodine-capped carbon rods align just perfectly, so that they undergo reaction upon sitting to form PIDA. This is a very sensitive process. Former group members were able to make PIDA cocrystals in decent quantities, but the process appeared to be highly sensitive to the environment. Eventually, an unknown variable changed, and cocrystals could no longer be obtained. This prompted new studies to optimize the conditions for forming PIDA cocrystals. After ruling out temperature and humidity changes, it was found that solvent had the biggest impact. Changing the solvent to acetonitrile made a big difference in the quantity of PIDA cocrystals made at a time.

With a much more reliable method for making PIDA cocrystals in hand, work was conducted to remove the iodine atoms from the material. Previous efforts by former group member Liang Luo focused on separating the PIDA from the host molecules before subjecting the material to conditions for iodine elimination. The free PIDA molecules, however, tend to

cluster together in groups. This clustering makes the strands on the inside harder to access rendering the internal PIDA strands inaccessible to the reagents that remove the iodine atoms. The end result is incomplete removal of the iodine atoms. The ideal reaction would involve removal of the iodine groups before the PIDA strands cluster together. The clustering before iodine removal can be avoided by using PIDA cocrystals and slowly dissolving away the host to expose fresh PIDA strands. The new work has shown that iodine can be completely removed, but other atoms take its place. The material is carbon-rich with inclusion of other atoms such as sulfur and phosphorus, depending on the reaction conditions. This new material may be interesting in its own right.

Finding optimal conditions for removing iodine from PIDA cocrystals required modeling the reaction. It is very difficult to figure out the structure of the large, complicated carbon-rich material made by removing iodine from PIDA. It would thus be easier to use a model compound that scientific instruments could obtain detailed structural information about. A model compound was made and tested under various conditions to see how the reactive iodine atoms in PIDA would behave. Chang Heon Lee conducted the reaction with pyrrolidine, and iodide ion, the material added to table salt as an iodine source. He found that the solvent used for the reaction had a dramatic effect on the speed of the reaction. The observations from Mr. Lee's experiments allowed us to propose optimal conditions to completely remove iodine from PIDA.

Further studies showed the pyrrolidine induced side-reactions, in addition to the removal of iodine. This made the overall reaction quite complex. The reaction of the PIDA model compound with the iodide ion is simpler, but also had many side-reactions associated with it. Ultimately, it was found that pyrrolidine and iodide ion can remove iodine to make carbon rods. This happens when 1 molecule of the model reacts with 1 molecule of the ammonia-like or

iodized salt-like species. The reaction was found to be general for molecules with similar reactive sites to PIDA. The new insight into the iodine removal reaction has brought PIDA one step closer to being transformed into carbyne and other carbon-rich materials.

Chapter 1: Background and Introduction

1.1 The Need for Organic Materials

As modern technology continues to develop there will be an increase in demand for new materials to make the functional components of these devices. Inorganic compounds such as silicon, SiGe, GaAs, GaP, and GaN are used in today's electronics as semiconductors or light emitting diodes. While these inorganic materials certainly have proven useful, they often suffer from issues like poor natural abundance and challenges in recycling. In addition, processing these materials often requires harsh chemicals and specialized equipment.

Silicon, for example, is at the heart of almost every semiconductor used in computing systems. It does not suffer from raw-material availability, but it does require hazardous chemical treatments and high temperature for processing.[1] The manufacturing of silicon requires etching chemicals such as hydrofluoric acid (HF) and a solution of conc. H_2SO_4 / H_2O_2. HF is highly toxic and corrosive. The H_2SO_4 / H_2O_2 solution is also highly corrosive and its preparation is highly exothermic. The raw material used in silicon production is silicon dioxide. Silicon dioxide (SiO_2) is reduced to silicon via a carbothermal reaction at 1900 °C. In this reaction, carbon reduces SiO_2 to silicon and forms the greenhouse gas, CO_2. In order to grow useable polycrystalline electronic grade silicon, it is necessary to liquefy the reduced Si at 1450 °C and use a seed crystal to form a boule. This process makes the production of silicon an energy intensive process that results in highly toxic waste that needs proper disposal. Some physical drawbacks of silicon include its rigidity and brittleness. These drawbacks make silicon and many other inorganic materials unsuitable for use in flexible displays. Other materials such as gallium arsenide and silicon germanium have been developed as potential replacements for silicon. These materials, however, suffer from poor natural abundance. The earth's crust only contains 1.8 ppm

germanium, 1.5 ppm arsenic, and 18 ppm gallium. Silicon by comparison comprises 277,100 ppm.

It is necessary to develop an alternative to inorganic materials given the numerous drawbacks of using such compounds. Organic materials can address many of the issues faced by their inorganic counterparts. One of the benefits of using organic materials is that organic synthesis can be used to build an almost limitless library of compounds with different structural features that give rise to different physical properties. Organic chemistry also lends itself to versatility in that there are often multiple synthetic pathways that can be used to obtain a single product. This characteristic of organic chemistry allows for flexibility in finding the most cost effective route to preparing a desired compound. Organic raw-materials are also available in abundance. Although hydrocarbons from the petroleum industry are the most common source of organic compounds, a great deal of effort has been given in recent years in using bacteria to synthesize basic building blocks like ethanol.[2]

Another major advantage in favor of using organic compounds is the possibility for solution state processing. Solution state processing allows the organic compound to be dissolved in common organic solvents and deposited by techniques such as spin coating, inkjet printing, and spray coating.[3] These techniques can be carried out cheaply on large scales. These methods do however require the organic compound to be appreciably soluble in the solvent of choice. For poorly soluble molecules, another technique such as organic molecular beam deposition (OMDB) can be used where the compound is evaporated onto a substrate under ultra high vacuum (UHV).[3]

1.2 History of Organic Materials

Conductive organic materials have been studied since the 1800's. The earliest work dates back to Henry Letheby in 1862.[4] Letheby was working with aniline in a sulfuric acid electrolyte

during an electrochemical experiment when he obtained a partially conductive compound that he was unable to fully characterize. The same conditions used by Letheby are now used to prepare the semiconductor polyaniline (PANI) but he did not have clear definitive characterization data to positively identify his compound.[5] Although organic semiconductors have been known for many years, inorganic semiconductors were favored because fewer technological hurdles exist in making these materials work well.[6]

In 1974, Proctor and coworkers[7] demonstrated a working organic transistor based on melanin. Melanin is a general term for a variety of naturally occurring pigments found in most organisms. These pigments have varying chemical structures but all contain a nitrogen heterocycle. The nitrogen heterocycle is commonly polymerized at the positions indicated by **Figure 1.1**. The R groups of melanins can be –COOH groups or simple –H groups. Another feature of the naturally occurring melanins is a conjugated backbone with electron-withdrawing carbonyls and electron-donating indole ring. The combination of electron-withdrawing and electron-donating groups creates donor-acceptor pairs that enhance charge carrier mobility. Proctor and coworkers[7] used isolated melanins from a human tumor and ones prepared synthetically by enzymes. Several forms of melanin may have been present in the working device due to the biological source of the materials. Confirmation of transistor activity was observed when an appropriately applied potential generated a measurable current. At other potentials no current was observed and the device was in an "off" state.

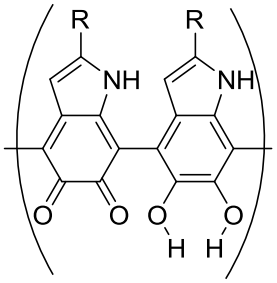

Melanin

Figure 1.1. Structure of naturally occurring Melanin

1.3 Theoretical Considerations

Organic materials have attracted interest in areas such as biosensors, organic field-effect transistors (OFETs), nonlinear optics (NLO), dye-sensitized solar cells (DSSCs), and organic light-emitting diodes (OLEDs). The organic compounds in these devices and disciplines can be small molecules or organic polymers. **Figure 1.2** below shows some organic materials that have been investigated in recent times for semiconductor applications.[8]

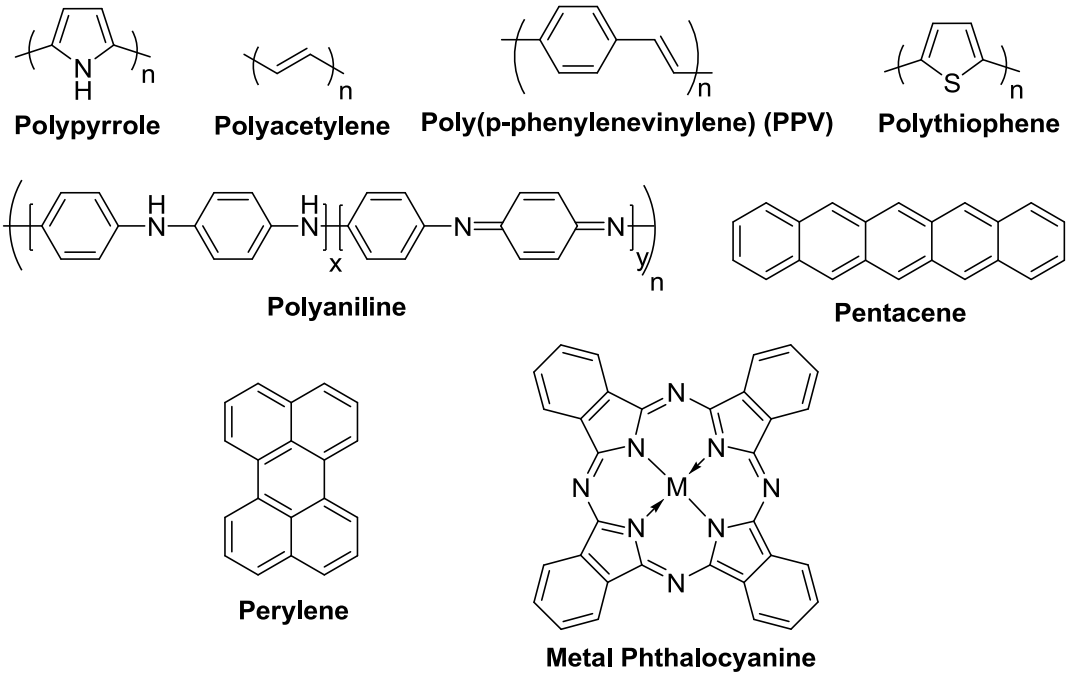

Polypyrrole **Polyacetylene** **Poly(p-phenylenevinylene) (PPV)** **Polythiophene**

Polyaniline **Pentacene**

Perylene **Metal Phthalocyanine**

Figure 1.2. Some common organic compounds showing the structural diversity of organic materials

The science used to describe semiconductor behavior is called band theory and focuses largely on inorganic compounds. Despite the focus on inorganic compounds, band theory can still be used with some modification to describe organic semiconductors. Band theory has roots

in molecular orbital theory. This theory specifically focuses on the highest occupied molecular orbital (HOMO) and lowest unoccupied molecular orbital (LUMO). **Figure 1.3** below shows the relationship between band theory and molecular orbital theory. **Figure 1.3A** shows that less energy is needed to promote an electron from the HOMO to the LUMO as more tightly packed atomic orbitals overlap with each other.[9] As multitudes of atoms bond, the discreet energy levels become indistinguishable. These indistinguishable energy levels are referred to as energy bands. The HOMO and LUMO are then referred to as the valence band and conduction band respectively (**Figure 1.3B**). Tight packing of orbitals is a consequence of the solid state. Furthermore, when the bands form, electrons can easily delocalize throughout the entire system. For metallic compounds, this involves promoting electrons from a *d*-orbital to the above *s*-orbital.[10] The energy required for this promotion is very small because metals have highly delocalized electrons resulting from multidirectional delocalization.[10] The ease of electron delocalization is what gives rise to the conductivity of metals. Organic semiconductors can be explained in a similar fashion with exception that electrons are excited from a π to π^* orbital. This excitation can be initiated with light or an applied potential.[11] When an electron returns to its lowest energy after excitation, emission of a photon is possible. The emission of photons is one reason why organic materials are of interest for both organic field-effect transistors (OFETs) and organic light-emitting diodes (OLEDs).[11]

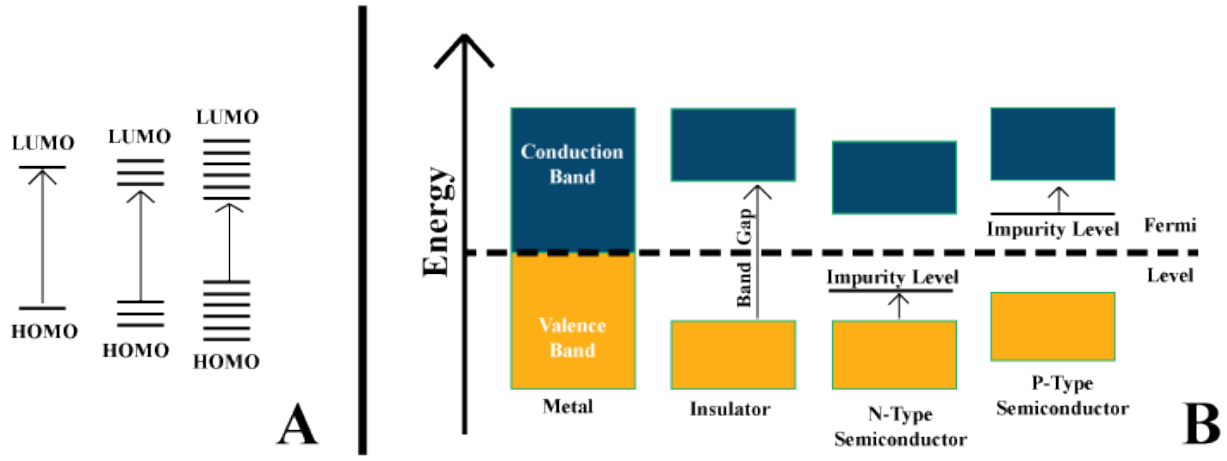

Figure 1.3. A) HOMO – LUMO energy gap lessens as more orbital overlap results in delocalization. B) Energetic differences between metals, insulators, and semiconductors.

Extensive delocalization accounts for the conductivity in metals but even the most highly conjugated polymers do not exhibit comparable conductivity to metals. The reason for the difference in conductivity can be seen in **Figure 1.3B**. **Figure 1.3B** shows the relative energy levels of the valence and conduction bands for metals, insulators, and semiconductors. The difference in energy between the valence band and conduction band is called the band gap. Metals typically have a band gaps less than 1 eV because the electrons delocalize easily. Insulators are defined as requiring energies of 5.5 eV or higher to promote electrons from the valence band to the conduction band.[12] At room temperature however there is not enough free energy to excite the electrons hence insulators lack appreciable conductivity. Semiconductors on the other hand can conduct electricity at room temperature because there is sufficient thermal energy to cause an excitation. The band gap for semiconductors is generally defined as being between 1-5 eV.[12]

Figure 1.3B also shows two other important factors in classifying materials for electronic applications. These factors include impurity energy levels and the Fermi level. Impurity energy levels arise from adding minute amounts of an impurity called a dopant to a semiconducting material. The purpose of the dopant is to modify the energy bands in a way that lowers the

energy needed to promote an electron into the conduction band. The effect of the added impurity is important for classifying the semiconductor as having n-type or p-type characteristics (**Figure 1.3B**). When the energy level of the dopant closely matches the valence band, the material is said to be an n-type semiconductor. If the energy level of the dopant is close to the conduction band energy the material is said to a p-type semiconductor. Organic semiconductors however are not doped like silicon.[6] Large amounts of dopant on the order of a few percent are required to observe a noticeable change in the electronics of organic materials as opposed to only a few ppm of dopant for silicon. When organic materials are doped however, the material becomes a conductor.[6] A material classified as a conductor is undesirable for applications in electronic devices such as transistors because the device would not function as it is needed to. A transistor is a switch which requires "on" and "off" states to perform logic operations. If a material is a conductor it will constantly be in an "on" state which makes logic operations impossible.

A material is defined as a conductor, semiconductor, or insulator based upon its Fermi level. The Fermi level is the chemical potential of an electron and depends on temperature (**Equation 1.1**).[13] At absolute zero, electrons cannot cross the Fermi level in a semiconductor, and it displays insulator characteristics. When a material is subjected to elevated temperatures, its electrons gain energy to occupy higher energy states, which gives rise to conductivity. The Fermi level also allows differentiation between extrinsic and intrinsic semiconductors. Insulators are said to be intrinsic semiconductors, which means that they are only perfect insulators at 0 K.[6] Temperatures above 0 K can impart sufficient thermal energy to allow electrons to populate the conduction band. Extrinsic semiconductors are made through doping an intrinsic semiconductor. Since organic materials cannot be doped in the same manner as inorganic materials, they are classified as intrinsic semiconductors. Despite such classification, the labels n-type and p-type

are still used when discussing organic semiconductors. The difference between the two types for organic materials is distinguished by what is said to be a charge carrier.

$$F_e(\varepsilon) = \frac{1}{e^{((\mu-\varepsilon)/(kT))} + 1}$$

Equation 1.1. F_e = fermi level, μ = chemical potential from Fermi-Dirac distribution, ε = energy of the HOMO, T = absolute temperature, k = Boltzmann's constant

1.4 Electronic Application of Organic Materials

Charge carriers are particles often referred to as holes or electrons.[6] As the name suggests, charge carriers carry charge. Holes carry positive charge where as electrons carry negative charge. Organic compounds better at carrying holes are referred to as p-type semiconductors where as better electron carriers are said to be n-type semiconductors. **Figure 1.4** below was redrawn from Gao and coworkers to demonstrate the injection of holes from a gold electrode into pentacene.[14] The energy diagram in **Figure 1.4** shows that the Fermi level of gold closely matches the HOMO of pentacene. Since the HOMO of pentacene is populated no electrons can be injected into it. Electrons can only be injected into the LUMO of pentacene but there is a substantial energy barrier from the Fermi level of gold to the LUMO which prevents such injection. Given these electronic constraints, an electron will be removed from the HOMO of pentacene creating a hole (+ charge). Organic materials are characterized as p-type or n-type using a current-voltage plot as seen in **Figure 1.5**.[15] The current-voltage plot in **Figure 1.5** shows the semiconducting behavior of poly(2,5-thienylene vinylene) (PTV). One can see that as a more negative gate voltage is applied a current is observed between the electrodes of the transistor. The negative gate voltage implies that positive charges are being induced at the source electrode of the transistor.[6] This behavior indicates p-type behavior for PTV. The exact opposite would be observed for n-type transistors.

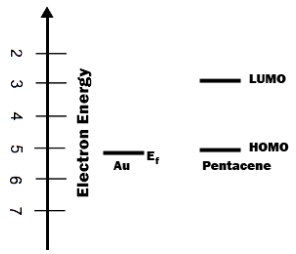

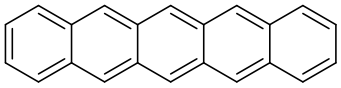

Pentacene

Figure 1.4. Energy diagram of pentacene at a gold electrode.[6] E_f = Fermi level of gold

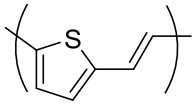

poly(2,5-thienylene vinylene) - (PTV)

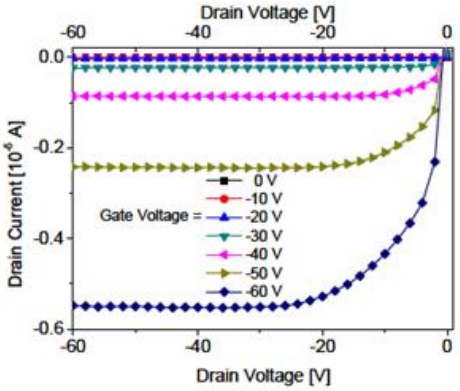

Figure 1.5. Voltage-current plot indicating p-type semiconductor behavior.[15] Annual review of materials research by ANNUAL REVIEWS. Reproduced with permission of ANNUAL REVIEWS in the format Republish in a thesis/dissertation via Copyright Clearance Center.

Organic field-effect transitors (OFETs) are of great interest because they can potentially be fabricated via ink jet printing onto flexible substrates. The block diagram of an OFET is presented below in **Figure 1.6** and was redrawn from Klauk.[6] The OFET has three electrical contacts which are called the source, drain, and gate. When a voltage is applied across the gate, a charge opposite in sign is induced across the semiconducting channel (**Figure 1.6 inset**). The insulator can be glass or a flexible plastic. It is important to note that charge in organic semiconductors is directional. When charge is directional, conductivity is only achieved in

specific directions depending upon the material. Graphite for instance, is mostly conductive along the carbon plane.[16]

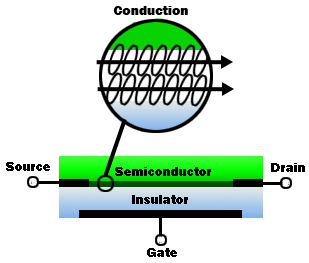

Figure 1.6. Block diagram showing key components of an OFET. Inset shows conduction pathway.[6, 11]

1.5 Optical Applications of Organic Materials

Conjugated organic materials have interesting optical properties such as undergoing color transitions when exposed to certain stimuli. One such device that functions based on a color transition is a biosensor. Biosensors are defined by IUPAC as "devices that use specific biochemical reactions mediated by isolated enzymes, immunosystems, tissues, organelles or whole cells to detect chemical compounds usually by electrical, thermal or optical signals."[17] This definition means that biosensors must be optimized for a specific application in order to work properly. One such use for biosensors is pathogen detection. Amano and Cheng[18] recently considered some of the common problems with current detection technologies for the influenza virus. Some common methods for viral detection are real-time polymerase chain reaction (RT-PCR), MDCK cell cultures, complement fixation, and hemagglutinin-inhibition.[18] These methods are either labor-intensive or require specialized training making them impractical for high volume detection. Anti-viral drugs can only be administered for the flu within 48 hours of the onset of the virus.[18] This property of anti-viral drugs makes rapid detection a requirement, with current detection technologies being a hurdle to better treatment.

Charych and coworkers[19] have experimented with a class of organic materials called polydiacetylenes (PDAs) (**Figure 1.7**) for influenza detection. The PDAs were cast into

Langmuir-Blodgett (LB) thin-films using a monolayer support and sialic acid functionalized PDA to bind the Hemaglutinin glycoprotein units found on the surface of the influenza virus (**Figure 1.8)**. The conjugated PDA backbone is a chromophore making these compounds useful for visual applications such as colorimetry. PDAs are particularly interesting because the optical properties of these compounds are strongly influenced by stress applied to the side-chains of the C=C double bonds.[20] The results of Charych's experiment showed that when the LB film was exposed to as little as 40 Hemagglutinin Units (40 x 10^7 particles) of virus a noticeable color change from blue to red was observed. The colorimetric result can be seen in **Figure 1.9** below. This colorimetric change is easy to observe without special instrumentation and the change is complete in 30 minutes.[19] One of the benefits of this method is that the LB film was easily prepared under mild conditions. Charych and cowokers speculate that as the influenza virus binds to the sialic acid receptor on the PDA backbone, stress affects the energy levels in conjugated network with a color change being made manifest. Schott and coworkers[20] use first-principles methods to probe the nature of electron delocalization on chromic shifts in PDAs. It was found that the red phase of PDAs is explained by diminished delocalization resulting from applied stresses.

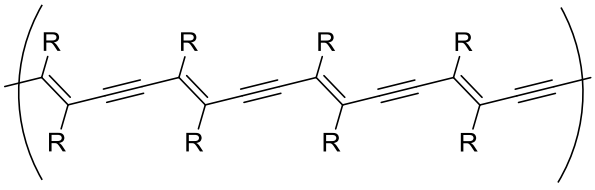

Figure 1.7. General structure of the material used by Charych and coworkers

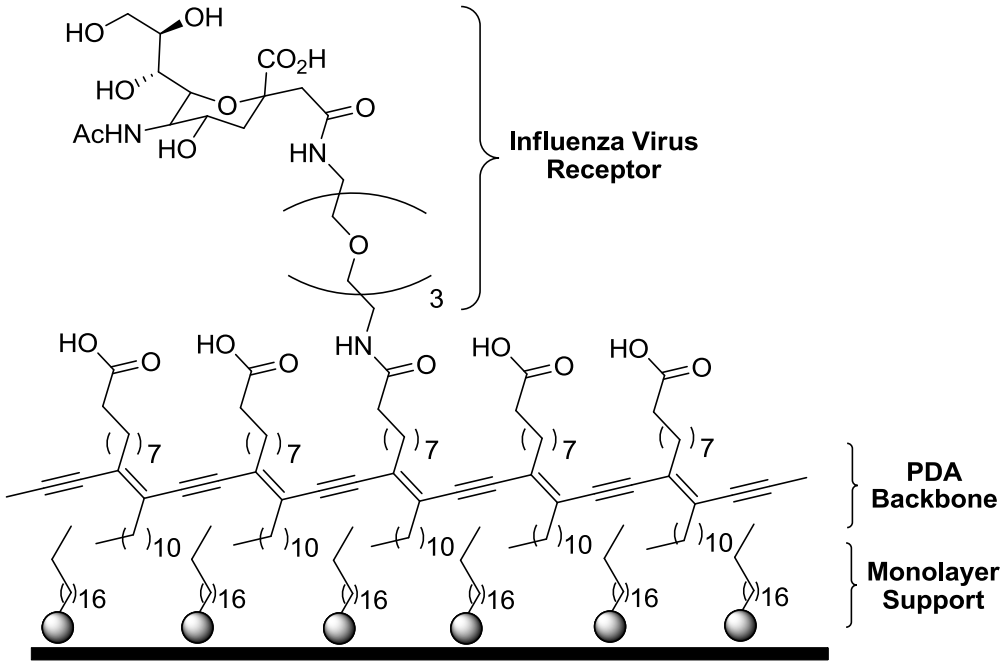

Figure 1.8. Redrawn schematic of the biosensor constructed by Charych and coworkers[19b]

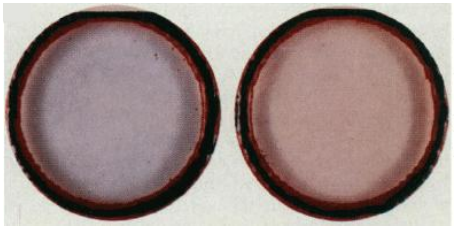

Figure 1.9. Biosensor thin-film before (blue) and after (red) exposure to influenza virus.[19b] Reprinted with permission from Ref. 19b. Copyright AAAS 1993.

Another field that exploits the optical properties of organic materials is non-linear optics (NLO). NLOs is the term used to study how light is affected by the optical properties of a material. The behavior of a material in an optical field is said to be nonlinear if the material responds nonlinearly to the strength of the applied optical field.[21] Weinreich and coworkers[22] are credited with first investigating the field of NLOs. They were the first group to observe second-harmonic generation with ruby optical microwave amplification by stimulated emission (MASER).[22] Second-harmonic generation results in a quadratically scaling atomic response to the strength of an applied optical field.[21] The atomic response is the emission of photons of different frequency than the applied optical field. **Equations 1.2** and **1.3** below shows a

simplified mathematical model for the behavior of NLOs and linear optics (LOs). One can see from **equations 1.2** and **1.3** that NLOs can be treated as a power series dependent upon higher order factors. As a result, it is important to consider first-order factors when discussing second-order ones. It thus follows that the third-order factors also have mathematical dependency on the second and first order ones. The relationships in **equations 1.2** and **1.3** only hold true if a material is a lossless and dispersionless system. For systems experiencing loss and dispersion NLO treatment must be more rigorous because the relationships in **equations 1.2** and **1.3** break down.

Linear Optics: $P(t) = \varepsilon_0 \chi^{(1)} E(t)$ **Equation 1.2**

Nonlinear Optics: $P(t) = \varepsilon_0 [\chi^{(1)} E(t) + \chi^{(2)} E^2(t) + \chi^{(3)} E^3(t) + \ldots]$ **Equation 1.3**

P(t) = polarization, χ^n = susceptibility constant, E(t) = energy of applied optical field, ε_0 = permittivity of free space

The source of NLO activity in organic systems is the conjugated π-systems. As delocalization of π-electrons gives rise to conductivity, it also enables NLO activity. The reason for this is that the π-electrons are more loosely bound to the nuclei and free to interact with an applied optical field.[22] It was known in the late 1980's that conjugated small organic molecules and organic polymers had large third-order NLO properties. One such organic polymer that has been extensively studied for NLO activity is poly(diacetylene toluene sulfonate) (PTS).[23] The structure of PTS can be found below in **Figure 1.10**. PTS was particularly hard to study by transmission spectroscopy experiments because it had a very strong exciton absorption leading to fluorescence.[23a] This phenomenon made it necessary to use solid samples as thin as 100 Å. This restraint was modestly overcome by Thakur and coworkers[24] in 1985 through developing a technique for the preparation of single-crystal thin-films. The preparation of the films was carried out by using high pressure to press a PDA between two optical plates while in a molten state. The molten state could be induced either by melting the PDA or dissolving it in a solvent

such as acetone if possible. This method allowed films as thick as 200 Å to be studied. In later work, Thakur and coworkers were some of the first to extensively study the NLO properties of PTS.[23a] They report observing third-order NLO susceptibility which is common for conjugated organic systems. One source of third-order nonlinear optical activity is multiphoton absorption. Multi-photon absorption is the term used to describe absorption of multiple photons of either the same or different frequency followed by an electronic excitation. The subsequent relaxation back to the ground state can result in the emission of a photon of different frequency than the exciting photon(s).[21] Stegeman and coworkers reported four-photon absorption for PTS.[25]

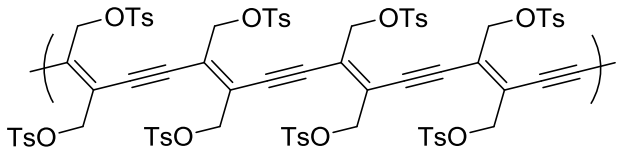

Polydiacetylene Toluene Sulfonate (PTS)

Figure 1.10. Molecular structure of poly(diacetylene toluene sulfonate) (PTS)

While NLO is its own discipline, it has broad applications in areas such as all-optical computing, optical storage, and telecommunications. One such area of extreme interest is all-optical computing. NASA scientists Donald Frazier, Hossin Abdeldayem, and Steve Paley are one such team amongst the many that have worked to develop optical computing systems.[26] Frazier states that current semiconductor technology using electrical conductivity for switching devices between the "on" and "off" limits computer networks speeds to 50 Gbits / sec.[26-27] Abdeldayem claims that terabit speeds will be needed to keep up with the growing demand for bandwidth over the internet for multimedia data.[26-27] Optical systems are well suited for this task because photonic devices work better in parallel than electronic devices. The multi-photon absorption properties of NLO materials are favorable for parallel operation.

Photonic devices also do not suffer from electromagnetic interference and generally work faster because photons can travel at almost the speed of light under ambient conditions.[28]

Semiconductors using electrical conductivity for logic operations are adversely affected by thermal energy which builds up as the device is working. If too much thermal energy builds up the semiconductor can short circuit. This break down occurs because the thermal energy is allowing the electrons to freely delocalize from the valence band to the conduction band. When this happens the semiconductor becomes a conductor, which will cause undesired operation and device failure. Photonic systems do not suffer from thermal energy break down in the same way. Abdeldayem and coworkers have built logic gates using a PDA and metal-free phthalocyanine that operate at the terabit level.[26] A major technological hurdle still remains to be overcome before such devices become used in mainstream computing. This hurdle is in the stability of the NLO material when subjected to a laser. Lasers are powerful beams of the light that often destroy the organic material.[29]

1.6 All-Carbon Materials

While the field of organic materials frequently includes heteroatomic systems with hydrogen groups, other systems containing mostly or all-carbon networks are also of great interest. Materials such as graphite and diamond are the well known forms (**Figure 1.11**) of carbon. Graphite, a well-known conductor, is a layered honeycomb structure of aromatic rings. Conductivity is imparted through graphite's vast π-electron delocalization in the plane of the graphite layer. The layers in graphite are held together by weak van der Waals forces which make it easy to rub graphite off on other surfaces.[30] This property is what makes graphite useful as pencil lead. Graphite itself is also used as a lubricant, electrode material, and other specialized commercial applications. In materials chemistry, graphite can serve as a precursor to the nanoscale carbon allotrope called graphene.

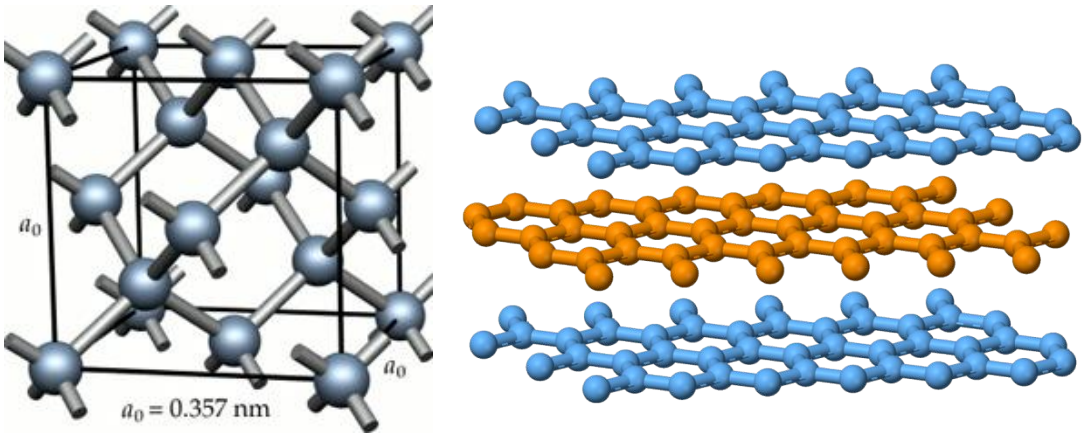

Figure 1.11. Molecular structure of diamond. Copyright 2011-2013 Element Six. All Rights Reserved. (left) and graphite. From Wikimedia Commons, the free media repository. (right)

Graphene is single atom thick layer of graphite (**Figure 1.12**). It was first studied by Hofmann in 1962 but not thoroughly investigated until recently.[31] Much of the recent interest in graphene can be attributed to the work of Andre Geim and Konstantin, who in 2010 were awarded the Nobel Prize in Physics for their efforts. They discovered graphene could be obtained simply by applying Scotch tape to graphite and removing it.[32] The result of this experiment was few layer graphene deposited on the Scotch tape. This technique has come to be known as the "Scotch tape" method. Geim and Novoselov studied the properties of graphene and found it to be extremely strong and highly conductive.[32] These findings generated great interest in the area of flexible displays and electronics. While the simplicity of the "scotch tape" method is tantalizing, it does have certain drawbacks. Once the Scotch tape has been removed from graphite the graphene must be located under a microscope. The Scotch tape contains layers of graphite varying in thickness with some being very thick and others less so.[32]

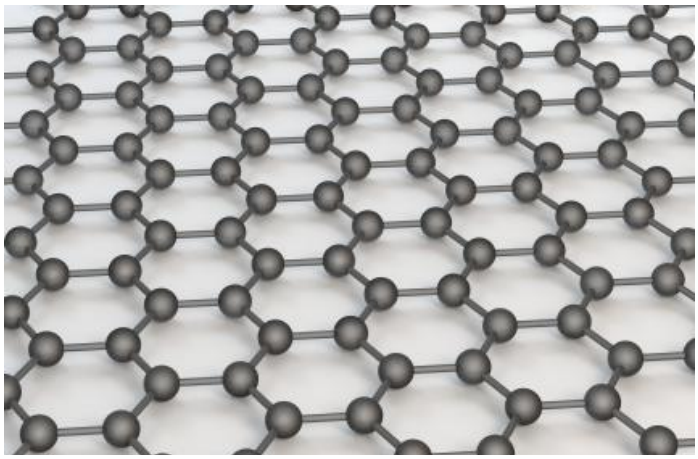

Figure 1.12. Molecular structure of monolayer graphene. ©iStockphoto.com/INchendio

In recent years, graphene has attracted a great deal of interest for a variety of applications.[33] One such application of graphene has been investigated by semiconductor giant, IBM. In 2010, IBM developed a 100 GHz transistor based on graphene (**Figure 1.13)**.[34] The highest switching frequency reported for Si semiconductors is 40 GHz making graphene more than twice as fast.[34] The major obstacle to commercialization of such graphene devices is finding reliable and mild methods for fabrication.

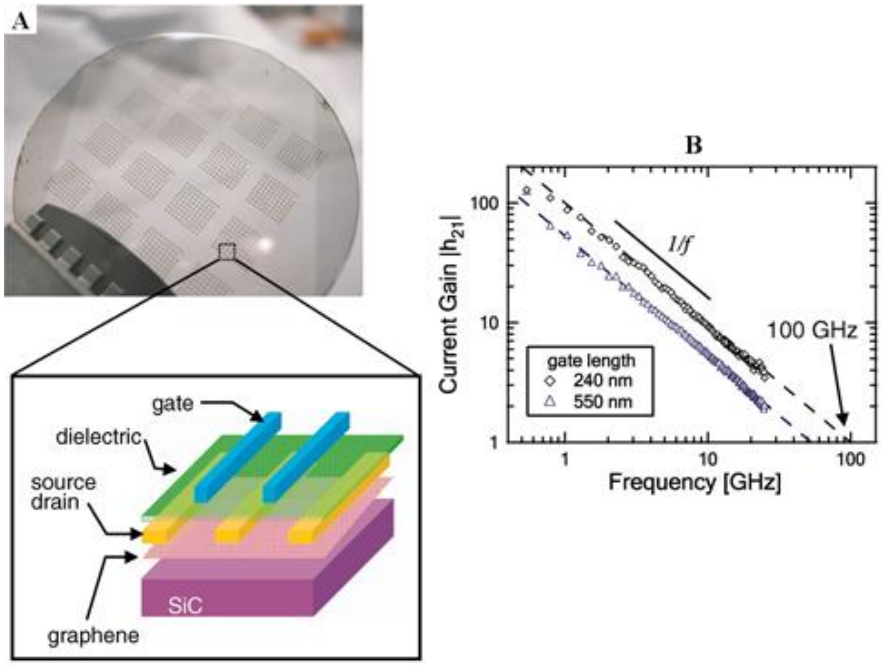

Figure 1.13. A) Graphene deposited on wafer; B) Current-frequency plot showing the max switching frequency of 100 GHz. Reprinted with permission from Ref. 34. Copyright AAAS 2010.

While the electronics industry has a great interest in graphene, other uses have been proposed. One such use is for hydrogen storage. Brus and coworkers experimented with hydrogenating 1 layer and 2 layer graphene.[35] They found that hydrogen reacts with monolayer graphene at room temperature. The reactivity was attributed to ripples in the graphene layer due to the absence of π-stacking which favors planarity. **Figure 1.14** below shows the Raman spectrum of the hydrogenated and pristine samples indicating reaction in the monolayer sample.

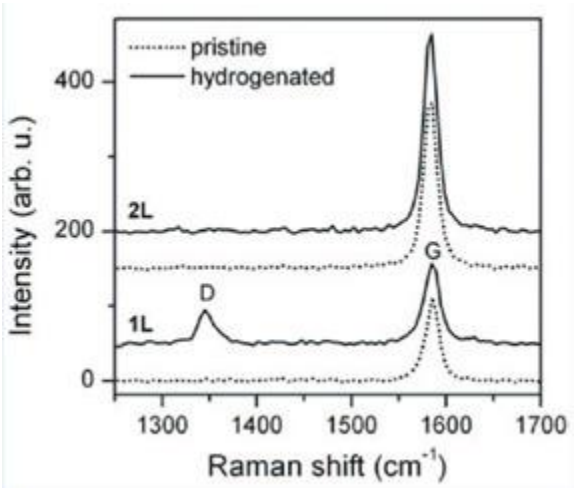

Figure 1.14. Raman spectra showing pristine (dotted) and hydrogenated graphene (solid). Reprinted with permission from Ref. 35. Copyright (2008) American Chemical Society.

In **Figure 1.14** the appearance of the D band in the hydrogenated sample indicates hydrogen was absorbed onto the monolayer. The bilayer graphene did not show any absorption of hydrogen. Equally import to absorption is desorption for the hydrogen to be used in a fuel cell application. Brus and coworkers also conducted experiments to release hydrogen from graphene by heating the sample (**Figure 1.15**). The results of the experiment showed the disappearance of the D band, which is indicative of the restoration of pristine graphene.[35]

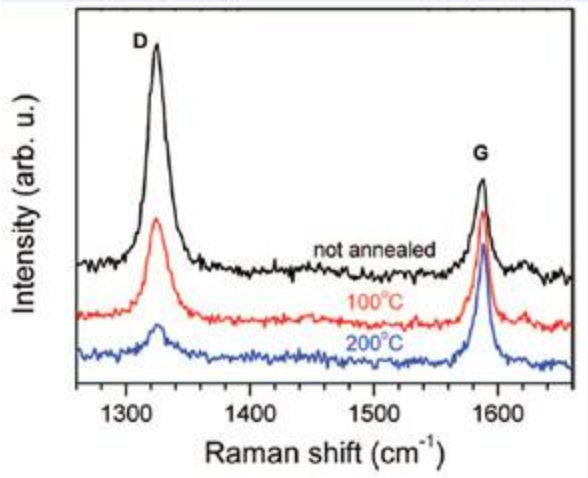

Figure 1.15. Raman spectra showing the release of hydrogen as the hydrogenated graphene is heated. Reprinted with permission from Ref. 35. Copyright (2008) American Chemical Society.

Monolayer devices are not best suited for hydrogen storage. Using them for such would require expensive preparation and the substrate would add unnecessary weight. As a result, the use of Li^+ decorated multi-layer graphene has been proposed as an alternative to monolayer graphene based on first-principle calculations.[36] According to Smith and coworkers, decorating multilayer graphene with Li^+ separates the layers enough so that hydrogen can fill the void.[36] The Li^+ ions thus effectively create a stabilized porous graphene. First-principle calculations show that as more hydrogen is adsorbed further incorporation requires less energy due to steric interactions between hydrogen molecules.[36] While these results are promising, more work is needed to understand how graphene materials can be prepared.

Although graphene has attracted much attention, other nanoscale carbon materials like carbon nanotubes and fullerenes are also investigated routinely (**Figure 1.16**). Fullerenes are spherical in shape and come in various sizes such as C_{60}, C_{70}, C_{76}, C_{82}, and C_{84}. C_{60} is frequently studied for applications in dye sensitized solar cells.[37] Carbon nanotubes vary more in length and diameter. The properties of the nanotubes are strongly influenced by diameter. Carbon nanotubes have been investigated for many applications included supercapacitors,[38] optical mirage

studies,[39] and fuel cell catalysis.[40] These nanoscale allotropes have shown to have interesting properties, and demonstrate the diversity nature of carbon.

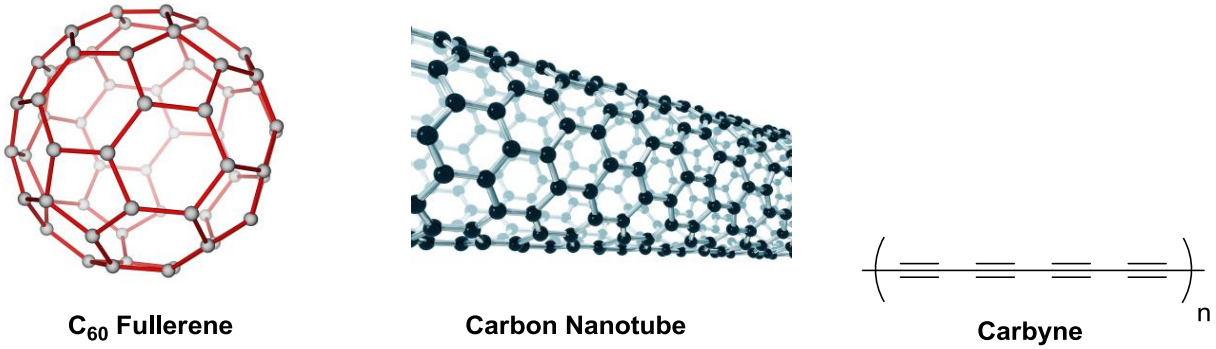

Figure 1.16. Molecular structure of C_{60}. ©iStockphoto.com/Leonid Andronov (left), carbon nanotube. ©iStockphoto.com/PaulFleet (middle), and carbyne (right).

Carbyne is the all-*sp*-hybridized allotrope of carbon, which is less well known than the previously discussed forms. It is highly unstable under ambient conditions which make studying it difficult. Many literature reports discuss observing carbyne or carbyne-like structures but the data is often inconclusive. Lagow and coworkers claimed to observe a linear *sp*-hybridized carbon chain of over 300 atoms long.[41] A mass spectrum is reported in their work however it shows the presence of fullerenes and does not definitively show evidence of carbyne. Observing carbyne formation under the conditions reported by Lagow and coworkers is unlikely. Milani and coworkers studied the stability of carbynoid structures in carbon films.[42] The films were prepared using supersonic carbon cluster beam deposition in an ultrahigh vaccum at room temperature. These films however consisted primarily of polyynes and polycumulene embedded in with sp^2 hybridized carbon. The carbynoid structures were found to react with oxygen and rapidly disappeared upon heating above room temperature. Despite these literature reports, definitive evidence of carbyne formation has not been observed to date.

1.7 Common Techniques for the Preparation of Carbon Materials

Wet chemical preparation of carbon rich materials is challenging. Graphene suspensions for instance are usually prepared by oxidizing graphite, thermally expanding it, and then reducing it to restore conductivity.[43] Graphite is commonly oxidized by a technique called the Hummers method.[43] This method involved the use of harsh oxidizing reagents such as H_2SO_4 / HNO_3, $KMnO_4$ in H_2SO_4, and $KMnO_4$ / $NaNO_3$ in H_2SO_4. These mixtures can be potentially explosive and make large scale processing infeasible. Newer methods using $KMnO_4$ in H_3PO_4 / H_2SO_4 have been developed but still require large amounts of concentrated acid.[44] Another drawback with this method is the need to reduce graphene oxide to graphene because the oxide is not conductive. The reduction often leaves behind imperfections in the carbon network making pristine graphene inaccessible through this method. Ajayan and coworkers succeeded in making close to pristine graphene by first reducing the expanded graphene oxide with sodium borohydride.[45] The product of the $NaBH_4$ reduction was then subject to annealing at 1100°C under an Ar / H_2 environment. These conditions however are still extreme and potentially dangerous.

Graphene can also be formed via chemical vapor deposition (CVD) by decomposition of a carbon source like methane.[46] Zhang and coworkers used electron beam evaporated copper film to serve as a catalyst to decompose methane. The quality of the copper film determined the quality of the graphene layers deposited. Full coverage of the quartz substrate however was not achieved but single and few-layer graphene could be detected by Raman spectroscopy. This method is less hazardous than harsh chemical oxidation but requires specialized equipment.

Carbon nanotubes are usually not prepared via wet chemistry. These materials are often prepared by techniques such as arc discharge,[47] laser ablation,[48] and CVD.[49] Arc discharge involves passing a large current through graphite electrodes. Laser ablation is the process by

which a pulsed laser vaporizes a graphite target in a high-temperature reactor under an inert environment. CVD involves coating a substrate with a metal layer to act as a catalyst in a similar manner as graphene is prepared. The substrate is then heated to high temperature and bombarded with a carbon gas such as acetylene, ethylene, or methane.[49] The diameter of the nanotubes is dependent upon the size of the metal catalyst particles. All of these methods involve extreme conditions and specialized equipment, which raises the cost of these materials.

Fullerenes can also be prepared from arc discharge methods.[47] This method is not ideal for large scale preparation because of the large currents required. It is also necessary to fine tune conditions to favor fullerenes over carbon nanotubes. Some have attempted to prepare fullerenes by methods other than arc discharge. In 2002, Scott and coworkers prepare C_{60} fullerene in less than 1% yield from simple organic compounds and flash vacuum pyrolysis.[50] It is clear that more reliable methodology is needed for widespread adoption of all-carbon materials for real applications. The ideal preparation would utilize mild reaction conditions with easy-to-access starting materials.

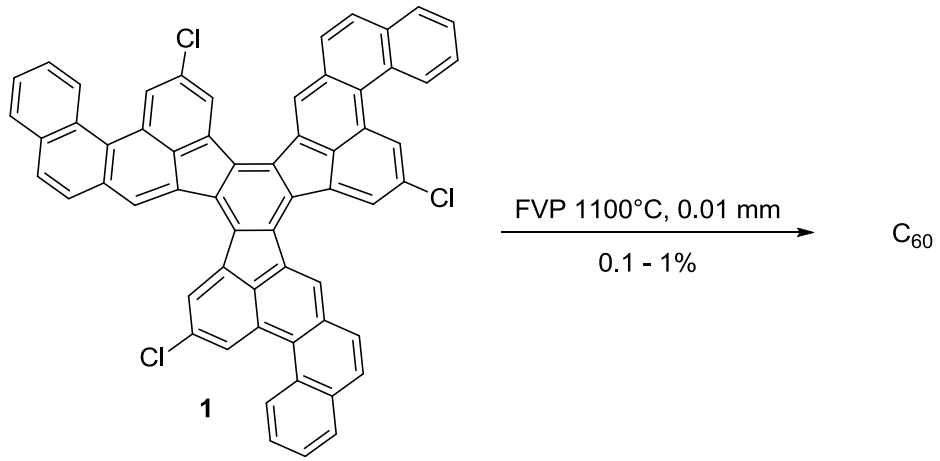

Scheme 1.1. Synthesis of C_{60} by Scott and coworkers from **1** by flash vacuum pyrolysis[50]

1.8 Polydiacetylenes

PDAs feature a highly conjugated all carbon π-system. This property makes PDAs an attractive starting material for carbon rich systems depending upon the choice of side-chain.

Accessing PDAs is challenging but work done by Fowler and Laugher has increased the accessibility of these compounds in recent years.[51] Fowler and Laugher devised the host/guest system in **Figure 1.17** to exploit hydrogen bonding to favor ordered 1,4 polymerization of diynes. The purpose of host molecule **2** in **Figure 1.17** is to align the diacetylene monomers **3** in the ideal parameters for ordered 1,4-polymerization.[51] The ideal parameters were studied extensively by Wegner and Baughman (**Figure 1.18**).[50, 52] The hydrogen bonding of the oxalamide groups in the host maintain the ideal repeat distance *r* of 5.0 Å through hydrogen bonding with other oxalamide groups. Host molecules also impart a distance *d* of 3.5 Å between C1 and C4 of an adjacent monomer. A host / guest system that satisfies these parameters can undergo a controlled polymerization to form a PDA. Before Fowler and Lauher's pioneering host/guest chemistry, it was necessary to align diyne monomers by other means. One such means typically involves the use of an alkyl tether with an amide group covalently bonded to one terminus of the diyne.[53] This system would afford an asymmetric diyne, which can be challenging to synthesize. Some monomers such as 1,6-bis(4-methylbenzenesulfonate)-2,4-hexadiyne-1,6-diol align according to the ideal parameters spontaneously.[52c] This monomer gives the PTS polymer in **Figure 1.10**. If the monomers do not align automatically it is necessary to incorporate an aligning group, which require additional synthetic work. The aligning group is typically one capable of intermolecular bonding such as hydrogen bonding.

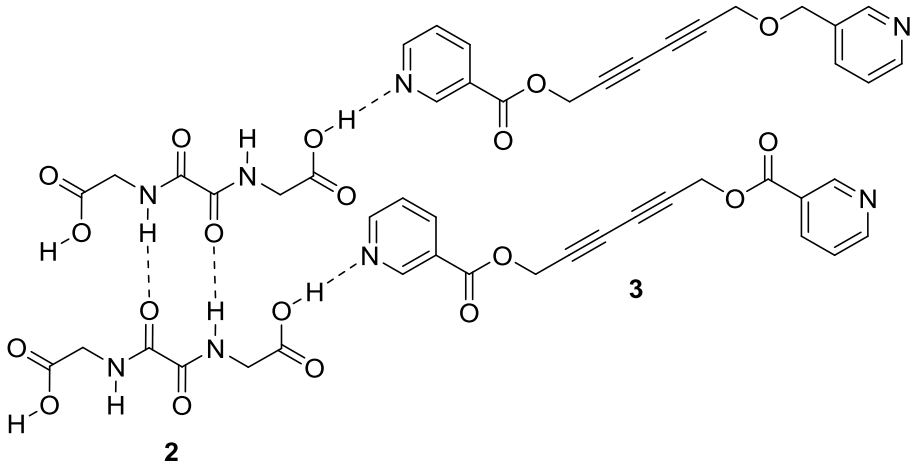

Figure 1.17. One of the first host / guest systems developed by Fowler and Lauher based on hydrogen bonding[51]

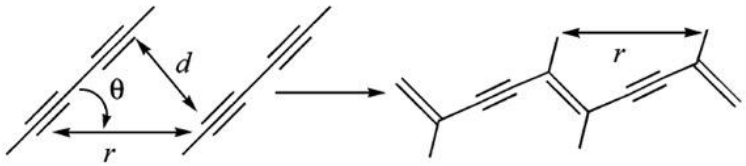

Optimal values for 1,4-polymerization are $r = 4.9–5.0$ Å, $\theta = 45°$, and $d = 3.5$ Å.

Figure 1.18. Ideal values for ordered 1,4-topochemical polymerization. Reprinted with permission from Ref. 54. Copyright (2008) American Chemical Society.

1.9 Carbon Rich Materials from Poly(diiododiacetylene)

In 2006 Sun, Lauher, and Goroff prepared the simplest PDA known featuring only iodine atoms as side groups.[55] This PDA, called poly(diiododiacetylene) (PIDA), is presented in **Figure 1.19** below. PIDA was prepared via topochemical polymerization using a host/guest strategy optimized for a halogen bond interaction.[55-56] The rationale behind selecting iodine as a side group is that it is a good Lewis acid when bonded to a sp carbon.[56] As a result the Lewis acidic iodine group will form a weak intermolecular interaction with a Lewis base. This type of interaction is often referred to as a halogen bond. Sun, Lauher, and Goroff used the halogen bond interaction as a means to allow host compound **4** to properly align diiodobutadiyne **5** (**Figure 1.20**). Once cocrystallization of **4** and **5** is complete, the system can undergo spontaneous controlled 1,4-polymerization in the solid state. The result is a cocrystallized PIDA system and shown in **Figure 1.21** below.

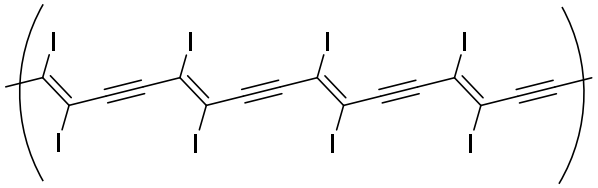

Figure 1.19. Molecular structure of poly(diiododiacetylene) (PIDA)

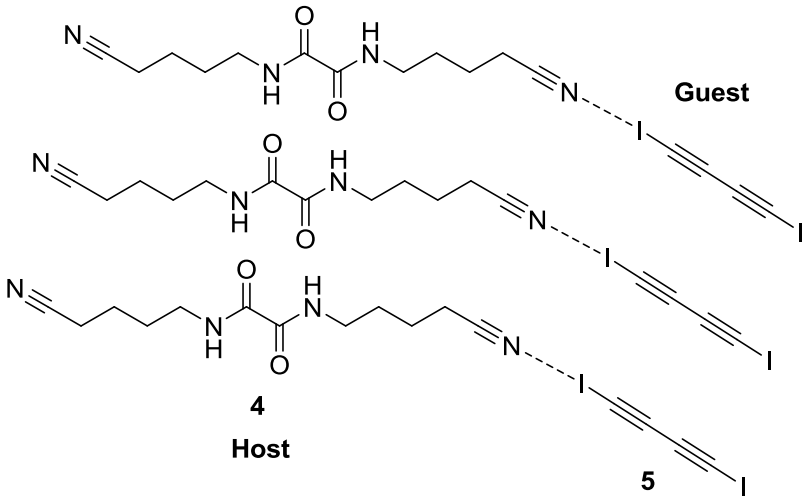

Figure 1.20. Schematic representation of halogen bonding between Lewis acid iodine and Lewis basic nitrile in a host/guest system

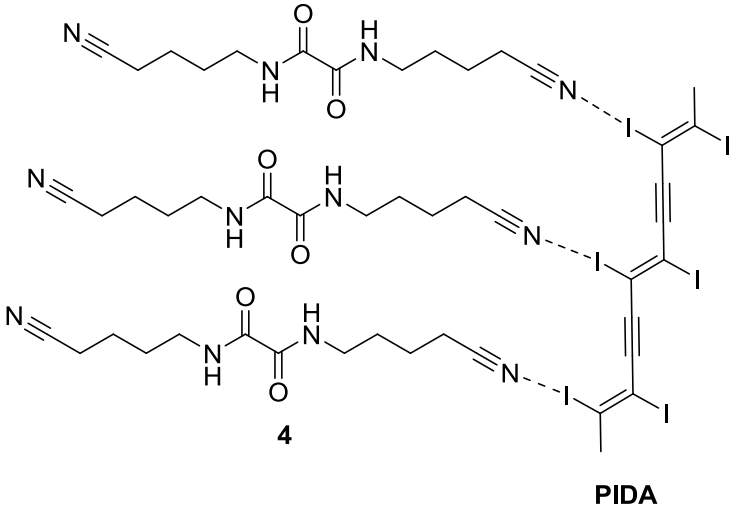

Figure 1.21. Molecular structure of PIDA cocrystal

In 2008, the Goroff group reported a more detailed study of PIDA including better optical microscope images and X-ray crystal structure confirmation.[57] New host molecules containing longer methylene chains were also synthesized and used to favor topochemical polymerization.

The same work also reports the isolation of PIDA from the cocrystal system alongside aggregation studies for isolated PIDA.[57] **Figure 1.22** below shows the optical microscopy and X-ray crystal structure data of the cocrystal system in **Figure 1.21**. With the successful isolation of PIDA, Luo studied the chemistry of the isolated polymer.[58] Luo had intentions to perform well-known coupling chemistry on the isolated PIDA but poor solubility hampered such work. Isolated PIDA forms aggregates in solution, which makes carrying out standard organic chemistry reactions such as the Sonogashira coupling difficult.[58] **Figure 1.23** below shows isolated PIDA aggregating in THF. In an attempt to make a homogenous solution of isolated PIDA, Luo tried to exploit the halogen bonding interaction to enhance the solubility. Lewis basic pyrrolidine was added to methanol in an effort to exploit the halogen bonding interaction with the Lewis acidic iodine groups in PIDA.[58]

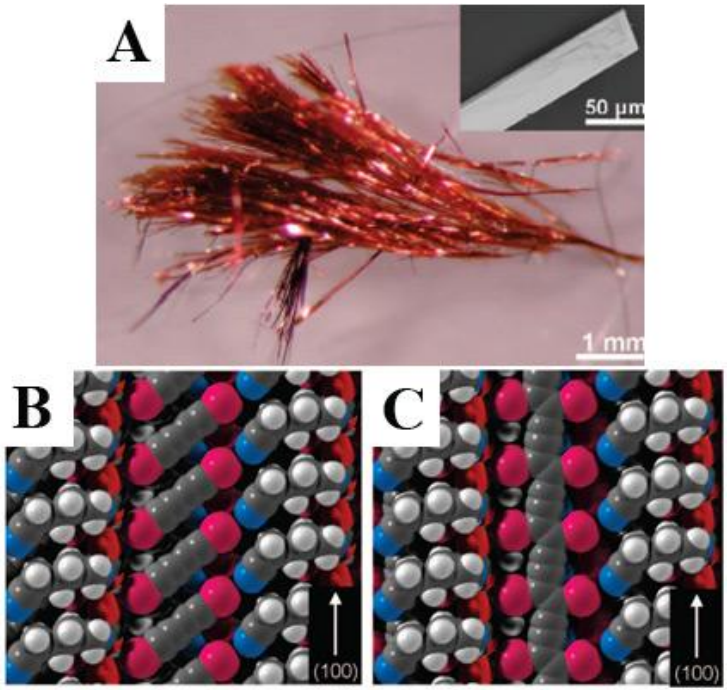

Figure 1.22. A) Optical microscope image of Host **4c** with PIDA; B) Crystal structure of Host **4c** with diiodobutadiyne **5**; C) Crystal structure of PIDA cocrystal. Reprinted with permission from Ref. 57. Copyright (2008) American Chemical Society.

Figure 1.23. Optical image of isolated PIDA aggregates in THF. Reprinted with permission from Ref. 57. Copyright (2008) American Chemical Society.

Unexpectedly, isolated PIDA was found to react with pyrrolidine.[58] The reaction was observed via UV-vis spectroscopy by Luo in **Figure 1.26** below. The reaction between isolated PIDA and pyrrolidine also gives rise to a visible color change as indicated in **Figure 1.25**. Luo studied the scope of this reaction and found that other Lewis bases such as pyridine and triethylamine also do the reaction albeit more slowly.[58] Further experiments done by Luo indicated that iodine is formed during the reaction. The observation of iodine formation was confirmed by analyzing the solutions with UV-vis spectroscopy. These experiments were conducted by adding $Na_2S_2O_3$ which reduces I_2 to I^-. I_2 can be seen in the visible spectrum but I^- cannot.[58] The disappearance of I_2 from the spectrum after addition of $Na_2S_2O_3$ indicated molecular iodine was present then reduced.[58] Further evidence for iodine elimination was obtained from pyrolysis studies by Luo and reported in 2011.[59] **Figure 1.26** below shows the TGA weight loss for isolated PIDA. The results of the TGA experiment (**Figure 1.26)** show about an 82% loss in weight. This weight loss corresponds closely to the 84% mass percent of iodine in isolated PIDA. Given the weak nature of C-I bonds it is not surprising iodine was eliminated under pyrolysis conditions.

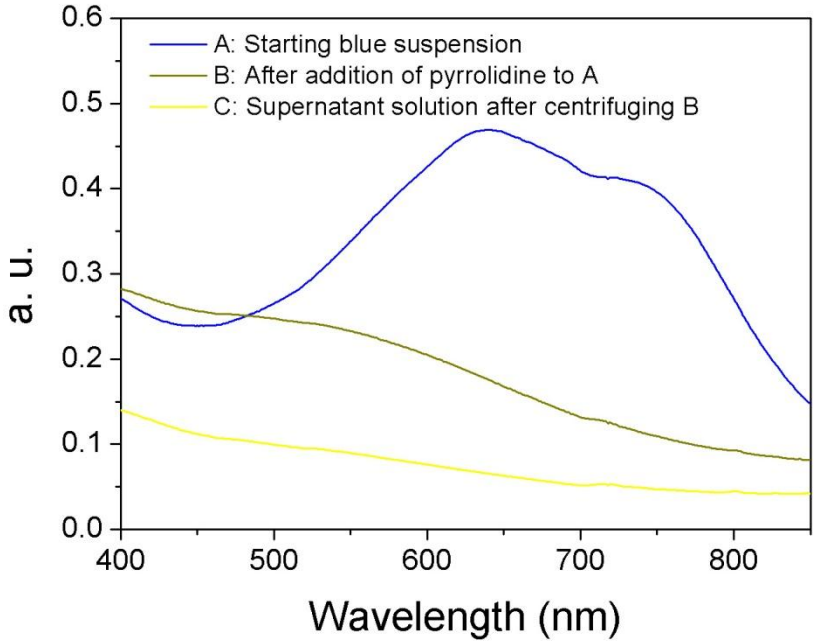

Figure 1.24. UV-vis spectra showing reaction between isolated PIDA and pyrrolidine. Reprinted with permission from Ref. 60. Copyright (2011) American Chemical Society.

Figure 1.25.[58] Before and after addition of pyrrolidine in methanol to isolated PIDA suspension. Reprinted with permission from Ref. 58. Copyright (2009) Liang Luo.

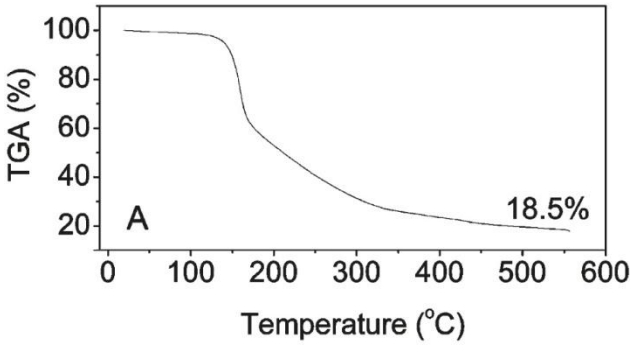

Figure 1.26. TGA of isolated PIDA showing weight loss corresponding to iodine. Reprinted with permission from Ref. 59. Copyright (2011) American Chemical Society.

Since PIDA is comprised of only carbon and iodine atoms it is expected that the product obtained from the elimination of iodine is carbon-rich. Luo attempted to characterize the product of pyrolysis but fine structural information was not obtained. **Figure 1.27** below shows the

polarized Raman spectra of the pyrolized samples.[59] The polarized Raman spectrum shows that the product contains sp^2-hybridized carbon, but lacks an ordered structure. Characterizing this sample further is challenging due to the limitation of NMR analysis and X-ray crystallography. ^{13}C-NMR MAS analysis would be difficult because the material lacks protons for relaxation. One would need to use long relaxation delays, which affects the quality and amount of data collected. If the material is a conductor as expected, eddy currents can make the sample difficult to spin.[58] The lack of order in the pyrolized product makes single crystal X-ray crystallography infeasible.

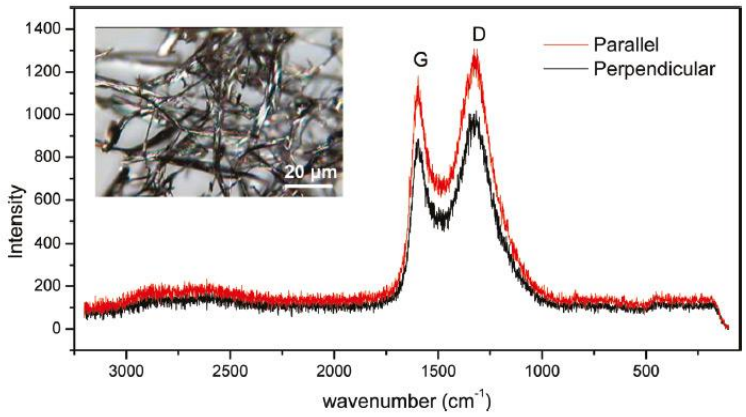

Figure 1.27. Polarized Raman spectra showing sp^2-carbon. Reprinted with permission from Ref. 59. Copyright (2011) American Chemical Society.

Despite the success of deiodinating PIDA by pyrolosis, the conditions are harsh and do not allow for controlled elimination. The Lewis base induced deiodination of PIDA, discovered by Luo, occurs under mild conditions and may serve as a means to accessing carbyne. If conditions can be found to completely deiodinate PIDA with a simple Lewis base like pyrrolidine, this would bring the polymer a step closer towards carbyne. Understanding the mechanism of Lewis base induced deiodination would allow for new conditions to be proposed for optimizing the reaction. The deiodination reaction can also be modeled on a small molecule system, to circumvent the difficulties of characterizing deiodinated PIDA. A small molecule

model would also allow for in depth understanding of the reaction scope as a means to apply the elimination chemistry elsewhere. The mild conditions warrant such an investigation especially if carbyne is to be accessed. The work presented in this thesis will focus on understanding the Lewis base-induced elimination reaction and increasing the reliability of the PIDA cocrystal synthetic protocol.

1.10 References

1. Kirk-Othmer, In *Encyclopedia of Chemical Technology*, John Wiley & Sons, Inc.: New York, 1985.
2. The DOE Bioethanol Pilot Plant: A Tool for Commercialization. http://www.nrel.gov/docs/fy00osti/28397.pdf (accessed April 25, 2011).
3. Kowarik, S.; Gerlach, A.; Schreiber, F., Organic molecular beam deposition: fundamentals, growth dynamics, and in situ studies. *J. Phys-Condens. Mat.* **2008,** *20*, 184005.
4. Inzelt, G.; Scholz, F., *Conducting Polymers: A New Era in Electrochemistry*. Springer: Leipzig, Germany, 2008.
5. Yakuphanoglu, F.; Basaran, E.; Şenkal, B. F.; Sezer, E., Electrical and Optical Properties of an Organic Semiconductor Based on Polyaniline Prepared by Emulsion Polymerization and Fabrication of Ag/Polyaniline/n-Si Schottky Diode. *J. Phys. Chem. B* **2006,** *110*, 16908-16913.
6. Klauk, H., *Organic Electronics*. 1st ed.; Wiley VCH Verlag GmbH & Co.: Strauss GmbH, Morlenbach, 2006.
7. McGinnes.J; Corry, P.; Proctor, P., Amorphous Semiconductor Switching in Melanins. *Science* **1974,** *183*, 853-855.
8. (a) Reynolds, J. R.; Ruiz, J. P.; Child, A. D.; Nayak, K.; Marynick, D. S., Electrically conducting polymers containing alternating substituted phenylenes and bithiophene repeat units. *Macromolecules* **1991,** *24*, 678-687; (b) Eley, D. D., Phthalocyanines as Semiconductors. *Nature* **1948,** *162*, 819-819; (c) Chiang, C. K.; Fincher, C. R., Jr.; Park, Y. W.; Heeger, A. J.; Shirakawa, H.; Louis, E. J.; Gau, S. C.; MacDiarmid, A. G., Electrical Conductivity in Doped Polyacetylene. *Phys. Rev. Lett.* **1977,** *39*, 1098-1101; (d) Gundlach, D. J.; Lin, Y. Y.; Jackson, T. N.; Nelson, S. F.; Schlom, D. G., Pentacene organic thin-film transistors - Molecular ordering and mobility. *IEEE Electr. Device L.* **1997,** *18*, 87-89.
9. (a) Huheey, J. E. K., E.A.; Keiter, R.L.;, *Inorganic Chemistry: Principles of Structure and Reactivity*. 4th ed.; HarperCollins College Publishers: New York, NY, 1993; (b) Anslyn, E. V.; Dougherty, D. A., Electronic organic materials. In *Mordern Physical Organic Chemistry*, University Science Books: Sausalito, California, 2004; pp 1001-1046.
10. Huang, X.; Zhai, H. J.; Kiran, B.; Wang, L. S., Observation of d-orbital aromaticity. *Angew. Chem. Int. Ed.* **2005,** *44*, 7251-7254.
11. Brutting, W., *Physics of Organic Semiconductors*. 1st ed.; Wiley-VCH Verlag GmbH &Co. LGaA: Strauss GmbH, Morlenbach, 2005.
12. Odonnell, K. P.; Chen, X., Temperature-Dependence of Semiconductor Band-Gaps. *Appl. Phys. Lett.* **1991,** *58*, 2924-2926.
13. Podesta, M. d., *Understanding the Properties of Matter*. 2nd ed.; Taylor and Francis Inc.: New York, NY, 2002.
14. Kahn, A.; Koch, N.; Gao, W., Electronic structure and electrical properties of interfaces between metals and π-conjugated molecular films. *J. Polym. Sci. Pol. Phys.* **2003,** *41*, 2529-2548.
15. Birendra, T. S.; Sariciftci, N. S., Progress in Plastic Electronics Devices. *Annu. Rev. Mater. Res.* **2006,** *36*, 199–230.
16. Dutta, A. K., Electrical Conductivity of Single Crystals of Graphite. *Phys. Rev.* **1953,** *90*, 187.
17. IUPAC. Compendium of Chemical Terminology, 2nd ed. (the "Gold Book"). Compiled by A. D. McNaught and A. Wilkinson. Blackwell Scientific Publications, Oxford (1997). XML

on-line corrected version: http://goldbook.iupac.org (2006-) created by M. Nic, J. Jirat, B. Kosata; updates compiled by A. Jenkins. ISBN 0-9678550-9-8. doi:10.1351/goldbook.
18. Amano, Y.; Cheng, Q., Detection of influenza virus: traditional approaches and development of biosensors. *Anal Bioanal Chem* **2005,** *381*, 156-164.
19. (a) Reichert, A.; Nagy, J. O.; Spevak, W.; Charych, D., Polydiacetylene Liposomes Functionalized with Sialic Acid Bind and Colorimetrically Detect Influenza Virus. *J. Am. Chem. Soc.* **1995,** *117*, 829-830; (b) Charych, D. H.; Nagy, J. O.; Spevak, W.; Bednarski, M. D., Direct colorimetric detection of a receptor-ligand interaction by a polymerized bilayer assembly. *Science* **1993,** *261*, 585-588.
20. Filhol, J.-S. b.; Deschamps, J. r. m.; Dutremez, S. G.; Boury, B.; Barisien, T.; Legrand, L.; Schott, M., Polymorphs and Colors of Polydiacetylenes: A First Principles Study. *J. Am. Chem. Soc.* **2009,** *131*, 6976-6988.
21. Boyd, R. W., *Nonlinear Optics (Third Edition)*. 3rd ed.; Elsevier Inc.: Burlington, MA, 2008.
22. Franken, P. A.; Weinreich, G.; Peters, C. W.; Hill, A. E., Generation of Optical Harmonics. *Phys. Rev. Lett.* **1961,** *7*, 118-119.
23. (a) Greene, B. I.; Mueller, J. F.; Orenstein, J.; Rapkine, D. H.; Schmittrink, S.; Thakur, M., Phonon-Mediated Optical Nonlinearity in Polydiacetylene. *Phys. Rev. Lett.* **1988,** *61*, 325-328; (b) Bolger, J.; Harvey, T. G.; Ji, W.; Kar, A. K.; Molyneux, S.; Wherrett, B. S.; Bloor, D.; Norman, P., Near-resonant third-order optical nonlinearities in p-toluene sulfonate polydiacetylene. *J. Opt. Soc. Am. B* **1992,** *9*, 1552-1557; (c) Yoshino, F.; Polyakov, S.; Stegeman, G. I., All-optical multiphoton absorption figures of merit: Polydiacetylene poly (bis para-toluene sulfonate) of 2,4-hexadiyne-1,6 diol. *Appl. Phys. Lett.* **2004,** *84*, 5362-5364.
24. Thakur, M.; Meyler, S., Growth of large-area thin-film single crystals of poly(diacetylenes). *Macromolecules* **1985,** *18*, 2341-2344.
25. Polyakov, S.; Yoshino, F.; Liu, M.; Stegeman, G. In *Effects of self-focusing on multiphoton absorption processes in polymer bis-paratoluene sulfonate (PTS)*, Quantum Electronics and Laser Science Conference, 2000. (QELS 2000). Technical Digest, 12-12 May 2000; 2000; pp 169-170.
26. (a) Abdeldayem, H.; Frazier, D. O.; Paley, M. S., An all-optical picosecond switch in polydiacetylene. *App. Phys. Lett.* **2003,** *82*, 1120-1122; (b) Paley, M. S.; Frazier, D. O.; Abdeldayem, H.; McManus, S. P., Photodeposition of Thin Polydiacetylene Films from Solution That Exhibit Large Third-Order Optical Nonlinearities. *Chem. Mater.* **1994,** *6*, 2213-2215.
27. Hossin Abdeldayem; Donald. O. Frazier; Mark S. Paley; Witherow, W. K. Now, Just A Blinkin' Picosecond! http://science.nasa.gov/headlines/y2000/ast28apr_1m.htm (accessed August 12, 2013).
28. (a) Green, P. E., *Fiber Optic Networks*. Prentice Hall: Upper Saddle River, NJ, 1993; (b) Palais, J. C., *Fiber Optic Communications*. 4th ed.; Prentice Hall: Upper Saddle River, NJ, 1998.
29. Bosch, M.; Fischer, C.; Linkatas, I.; Bosshard, C.; Gunter, P. In *Photochemical stability of highly nonlinear optical chromophores for electro-optic applications*, Lasers and Electro-Optics Europe, 2000. Conference Digest., 10-15 Sep 2000.
30. Charlier, J. C.; Gonze, X.; Michenaud, J.-P., Graphite Interplanar Bonding: Electronic Delocalization and van der Waals Interaction. *Europhys. Lett.* **1994,** *28*, 403.
31. Boehm, H. P.; Clauss, A.; Fischer, G. O.; Hofmann, U., Das Adsorptionsverhalten sehr dünner Kohlenstoff-Folien. *Z. Anorg. Allg. Chem.* **1962,** *316*, 119-127.

32. Novoselov, K. S.; Geim, A. K.; Morozov, S. V.; Jiang, D.; Zhang, Y.; Dubonos, S. V.; Grigorieva, I. V.; Firsov, A. A., Electric field effect in atomically thin carbon films. *Science* **2004,** *306*, 666-669.
33. (a) Geim, A. K., Graphene: Status and Prospects. *Science* **2009,** *324*, 1530-1534; (b) Geim, A. K.; Novoselov, K. S., The rise of graphene. *Nat Mater* **2007,** *6*, 183-191.
34. Lin, Y. M.; Dimitrakopoulos, C.; Jenkins, K. A.; Farmer, D. B.; Chiu, H. Y.; Grill, A.; Avouris, P., 100-GHz Transistors from Wafer-Scale Epitaxial Graphene. *Science* **2010,** *327*, 662-662.
35. Ryu, S.; Han, M. Y.; Maultzsch, J.; Heinz, T. F.; Kim, P.; Steigerwald, M. L.; Brus, L. E., Reversible Basal Plane Hydrogenation of Graphene. *Nano Lett.* **2008,** *8*, 4597-4602.
36. Du, A.; Zhu, Z.; Smith, S. C., Multifunctional Porous Graphene for Nanoelectronics and Hydrogen Storage: New Properties Revealed by First Principle Calculations. *J. Am. Chem. Soc.* **2010,** *132*, 2876-2877.
37. Langa, F.; Nierengarten, J.-F., *Fullerenes: Principles and Applications*. The Royal Society of Chemistry: Cambridge CB4 0WF, UK, 2007.
38. Pan, H.; Li, J.; Feng, Y., Carbon Nanotubes for Supercapacitor. *Nanoscale Res. Lett.* **2010,** *5*, 654 - 668.
39. Aliev, A.; Gartstein, Y.; Baughman, R. H., Mirage effect from thermally modulated transparent carbon nanotube sheets. *Nanotechnology* **2011,** *43*, 435704.
40. Kaempgen, M.; Lebert, M.; Nicoloso, N.; Roth, S., Multifunctional carbon nanotube networks for fuel cells *Appl. Phys. Lett.* **2008,** *92*, 094103.
41. Lagow, R. J.; Kampa, J. J.; Wei, H. C.; Battle, S. L.; Genge, J. W.; Laude, D. A.; Harper, C. J.; Bau, R.; Stevens, R. C.; Haw, J. F.; Munson, E., Synthesis of Linear Acetylenic Carbon - The sp Carbon Allotrope. *Science* **1995,** *267*, 362-367.
42. Casari, C. S.; Li Bassi, A.; Ravagnan, L.; Siviero, F.; Lenardi, C.; Piseri, P.; Bongiorno, G.; Bottani, C. E.; Milani, P., Chemical and thermal stability of carbyne-like structures in cluster-assembled carbon films. *Phys. Rev. B* **2004,** *69*, 075422.
43. Hummers, W. S.; Offeman, R. E., Preparation of Graphitic Oxide. *J. Am. Chem. Soc.* **1958,** *80*, 1339-1339.
44. Marcano, D. C.; Kosynkin, D. V.; Berlin, J. M.; Sinitskii, A.; Sun, Z.; Slesarev, A.; Alemany, L. B.; Lu, W.; Tour, J. M., Improved Synthesis of Graphene Oxide. *ACS Nano* **2010,** *4*, 4806-4814.
45. Gao, W.; Alemany, L. B.; Ci, L.; Ajayan, P. M., New insights into the structure and reduction of graphite oxide. *Nat. Chem.* **2009,** *1*, 403-408.
46. Ismach, A.; Druzgalski, C.; Penwell, S.; Schwartzberg, A.; Zheng, M.; Javey, A.; Bokor, J.; Zhang, Y., Direct Chemical Vapor Deposition of Graphene on Dielectric Surfaces. *Nano Lett.* **2010,** *10*, 1542-1548.
47. Iijima, S., Helical Microtubules of Graphitic Carbon. *Nature* **1991,** *354*, 56-58.
48. Guo, T.; Nikolaev, P.; Rinzler, A. G.; Tomanek, D.; Colbert, D. T.; Smalley, R. E., Self-Assembly of Tubular Fullerenes. *J. Phys. Chem.* **1995,** *99*, 10694-10697.
49. Joseyacaman, M.; Mikiyoshida, M.; Rendon, L.; Santiesteban, J. G., Catalytic Growth of Carbon Microtubules with Fullerene Structure. *Appl. Phys. Lett.* **1993,** *62*, 657-659.
50. Scott, L. T.; Boorum, M. M.; McMahon, B. J.; Hagen, S.; Mack, J.; Blank, J.; Wegner, H.; de Meijere, A., A rational chemical synthesis of C-60. *Science* **2002,** *295*, 1500-1503.
51. Fowler, F. W.; Lauher, J. W., A rational design of molecular materials. *J. Phys. Org. Chem.* **2000,** *13*, 850-857.

52. (a) Baughman, R. H., Solid-State Synthesis of Large Polymer Single Crystals. *J. Polym. Sci., Part B: Polym. Phys.* **1974,** *12*, 1511-1535; (b) Wegner, G., Topochemical polymerization of monomers with conjugated triple bonds. *Macromol. Chem. Phys.* **1972,** *154*, 35-48; (c) Wegner, G., Topochemical reactions of monomers with conjugated triple-bonds. IV. Polymerization of bis-(p-toluene sulfonate) of 2.4-hexadiin-1.6-diol. *Macromol. Chem. Phys.* **1971,** *145*, 85-94.
53. (a) Kim, J.-M.; Lee, Y. B.; Yang, D. H.; Lee, J.-S.; Lee, G. S.; Ahn, D. J., A Polydiacetylene-Based Fluorescent Sensor Chip. *J. Am. Chem. Soc.* **2005,** *127*, 17580-17581; (b) Ahn, D. J.; Chae, E.-H.; Lee, G. S.; Shim, H.-Y.; Chang, T.-E.; Ahn, K.-D.; Kim, J.-M., Colorimetric Reversibility of Polydiacetylene Supramolecules Having Enhanced Hydrogen-Bonding under Thermal and pH Stimuli. *J. Am. Chem. Soc.* **2003,** *125*, 8976-8977; (c) Fujita, N.; Sakamoto, Y.; Shirakawa, M.; Ojima, M.; Fujii, A.; Ozaki, M.; Shinkai, S., Polydiacetylene Nanofibers Created in Low-Molecular-Weight Gels by Post Modification: Control of Blue and Red Phases by the Odd−Even Effect in Alkyl Chains. *J. Am. Chem. Soc.* **2007,** *129*, 4134-4135.
54. Wilhelm, C.; Boyd, S. A.; Chawda, S.; Fowler, F. W.; Goroff, N. S.; Halada, G. P.; Grey, C. P.; Lauher, J. W.; Luo, L.; Martin, C. D.; Parise, J. B.; Tarabrella, C.; Webb, J. A., Pressure-Induced Polymerization of Diiodobutadiyne in Assembled Cocrystals. *J. Am. Chem. Soc.* **2008,** *130*, 4415-4420.
55. (a) Sun, A. W.; Lauher, J. W.; Goroff, N. S., Preparation of poly(diiododiacetylene), an ordered conjugated polymer of carbon and iodine. *Science* **2006,** *312*, 1030-1034; (b) Lauher, J. W.; Fowler, F. W.; Goroff, N. S., Single-Crystal-to-Single-Crystal Topochemical Polymerizations by Design. *Acc. Chem. Res.* **2008,** *41*, 1215-1229.
56. Goroff, N. S.; Curtis, S. M.; Webb, J. A.; Fowler, F. W.; Lauher, J. W., Designed Cocrystals Based on the Pyridine−Iodoalkyne Halogen Bond. *Org. Lett.* **2005,** *7*, 1891-1893.
57. Luo, L.; Wilhelm, C.; Sun, A.; Grey, C. P.; Lauher, J. W.; Goroff, N. S., Poly(diiododiacetylene): Preparation, Isolation, and Full Characterization of a Very Simple Poly(diacetylene). *J. Am. Chem. Soc.* **2008,** *130*, 7702-7709.
58. Luo, L. Preparation and Comprehensive Characterization of Poly(diiododiacetylene) and Spectroscopic Studies of Its Reactions with Lewis Bases. Stony Brook University, Stony Brook, NY, 2009.
59. Luo, L.; Wilhelm, C.; Young, C. N.; Grey, C. P.; Halada, G. P.; Xiao, K.; Ivanov, I. N.; Howe, J. Y.; Geohegan, D. B.; Goroff, N. S., Characterization and Carbonization of Highly Oriented Poly(diiododiacetylene) Nanofibers. *Macromolecules* **2011,** *44*, 2626-2631.
60. Luo, L.; Resch, D.; Wilhelm, C.; Young, C. N.; Halada, G. P.; Gambino, R. J.; Grey, C. P.; Goroff, N. S., Room-Temperature Carbonization of Poly(diiododiacetylene) by Reaction with Lewis Bases. *J. Am. Chem. Soc.* **2011,** *133*, 19274-19277.

Chapter 2: Poly(diiododiacetylene) – Preparation and Challenges

2.1 Introduction

The preparation of poly(diiododiacetylene) PIDA is an extremely sensitive process as there are numerous factors that contribute to cocrystal formation. Some of these factors include the stability of the diiodobutadiyne **5**, solubility of the host compound, presence of solid impurities, initial concentration, and evaporation rate. Compound **5** is prepared and stored in the dark as it is light-sensitive (**Scheme 2.1**). It is also important to prepare diiodobutadiyne **5** in quantities no greater than 1 g according to the standard operating procedures (SOPs). Since **5** is a shock explosive, working with it in small quantities is necessary for proper safety. It is also best to store **5** in solution in a freezer as to minimize decomposition and make for safer handling. Solutions of **5** that are older than 2 weeks should be discarded in the appropriate waste container. These precautions ensure both the integrity of the compound to maximize the yield of PIDA and adherence to proper safety guidelines.

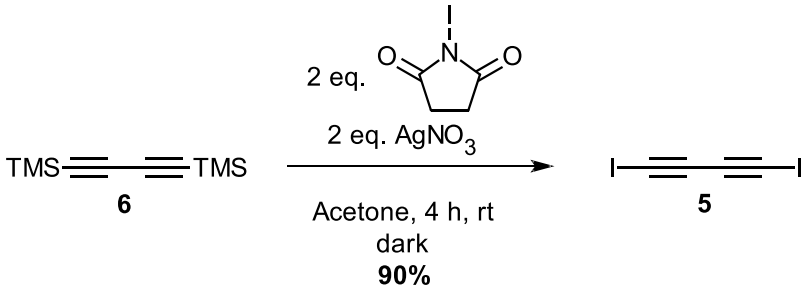

Scheme 2.1. Synthesis of diiodobutadiyne **5**

Host solubility is another critical parameter to consider when preparing PIDA cocrystals. The host molecules possess nitrile and an oxalamide groups which makes these compounds very polar (**Figure 2.1**). The hydrogen bond network between the oxalamide groups favors crystallization of the host molecules. Choosing an appropriate solvent based on the solubility of the host compounds is essential to prevent asynchronous crystallization. If the host compound and diiodobutadiyne **5** monomer do not precipitate at the same time, cocrystals will not form.

The Goroff group found that host **4a** has particularly poor solubility in organic solvents and precipitates without forming cocrystals.[1] Host **4b** is able to form cocrystals with **5** but polymerization does not occur as there is not enough flexibility to allow the monomer to conform to the geometrical requirements for ordered 1,4-polymerization.[1] Polymerized cocrystals were obtained with host **4c** and monomer **5** although reproducibility remained a challenge.[1]

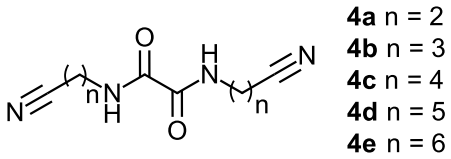

4a n = 2
4b n = 3
4c n = 4
4d n = 5
4e n = 6

Figure 2.1. Host compounds previously reported[1-2]

The Goroff group later reported the preparation of PIDA cocrystals using hosts **4d** and **4e** and demonstrated an improvement in the cocrystallization method.[2] Host **4d** afforded unpolymerized blue cocrystals in better yield than host **4c**. After heating, the blue **4d·5** cocrystal turned dark grey and polymerization was observed by ^{13}C-NMR MAS. Host **4e** was found to give the best results, as it was able to afford polymerized shiny-golden cocrystals in good yield at room temperature. One of the advantages of host **4e** is that the longer alkyl tether imparts more flexibility for meeting the geometric requirements of an ordered 1,4-polymerization. One modification in the cocrystallization that helped improve the yield was the use of centrifugation. Luo found that centrifugation could be used to remove any insoluble particles such as host that had not fully dissolved.[3] These undissolved particles can induce premature nucleation of host so it is desirable to remove them. Luo also explored the solubility of host **4c** in various solvents, but found that methanol was still the best for dissolving **4c**.

Another two factors that make cocrystal formation challenging are the initial concentration of diiodobutadiyne **5** and host and the solvent evaporation rate. These factors are

closely related as more concentrated solutions require less solvent and thus less time for evaporation. There is a balance though that must be achieved between solvent evaporation rate and concentration. If the cocrystal solution is too concentrated and takes too long to evaporate, decomposition of **5** is more likely. The decomposition of **5** will not give PIDA cocrystals. If the solvent evaporates too quickly however, the necessary halogen bond interaction between the host and **5** may not form. It is thus necessary to find the ideal concentration given the evaporation rate of any solvent.

Luo first made the long term observation that cocrystals grew in better yield in one laboratory environment over another. The exact variable that caused this varied rate of success remains unknown . Another long term observation, first made by Luo, showed that cocrystals appeared to grow in better yield during the summer months. One factor that could explain this seasonal dependency is humidity. During the summer months there is more humidity in the air. It could also be due to temperature however. In the summer months the laboratory is air conditioned which may affect crystal growth. The difficulties with the reproducibility of cocrystal formation in different laboratories and overall yield worsened. This prompted the further investigations discussed later in this chapter.

The characterization of PIDA cocrystals has its own challenges as well. Single crystal X-ray crystallography is one technique used for characterization both before and after polymerization. The crystal structure of **4c·5** has been reported by Goroff and coworkers both before and after polymerization.[1-2] Due to the mosaicity of the crystals of **4d·5** and **4e·5**, the crystal structures were not obtained. Raman spectroscopy can also be used to characterize PIDA cocrystals (**Figure 2.2**).[2]

The polydiacetylene (PDA) backbone has characteristic peaks at υ(C-C) 971 cm^{-1}, υ(C=C) 1415 cm^{-1}, and υ(C≡C) 2071 cm^{-1}. PDAs have a very strong Raman signal due to the highly polarizable nature of the backbone. This also means that small amounts of polymer can dwarf the other peaks in the spectrum.

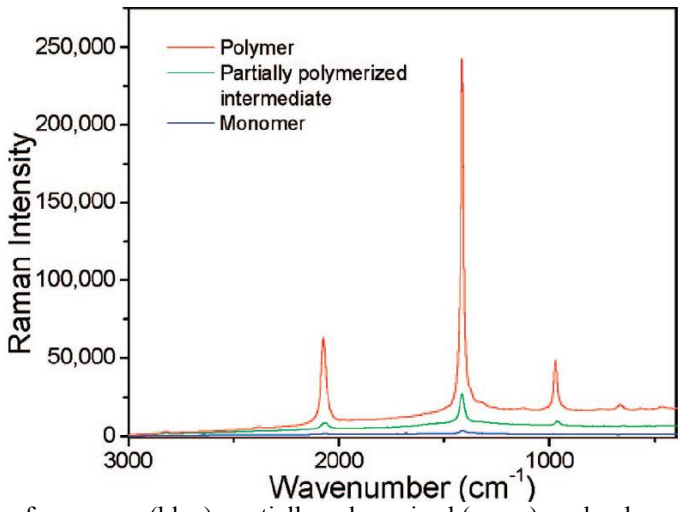

Figure 2.2. Raman spectra of monomer (blue), partially polymerized (green), and polymer (red) cocrystal **4c·5**. Reprinted with permission from Ref. 2. Copyright (2008) American Chemical Society.

^{13}C-NMR MAS gives a better measure of the amount of polymer in the sample, (**Figure 2.3**) as it is possible to obtain quantitative data on the degree of polymerization.[2] The results of ^{13}C-NMR MAS showed exclusively polymerized **4c·5**.[2] Although ^{13}C-NMR MAS is a good method for characterizing both the cocrystals before and after polymerization, it does have drawbacks. This technique requires an appreciable amount of material and poor signal to noise can make integration difficult.

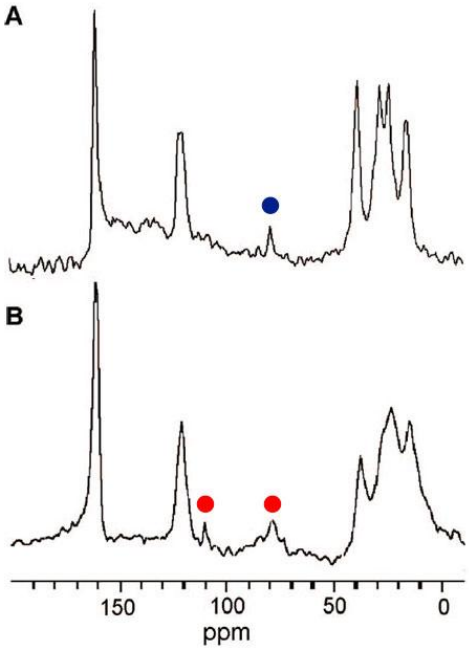

Figure 2.3. ^{13}C-NMR MAS showing A) monomer peak (blue dot) of **4c·5** and B) polymer peaks (red dots) of **4c·5**. Reprinted with permission from Ref. 2. Copyright (2008) American Chemical Society.

2.2 Scaling Up Synthesis of Host 4e

One of the first efforts to improve the cocrystallization method involved large scale synthesis of host **4e**. This host gave the best results for preparing PIDA cocrystals in terms of yield and ability to polymerize spontaneously at room temperature. Having a large supply of host would enable rapid screening of cocrystallization conditions since the synthesis of **4e** requires multiple time consuming steps. The traditional synthesis of **4e**, as reported by the Goroff group, continued to be employed at first in the work reported here (**Scheme 2.2**).[2] The conversion of bromide **7** to azide **8** was also found to work well at a scale of 5 g of starting material **7**. Vaccaro and coworkers[4] published a reaction for converting azides to amines using an in situ generated cobalt boride species as the reducing agent, and Liang Luo and coworkers successfully prepared **9** using their conditions on a 1 g scale. However, when the conversion of azide **8** to amine **9** was carried out on a 5 g scale, an appreciable amount of heat was generated. For safety reasons, this

reaction was never repeated. The ^{1}H-NMR spectra of the product of this reaction contained numerous unidentifiable peaks that overlapped with product peaks.

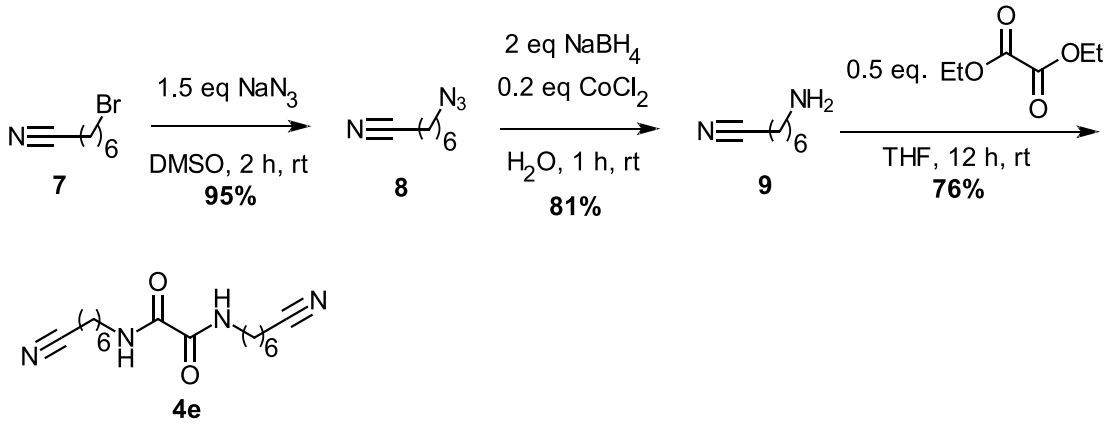

Scheme 2.2. Synthesis of host **4e** at a scale of less than 1 g of **7**

Ganem and coworkers reported the cobalt(II)-$NaBH_4$ catalyzed reduction of aromatic nitriles and cobalt(II)-$LiAlH_4$ catalyzed reduction of alkyl nitriles is highly exothermic at room temperature.[5] It is possible that the heat generated from the large scale reduction of azide **8** enabled the Co_2B species to reduce the nitrile group in addition to the azide group, which afforded a mixture of products. For this reason, the cobalt(II) catalyzed reduction of **8** was replaced with the Staudinger azide reduction (**Scheme 2.3**). It is essential to properly vent the reaction vessel when performing the Staudinger azide reduction as nitrogen gas is slowly generated from the reaction mixture.

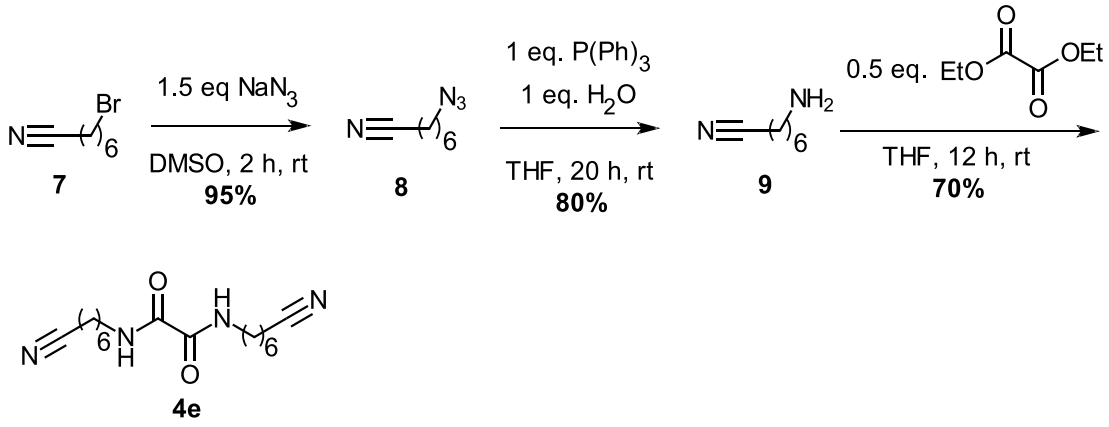

Scheme 2.3. Large scale preparation of **4e** using 5 g of starting material **7**

2.3 Improving the Cocrystallization Method

In order to improve the cocrystallization method it is necessary to understand the failed experiments. When a cocrystallization experiment fails, an off white solid or mixed shiny-golden / white solid (**Figure 2.4**) is obtained. The golden fibers in **Figure 2.4** are the polymerized cocrystals of **4e·5**. In general, when a cocrystallization experiment fails, the result is almost always as is seen on the right in **Figure 2.4**. On several occasions however, the result as seen on the left in **Figure 2.4** was observed. The white solid melted at 94-98°C after which a color change to black is observed indicating decomposition. This data suggests the white solid is host **4e** (m.p. 98-99°C[3]) with at least trace amounts of diiodobutadiyne **5** present. The off-white solid decomposed immediately between 94-98°C. The decomposition temperatures of both the white and off-white solids indicate diiodobutadiyne **5** is present after solvent evaporation. This result shows that either host **4e** or diiodobutadine **5** precipitates out of solution before cocrystal formation. Given the relative solubility of **4e** and **5** in methanol host **4e** is first to precipitate.

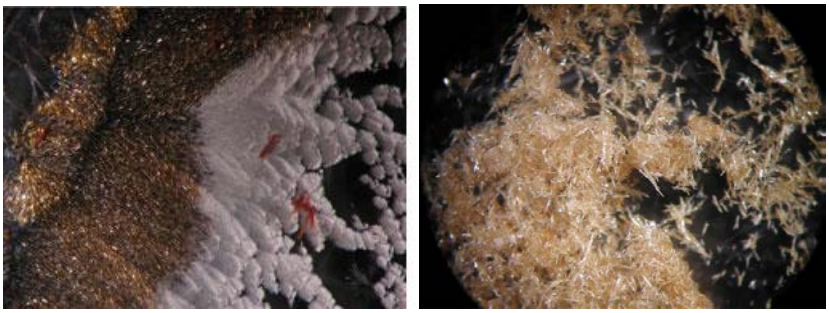

Figure 2.4. Left: Mixed **4e·5** cocrystal product with host **4e**; Right: Diiodobutadiyne **5** deposited on host **4e** without any cocrystal formation

Early precipitation can be attributed to temperature-induced change in solubility or nucleation caused by solid impurities in the solution. One potential impurity is host that did not completely dissolve. Luo removed this impurity from the host / guest solution in methanol by centrifugation at 2500 RPM prior to transferring it to a crystallization dish.[3] This technique was found to give an increase in the yield of PIDA cocrystals. In an attempt to further increase the yield and reliability of PIDA cocrystal formation, the host-monomer solutions were subjected to

centrifugation at 3000 RPM. The solution was then carefully decanted into a crystallization dish as Luo had done. This value of 3000 RPM corresponds to full power on the centrifuge whereas Luo's method used ¾ power. An off-white solid without any PIDA cocrystal formation resulted from the solution spun at 3000 RPM. In a different experiment, the host-monomer solution was subjected to centrifugation for 30 minutes at 3000 RPM as opposed to 10 minutes, but the off-white solid was still the only product. These centrifugation experiments suggest solid impurities are not likely to be the cause of failed cocrystallization.

The role of moisture in the air was taken into consideration because cocrystal formation appeared to be more reliable in the summer months. During this time, the air is more humid. Methanol is miscible with water and can absorb water from the atmosphere over time. Host **4e** is not soluble in water so it is possible for it to have reduced solubility in wet methanol. The affect of humidity was studied using 2 different environmental enclosures to control the available moisture. The results of the humidity study showed that both Setup A and B in **Figure 2.5** afforded PIDA cocrystals. Further trials also showed that the familiar off-white solid was obtained on occasion as had been observed when a humidity chamber is not used. This experiment showed that a moisture-saturated system did not have a drastic or detrimental effect on cocrystal formation.

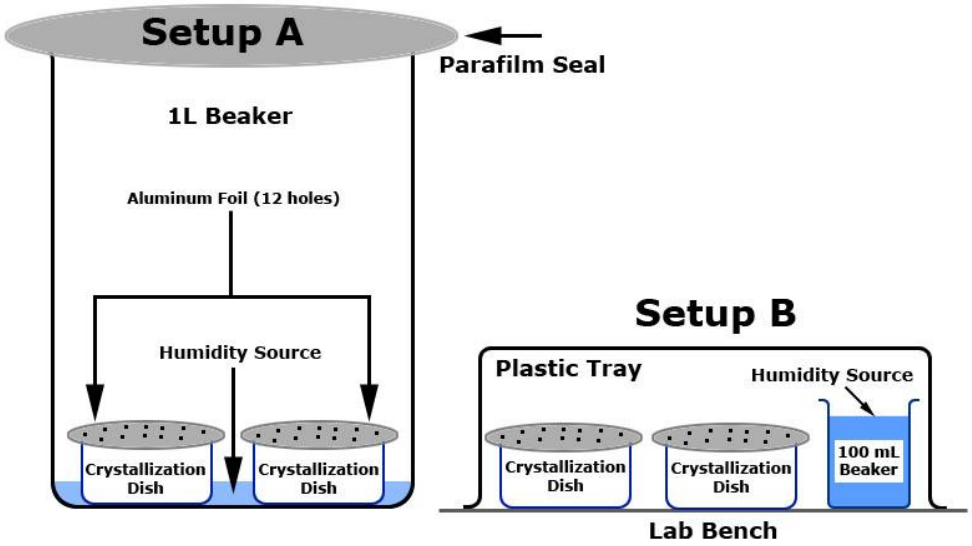

Figure 2.5. Humidity chamber block diagrams

Another variable that was probed for having an effect on the cocrystallization is temperature. The laboratory temperature was measured at the beginning and end of each cocrystallization experiment. The results were pooled for about 1 month and can be seen in **Table 2.1.** The results in **Table 2.1** show there is little fluctuation in the laboratory temperature. Experiments 12-14 failed in a cluster though the laboratory temperature for those days did not differ significantly from the days when the experiments were successful. Cocrystallizaton experiments were also attempted at temperatures of 30°C and 40°C. These experiments were conducted such that each crystallization dish was put in an oil bath of the appropriate temperature and another 2 were left on the benchtop as a control. The dishes in the oil baths had tiny bits of golden PIDA cocrystals but the yield was too small to obtain an accurate mass. The dishes on the benchtop had fibrous golden PIDA cocrystals in 8% yield as commonly found in **Table 2.1**.

Table 2.1. Cocrystallization and Laboratory Temperature[a]

Exp #	Date	Start Temp	Final Temp	Yield (%)
1	14-Feb	21	23	8
2	16-Feb	22	24	5
3	18-Feb	22	21	7
4	21-Feb	23	21	7
5	23-Feb	23	22	5
6	25-Feb	22	23	5
7	28-Feb	24	22	8
8	2-Mar	22	21	7
9	4-Mar	23	22	3
10	6-Mar	23	21	5
11	8-Mar	22	23	10
12	11-Mar	22	22	0
13	15-Mar	23	21	0
14	18-Mar	22	21	0
15	21-Mar	22	24	8

a) Temperature profile of 15 cococrystal experiments

Another factor that was given consideration in the preparation of PIDA cocrystals was the material of the crystallizing dish. Glass crystallization dishes are typically used for growing crystals and have a hydrophilic surface. The hydrophilic nature of glass often leads to the solvent being drawn up onto the walls of the dish as methanol is protic and can interact with the glass surface. PIDA cocrystals are thus often formed on the walls of the crystallization dish. Cleaning the glass dishes is also problematic depending on the nature of the cleaning solution. Base bath, which is typically used to clean the crystallization dishes, etches the glass surface. The etching of glass can affect nucleation if the surface is not uniform.

Given the drawbacks of using a glass recrystallizing dish, Teflon was considered as an alternative material. Teflon is non-polar and will not draw the polar solvent up onto the walls. It also has a low friction coefficient making it easy to remove any material from its surface. After subjecting the host **4e** / monomer **5** solution to centrifugation, the mixture was transferred to several different Teflon beaker liners placed inside a glass crystallization dish for structural

support. The Teflon beaker liners (7.5 mil and 10 mil in thickness) are flimsy and require a solid container to prevent accidental spillage. Both the 7.5 mil and 10 mil beaker liners were purchased in sizes of 100 mL and 50 mL. The crystallization experiments in Teflon liners did not show any visual improvement in crystal quality. As expected, the crystals were much easier to remove from the dish and did not require scraping or a wash with methanol to retrieve from the dish. For Teflon beaker liners of both thicknesses, the 50 mL liner afforded similar results to the glass crystallization dish but the 100 mL liner did not contain any PIDA cocrystals. This is most likely due to an uneven distribution of solvent in the 100 mL liner. The glass crystallization dishes are about the same diameter of the 50 mL Teflon liners.

Reproducibility of the cocrystallization experiments continued to be an issue until finally, the standard method originally developed by Luo[3] no longer produced PIDA cocrystals at all. In several successive experiments the only product obtained was the off-white solid that decomposed at 94°C. One important factor that had not been initially considered for the cocrystallization experiments involving host **4e** with **5** is solvent. Luo optimized the system for host **4c** but not host **4e**. Solvent plays a critical role in crystal formation as solubility of the host and guest directly influence cocrystallization. The solvent dependency of the cocrystallization process was probed with dry acetonitrile, regular acetonitrile, acetone, dimethoxyethane, and THF. Dimethoxyethane took 3-4 days to evaporate and afforded a yellow film. Acetone evaporated in less than a day but resulted in the characteristic off-white solid that decomposed at 94°C. THF yielded a mix of black and shiny golden solids. These solids were irregular in size and shape with platelet morphology. No further analysis was carried out on this sample as the material appeared to be of poor quality. Acetonitrile, whether dry or not, afforded the best result, giving shiny golden fibers in 65% yield. The cocrystallization experiment was repeated several

times in acetonitrile for reproducibility, and shiny golden fibers were always obtained in good yield. Raman spectroscopy (**Figure 2.6**) supports the formation of PIDA cocrystals as evidenced by the PDA peaks at 2082, 1409 and 976 cm^{-1}.

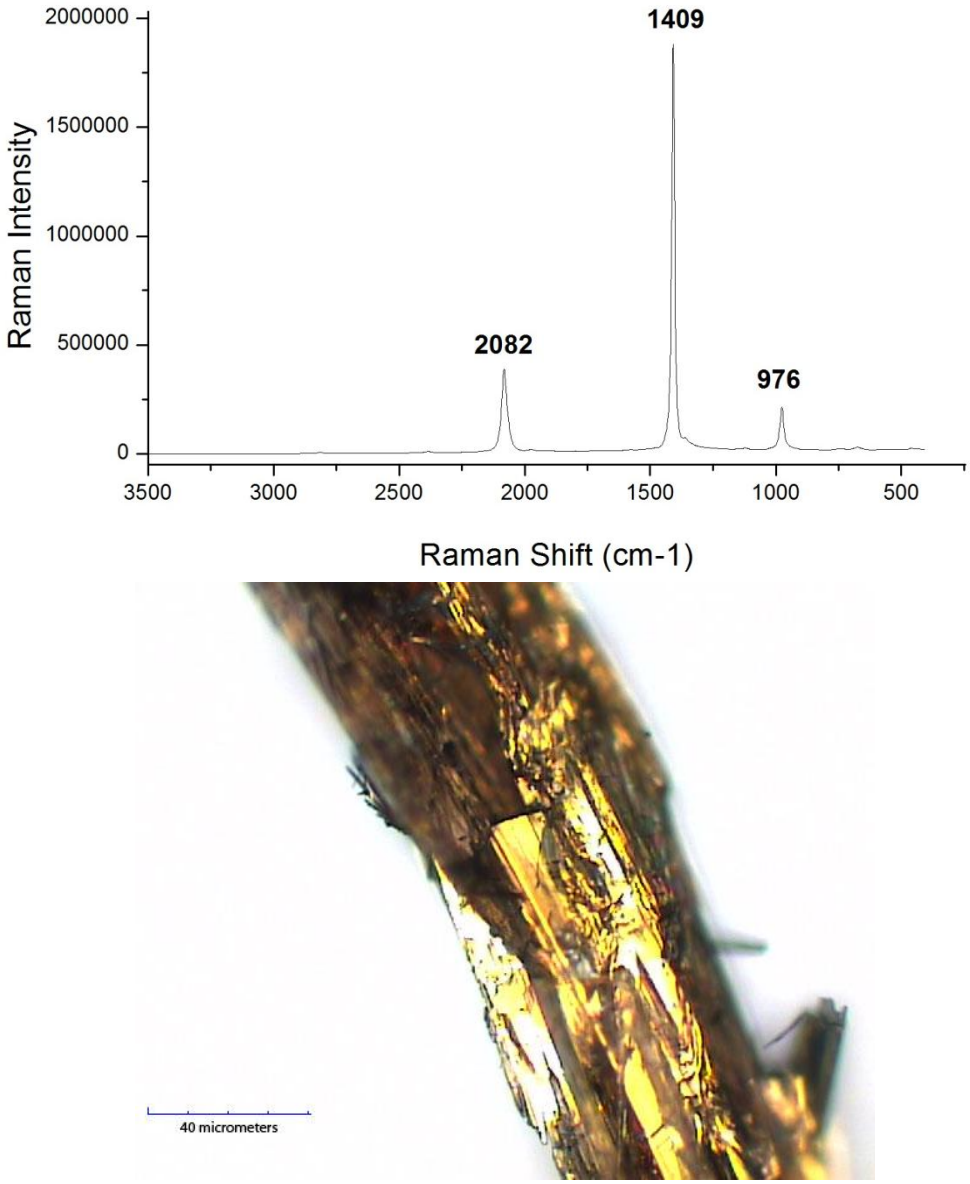

Figure 2.6. Top: Raman spectra of **4e·5** formed in acetonitrile; Bottom: Optical image of **4e·5** fiber.

The solvent experiments demonstrated that acetonitrile is the optimal solvent for cocrystallization of host **4e** with **5**. Undergraduate research student Siew Yoong Tan used this observation to further improve the cocrystallization method by finding the optimal concentration

of the reagents. Initial cocrystallization experiments were conducted at concentrations of 1.67 mg of **5** per mL (5.5 mM) of acetonitrile. Siew Yoong Tan was able to successfully grow cocrystals on a large scale at concentrations of either 3.3 or 13 mg/mL of **5** (**Figure 2.7**). The crystals grown at 3.3 mg/mL of **5** were shiny and golden in color and by visual inspection contained mostly cocrystal. A yield for these crystals was not reported however. At a concentration of 13 mg/mL of **5**, a PIDA cocrystal yield of up to 80% is obtained. In this experiment, Siew Yoong Tan was able to use less solvent, such that blue cocrystal formation occurs in 1 day. In an additional day, the characteristic golden fibers of PIDA are obtained. The benefit of faster crystallization is that **5** will have less time to decompose. One possible reason for the improvement in cocrystal yield is compound **5** having less time to decompose. Another measure taken to minimize the decomposition of **5** is total exclusion of light. Light was thoroughly excluded by fully wrapping the crystallization dish with aluminum foil as opposed to just covering the top of it as was done in past experiments.

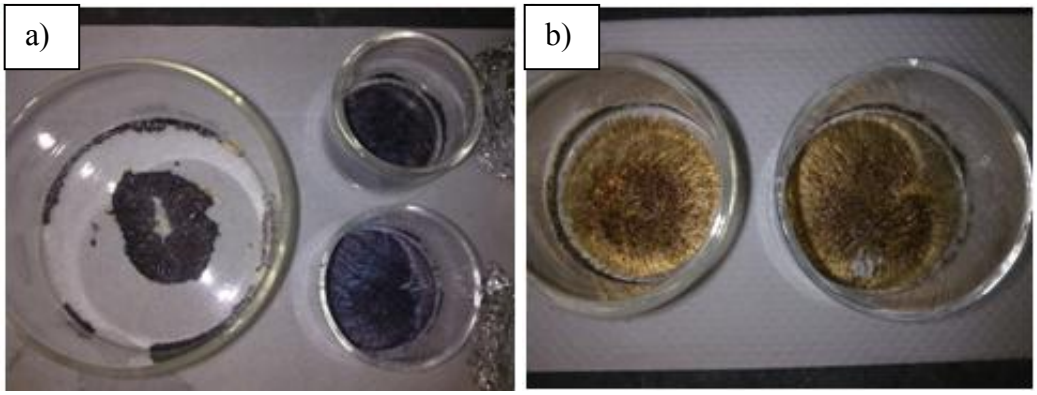

Figure 2.7. a) Unpolymerized and b) polymerized **4e·5** cocrystals grown in acetonitrile with C_4I_2 concentration of 13 mg/mL

2.4 Conclusion

The reproducibility of PIDA cocrystal synthesis can be significantly improved by using acetonitrile as a solvent for crystallization. Also, more concentrated cocrystal solutions allow for less solvent to be used without impacting crystal quality or yield. The yield of cocrystals

obtained under the optimized conditions reported here is greatly improved over past methods. Large scale preparation of PIDA cocrystals is now possible. Obtaining an X-ray crystal structure of cocrystal **4e·5** remains to be accomplished in future work. Another outlook for future investigation is detailed analysis of the crystals grown in THF. These crystals formed irregular platelet-like crystals, which are very different than the ones grown from an acetonitrile solution.

2.5 Experimental

Tetrahydrofuran was freshly distilled under argon and used immediately unless otherwise stated. All other reagents and solvents were used from stock bottles without further purification. NMR data was collected in $CDCl_3$ purchased from Cambrige Isotope Laboratories. Experiments were carried out under argon unless otherwise stated.

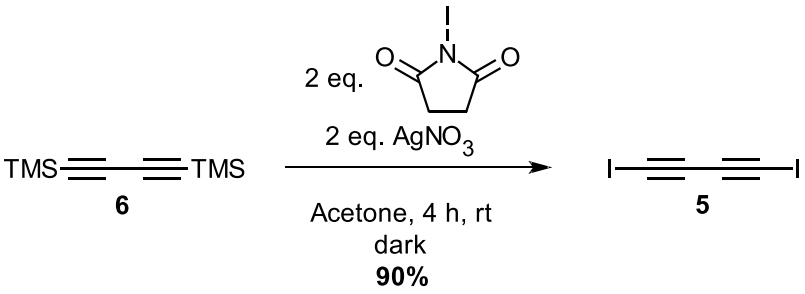

Diiodobutadiyne (5):[3] 1,4-Bis(trimethylsilyl)butadiyne **6** (0.500 g, 2.57 mmol) was added to an aluminum foil wrapped rbf. Acetone (125 mL) was then added to the flask. N-Iodosuccinimide (1.156 g, 5.14 mmol) and $AgNO_3$ (0.873 g, 5.14 mmol) were added to the solution of **9**. The reaction mixture was allowed to stir for 4 h before the solvent was removed in vacuo and 100 mL hexanes was added. The contents of the reaction flask were swirled and subjected to vacuum filtration. Water (100 mL) was then added to the filtrate and the liquid was transferred to a separatory funnel. The hexanes layer was separated and fresh hexanes (80 mL) were added to the separatory funnel. The water layer was extracted 3 × with hexanes. The organic layers were combined, dried with $MgSO_4$, and filtered. The solvent was removed in vacuo to afford a faintly yellow solid in 90% yield: ^{13}C-NMR (125 MHz, $CDCl_3$) δ 79.7, -3.4[3]

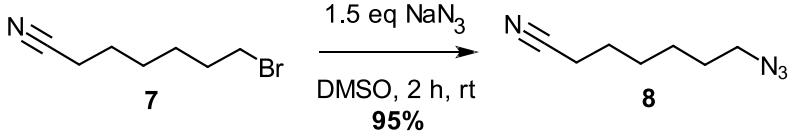

7-Azidoheptanenitrile (**8**):[3] 7-Bromoheptanenitrile (5.001 g, 26.3 mmol) was weighed out into a flask and 30 mL dimethylsulfoxide was added. Sodium azide (2.573 g, 39.5 mmol) was then added and the reaction was allowed to stir for 24 hours. The reaction was then diluted with 90 mL de-ionized water, followed by extraction with ether (4 × 50 mL). The combined ether layers were concentrated *in vacuo* to half volume, washed with water (2 × 50 mL), and finally the ether was removed *in vacuo*. The resulting faint yellow oil (3.800 g, 25.0 mmol) was obtained in 95% yield: ^{1}H NMR (300 MHz, $CDCl_3$) δ 3.28 (t, 2H), 2.35 (t, 2H), 1.77 – 1.53 (m, 4H), 1.53 – 1.07 (m, 4H).[3]

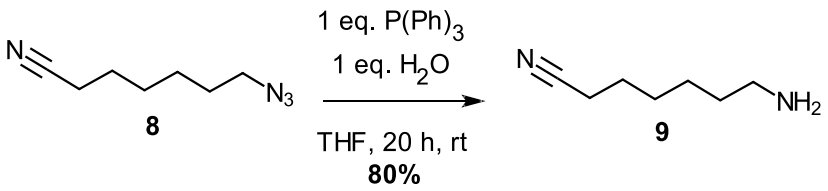

7-Aminoheptanenitrile (**9**):[3] 7-Azidoheptanenitrile (4.002 g, 26.3 mmol) was dissolved in 30 mL of wet THF with triphenylphosphine (6.900 g, 26.3 mmol). Deionized water (2 mL) was then added to the flask, and the reaction was stirred at room temperature for 24 hours. It is important to vent the reaction as to allow the nitrogen gas product to escape. The solvent was then removed *in vacuo*. Ethyl acetate (60 mL) was then added to dissolve the triphenylphosine oxide byproduct. The ethyl acetate layer was extracted with 1M HCl (5 × 40 mL). The combined acid extracts were basified to pH > 14 with NaOH. The basified solution was then extracted with ethyl acetate (4 × 50 mL). The combined organic layers were dried with $MgSO_4$, filtered, and the solvent was removed *in vacuo*. A yellow oil (2.65 g, 21.0 mmol) was obtained in 80% yield: ^{1}H

NMR (400 MHz, $CDCl_3$) δ 2.68 (t, *J* = 6.8 Hz, 2H), 2.33 (t, *J* = 9.6, 4.6 Hz, 2H), 1.64 (dd, *J* = 15.2, 7.2 Hz, 1H), 1.57 – 1.30 (m, 3H), 1.27 (s, 1H).[3]

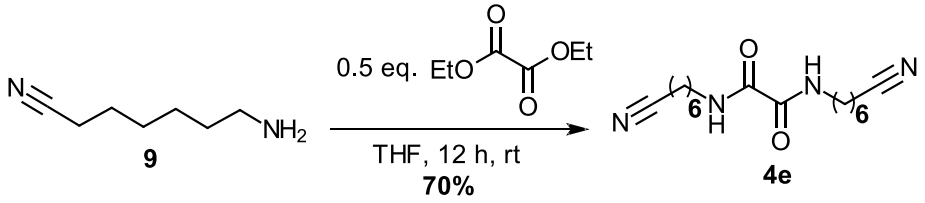

N,N-bis(6-cyanohexyl)oxalamide (**4e**):[3] 7-Aminoheptanenitrile (2.650 g, 21.0 mmol) was dissolved in 30 mL of THF in an argon-flushed flask. Diethyl oxalate (1.534 g, 10.5 mmol) was then added to the solution. The reaction solvent was removed *in vacuo* after 12 h. The resulting white solid was then recrystallized from ethanol and filtered. After recrystallization, the solid was subjected to reduced pressure for 30 minutes to ensure the thorough removal of ethanol. The resulting white solid (4.500 g, 14.7 mmol) was obtained in 70% yield: ^{1}H NMR (300 MHz, $CDCl_3$) δ 7.47 (s, 2H), 3.32 (t, *J* = 6.9 Hz, 4H), 2.35 (t, *J* = 7.0 Hz, 4H), 1.75 – 1.29 (m, 16H).[3]

General procedure for preparing PIDA Cocrystals
Host 4e / Diiodobutadiyne 5 Cocrystal:[3] Host **4e** (20 mg, 0.065 mmol) and diiodobutadiyne **5** (40 mg, 0.132 mmol) of C_4I_2 **5** were weighed and placed into a medium size test tube. Solvent (12 mL) was then added to the test tube. The test tube was then subjected to sonication for 10 min to ensure all solid was dissolved. The resulting solution was then divided evenly amongst 4 small test tubes and subjected to centrifugation for 10 minutes to remove impurities. The liquid contents of each test tube were transferred into separate crystallization dishes. Each crystallization dish was then covered with aluminum foil with 12 pin holes in it. On the morning of the third day from the start of the experiment, the crystals were removed from the dishes and observed. The cocrystals were then transferred into a cap-sealed vial for storage.

General procedure for preparing PIDA cocrystals (Siew Yoong Tan)
Host **4e** (0.020 g, 0.065 mmol) and diiodobutadiyne **5** (0.040 g, 0.13 mmol) were dissolved in 3

mL acetonitrile to give a solution with a guest concentration of 13 mg/mL. The solution was subjected to centrifugation for 10 min and decanted into a small crystallization dish. The crystallization dish was completely wrapped in foil. The foil covering the opening of the dish was punctured to allow slow evaporation of solvent. Cocrystals were left to grow at room temperature. Blue cocrystals were observed after 1 day, and these crystals turned gold within 2 – 3 days. Cocrystal yields were generally between 60 – 80%. The experiment was scaled appropriately for large scale cocrystallizations. A 12 cm diameter crystallization dish was used to prepare cocrystals from 12 mL solution of host **4e** / monomer **5** in acetonitrile. The concentration of this solution was 13 mg/mL.

2.6 References

1. Sun, A. W.; Lauher, J. W.; Goroff, N. S., Preparation of poly(diiododiacetylene), an ordered conjugated polymer of carbon and iodine. *Science* **2006,** *312*, 1030-1034.
2. Luo, L.; Wilhelm, C.; Sun, A.; Grey, C. P.; Lauher, J. W.; Goroff, N. S., Poly(diiododiacetylene): Preparation, Isolation, and Full Characterization of a Very Simple Poly(diacetylene). *J. Am. Chem. Soc.* **2008,** *130*, 7702-7709.
3. Luo, L. Preparation and Comprehensive Characterization of Poly(diiododiacetylene) and Spectroscopic Studies of Its Reactions with Lewis Bases. Stony Brook University, Stony Brook, NY, 2009.
4. Fringuelli, F.; Pizzo, F.; Vaccaro, L., Cobalt(II) Chloride-Catalyzed Chemoselective Sodium Borohydride Reduction of Azides in Water. *Synthesis* **2000,** *2000*, 646-650.
5. Osby, J. O.; Heinzman, S. W.; Ganem, B., Studies on the mechanism of transition-metal-assisted sodium borohydride and lithium aluminum hydride reductions. *J. Am. Chem. Soc.* **1986,** *108*, 67-72.

Chapter 3: Poly(diiododiacetylene) – A Potential Precursor to Carbon Rich Materials

3.1 Carbyne: Progress Towards the Elusive Allotrope of Carbon

As discussed in **Chapter 1**, the *sp*-hybridized allotrope carbyne (**Figure 3.1**) remains an unmet synthetic challenge. The preparation, isolation, and characterization of carbyne is challenging because of its instability. Although carbyne is defined as an infinitely long all-sp-carbon rod, its properties can be modeled using finite systems called polyynes. Some of the most recent and prominent work in using polyynes to model carbyne has been reported by Chalifoux and Tykwinski.[1] The polyyne in **Figure 3.2** contains 22 carbon-carbon triple bonds for a total of 44 carbon atoms. The purpose of the Tr^* group at the ends is to provide steric bulk to prevent the polyyne rods from undergoing an uncontrolled polymerization and forming the lowest energy carbon species.

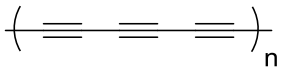

n = ∞

Figure 3.1. General structure of carbyne

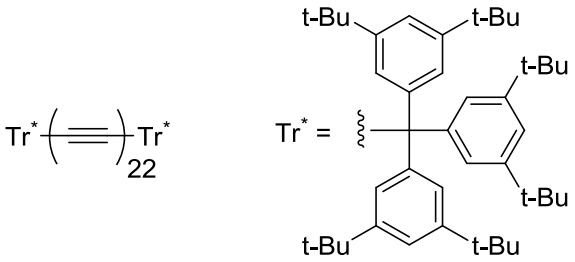

Figure 3.2. Chalifoux and Tykwinski reported the longest polyyne in the literature[1]

One of reasons Chalifoux and Tykwinski synthesized the 22 carbon-carbon triple bond polyyne was to gather UV absorbance data for predicting the λ_{max} of carbyne. **Figure 3.3** summarizes the UV data Chalifoux and Tykwinski collected. Chalifoux and Tykwinski observed an asymptote (purple dashed line) at 486 nm when wavelength is plotted as a function of the number of triple bonds in a polyyne. The asymptote is expected to be the λ_{max} of carbyne. This study also helped reveal the approximate length a polyyne would need to be in order to serve as a

model for carbyne. From **Figure 3.3** it is estimated that a polyyne of about 44 C≡C bonds (88 carbons) in length meets the lower threshold to be considered carbyne. Such a polyyne would be twice as long as the longest one Chalifoux and Tykwinski prepared.

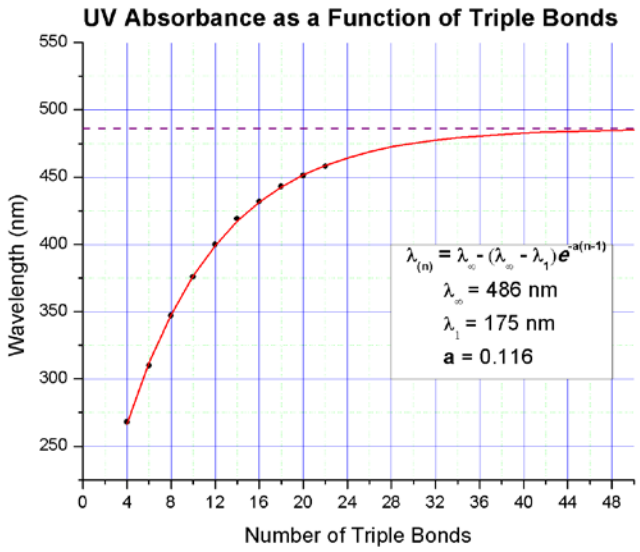

Figure 3.3.[1] Wavelengths of maximum absorption for polyynes taken from Ref. 1to extrapolate the λ_{max} of carbyne

The enormous effort by Chalifoux and Tykwinski to synthesize the necessary polyynes to make carbyne models suggests direct synthesis of carbyne itself is unfeasible. The intermediates involved in making carbyne would require handling of highly unstable compounds, which are often difficult to obtain in good yield. Polyynes are typically made from either metal-catalyzed alkyne coupling or a Corey-Fuchs reaction followed by a Fritsch-Buttenberg-Wiechell (FBW) rearrangement. **Figure 3.4** below shows typical conditions and substrates for polyyne synthesis.

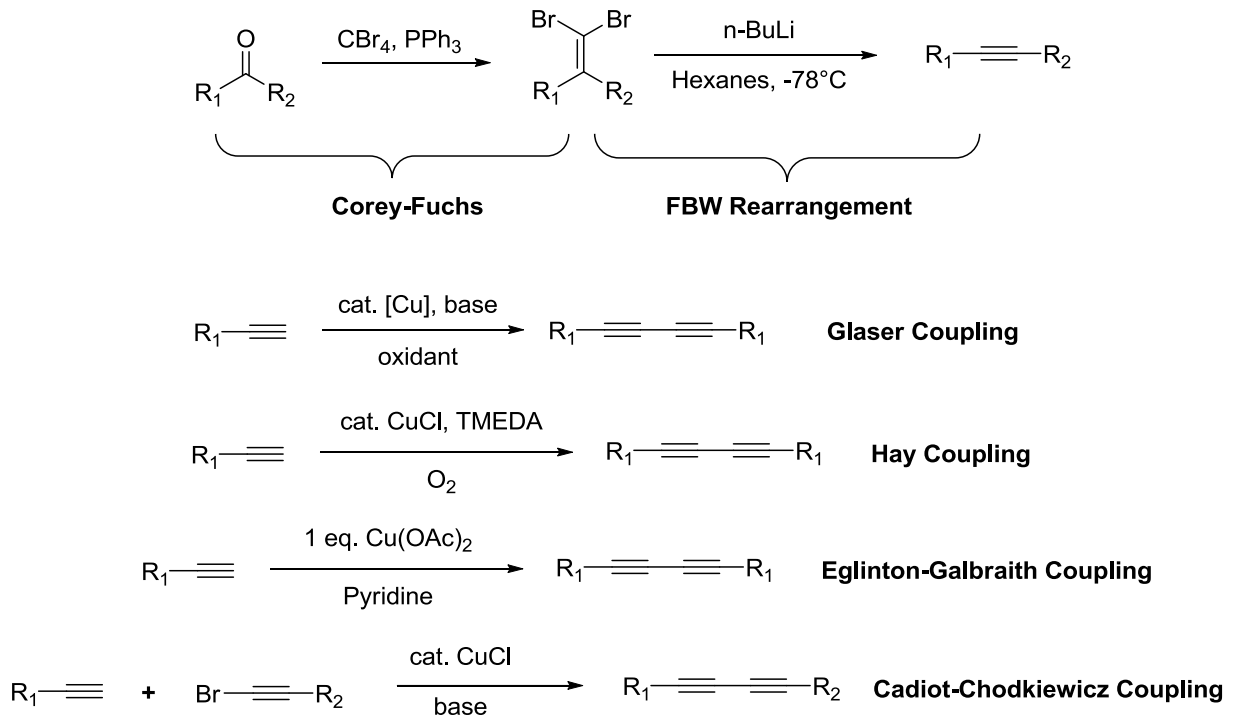

Figure 3.4. Synthetic reactions commonly used for making polyynes

The C-C coupling reactions offer some benefits over the FBW rearrangement as they are carried out under milder conditions.[2] When using these reactions, however, it is necessary to perform a series of desilylations for accessing terminal alkyne that are used as intermediates to build longer polyynes.[1] One of the limitations of the C-C bond forming reactions in **Figure 3.4** is that only symmetrical polyynes are obtained with the exception of the Cadiot-Chodkiewicz coupling. Group member Allison Black has studied the Cadiot-Chodkiewicz reaction thoroughly and found asymmetric coupling is not always possible with this reaction. Another issue is that almost all polyynes are derived from starting materials with one or two triple bonds. A direct synthetic method to prepare carbyne is infeasible, thus an alternative approach is desirable.

3.2 PIDA as a Potential Precursor for Carbyne and Other Carbon Materials

PIDA is potentially a precursor to carbyne because the C-I bonds are weak and easily broken. The polymer consists entirely of carbon and iodine. The complete deiodination of PIDA would thus result in an all carbon material (**Scheme 3.1**). Goroff and coworkers reported that

PIDA can be carbonized under pyrolysis conditions, but this technique requires high temperature.[3] The high temperature will favor the lowest energy carbon species, which is an amorphous graphite-like carbon (AGLC). The preparation of carbyne or carbyne-like species is more likely to be accomplished under mild conditions.

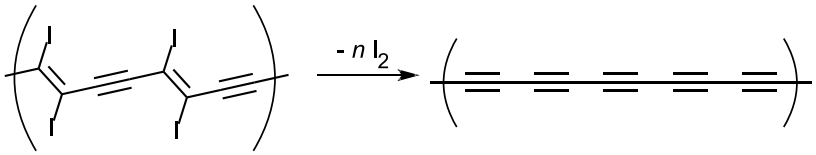

Scheme 3.1. Carbonization of PIDA

Goroff and coworkers showed that it is possible to eliminate iodine from isolated PIDA (**Figure 3.5**) using the Lewis-base triethylamine.[4] The elimination of iodine can also be induced with other Lewis-bases such as pyridine or pyrrolidine under mild conditions. Elemental analysis of the products of pyridine and pyrrolidine treated PIDA showed iodine was not completely eliminated (**Table 3.1**). Sample S4 was found to contain an appreciable amount of nitrogen which could come from the host or pyrrolidine. Given the thorough washing procedure to remove host, the source of nitrogen must be pyrrolidine. If conditions can be found to completely deiodinate PIDA without incorporating heteroatoms, the polymer would present itself as a potential precursor for preparing carbyne.

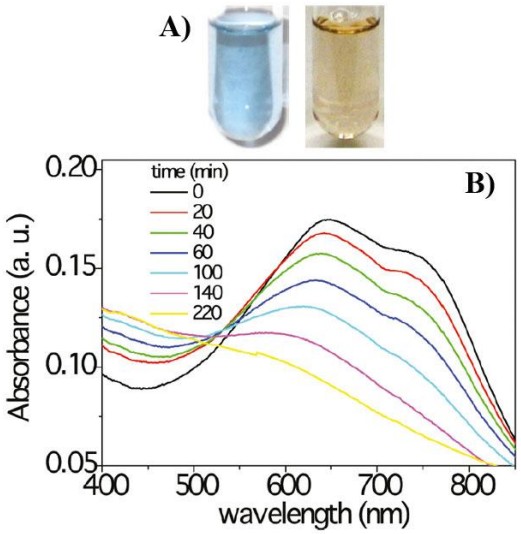

Figure 3.5. A) Isolated PIDA suspensenion in methanol (left) turns yellowish-brown after addition of triethylamine (right). B) UV-vis reaction monitoring as the color changed from blue to yellowish-brown. Adapted with permission from Ref. 4. Copyright (2011) American Chemical Society.

Table 3.1.[5] Results of bulk elemental analysis obtained by Luo.

Sample	Carbon (wt %)	Hydrogen (wt %)	Nitrogen (wt %)	Iodine (wt %)
S1	18.42	0.34	0.44	76.61
S2	26.55	1.37	2.18	70.55
S3	26.80	1.08	2.31	63.84
S4	51.74	4.95	8.46	N/A

S1: Isolated PIDA; S2: product of neat pyridine treated isolated PIDA; S3: product of isolated PIDA treated with stroichiometric pyrrolidine in methanol; S4: isolated PIDA treated with a large excess of pyrrolidine in methanol.

In Luo's experiments, the elimination of iodine from PIDA was typically carried out on the isolated polymer.[3, 5-6] Isolation of the polymer requires extensive sonication, and results in the formation of PIDA aggregates. The aggregation is potentially problematic because the internal strands may not be accessible to the reaction mixture. If the elimination reagent cannot access the internal iodine groups, complete deiodination cannot be achieved. This problem may be rectified by using PIDA cocrystals instead of isolated PIDA. Aggregation is less of an issue when PIDA cocrystals are used because the elimination reaction can occur as the polymer strands are exfoliated from the surface of the material. If this scenario is achieved, it ideally allows for the elimination reaction to preempt PIDA aggregation.

3.3 New Directions for Pyrrolidine-Induced Deiodination of PIDA

One of the more recent attempts to carbonize PIDA involved using PIDA cocrystals (**4e·5**) and an excess of pyrrolidine. An excess of pyrrolidine would ensure quick reaction so as to eliminate the iodine groups in PIDA before the polymer forms aggregates. Sonication was also used to aid in exfoliating the polymer from the cocrystal. Treating cocrystallized PIDA with a large excess of pyrrolidine resulted in the product shown in **Scheme 3.2** below. After 30 minutes of sonication a reddish-brown color was observed. The reaction was allowed to progress further for 24 hours before being subjected to acetone washing. The purpose of the washes is twofold. Acetone can dissolve any residual host, as well as dry the sample. Each wash was collected and subjected to NMR analysis after rotary evaporation. Peaks corresponding to pyrrolidine ^{1}H-NMR (2.61, 2.22, 1.69 ppm) were apparent in the first two washes. The third wash had several very small unidentifiable peaks at 2.82, 2.15, 1.30, and 0.14. NMR indicates that the fourth and fifth washes were entirely solvent.

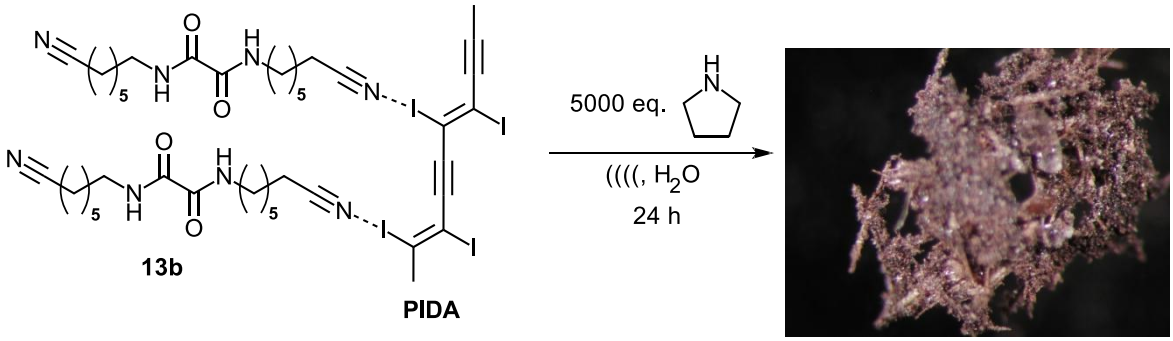

Scheme 3.2. Reaction between PIDA cocrystals and excess pyrrolidine

The product of the pyrrolidine-induced deiodination was subjected to Raman spectroscopy, UV-vis spectroscopy, and SEM/EDS analysis. Orange and black particles were observed under the Raman microscope indicating a heterogeneous mixture. Most of the particles were black in color. With the help of Christopher Young of the Halada group, the Raman data were collected for both the orange and black particles (**Figure 3.6**). The black particles seem to consist of disordered sp^2 carbon, as signified by the broad peaks between 1750 – 1000 cm^{-1}. The

signal to noise ratio of the data is poor, however. The Raman spectrum of the orange particles is of worse quality that the one for the black particles. It does not show any significant peaks.

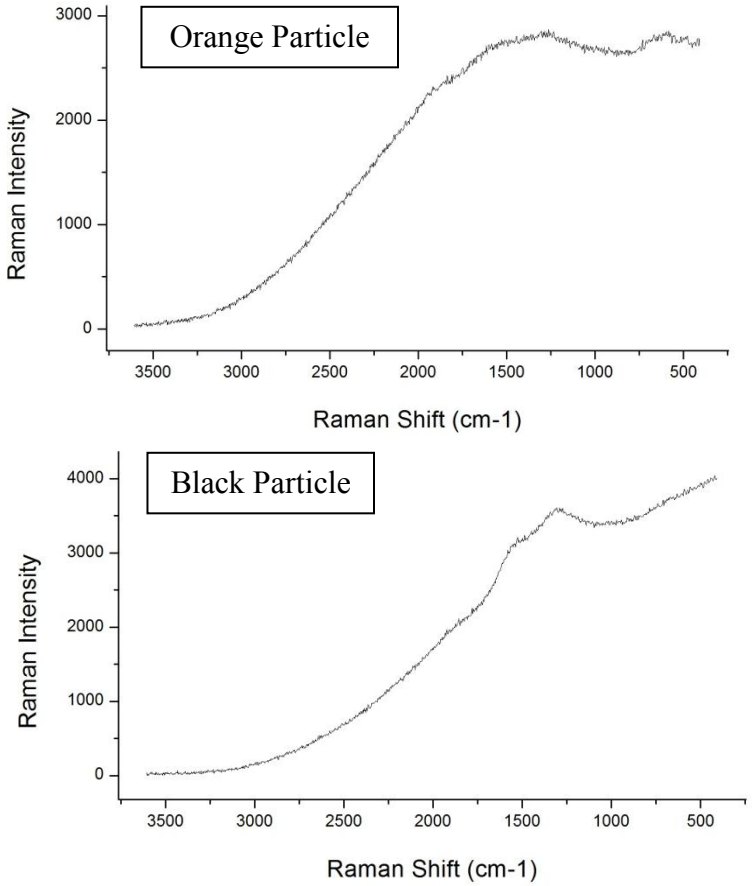

Figure 3.6. Raman spectroscopy of the carbonized product from the reaction of polymerized **4e·5** with excess pyrroldine (**Scheme 3.2**)

The UV-vis spectrum of the suspension of the base-treated material did not reveal any identifiable peaks. The UV spectra in **Figure 3.7** show two trials. Run #1 in **Figure 3.7** was more concentrated and as such the beam could not pass through the sample. A diluted sample was also subjected to UV-vis analysis but the instrument was not zeroed prior to data collection. This is the reason for the negative absorbance in Run #2. Run #2 however, does not contain any obvious peaks aside from the peak at 225 nm in the UV region.

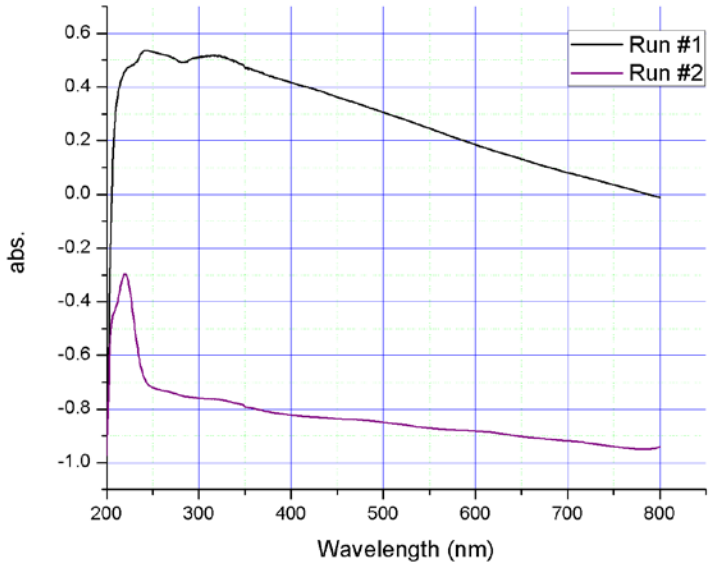

Figure 3.7. UV-vis spectrum of the suspended product of pyrrolidine induced deiodination

SEM imaging and EDS analysis of the product of pyrrolidine-induced deiodination showed the sample is not homogeneous (**Figure 3.8**). There are particles of varying size and composition. Some of these particles contain a significant amount of iodine, as shown by the EDS spectrum **Figure 3.8,** whereas others do not. It is important to note that EDS spectra only show the surface chemistry (about 10 nm) and are not necessarily representative of bulk composition.

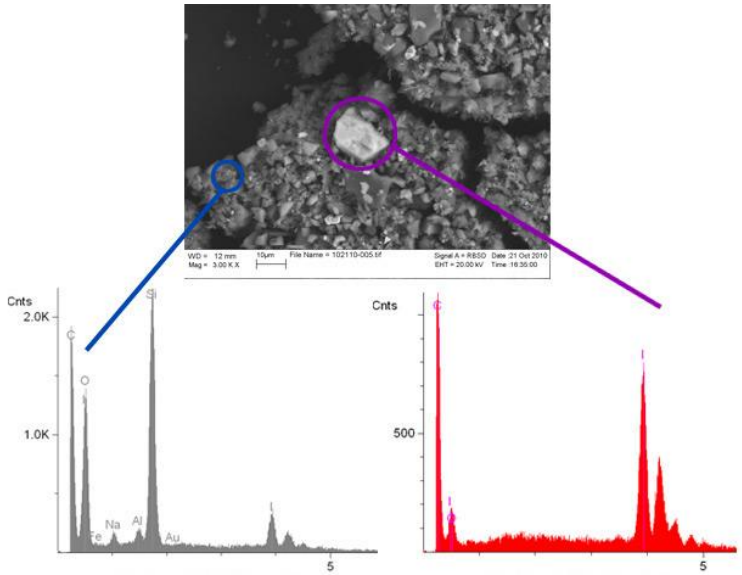

Figure 3.8. Top: SEM image of the product of pyrrolidine induced deiodination of PIDA cocrystals; Bottom: EDS results of the elements present in the sample

It is clear from the data that the reaction conditions used in **Scheme 3.2** with pyrrolidine are not optimal for the complete deiodination of PIDA cocrystals. One possible explanation for this observation is incomplete reaction. The model studies (**Chapter 4**) that were conducted after this experiment showed that the deiodination reaction proceeds very slowly in protic solvents without reaching full conversion. The reaction time of only 24 hours and use of water as a solvent would be an impediment to complete deiodination. Another possible explanation for the presence of iodine in the product is adsorption of a pyrrolidinium iodide species onto the carbonaceous material. The structure and reactivity of this species is discussed in more detail in **Chapter 4**.

Another attempt was made to deiodinate PIDA with pyrrolidine in a polar aprotic solvent. The model reaction studies described in **Chapter 4** showed that 2 equivalents of pyrrolidine in a polar aprotic solvent could induce the complete deiodination of a simple diiodoalkene in 15 hours. The use of acetonitrile as a solvent for the reaction, as shown in **Scheme 3.3** provides the polar aprotic medium that favors complete deiodination. The host also has excellent solubility in acetonitrile. An excess of pyrrolidine was used to ensure fast reaction. The reaction was also subjected to simple stirring rather than sonication. This eliminated the possibility of any side reaction induced by sonication.[7] In about 1 hour a dark reddish-brown solution was observed, though the solution was too dark to clearly see any solid material. The color change is a promising sign that reaction occurred without the need for sonication. UV-vis analysis of the reaction mixture was carried out after 48 hours, but did not show any characteristic peaks (**Figure 3.9**). The leveling off of the data from 250-200 nm is a result of detector saturation. There do appear to be other minor peaks in the UV spectrum at 400 nm and around 350 nm. These features are not well defined however. The reaction mixture was subjected to

centrifugation at 3000 rpm for 20 minutes as workup. After centrifugation, the liquid was decanted and a dark-colored sludge was left at the bottom of the centrifuge tube. The decanted liquid still had a dark reddish-brown color. In order to analyze the supernatant, the reaction solvent was evaporated to give a viscous reddish-brown oil. This oil is soluble in acetone, water, methanol, isopropyl alcohol, and dicholoromethane.

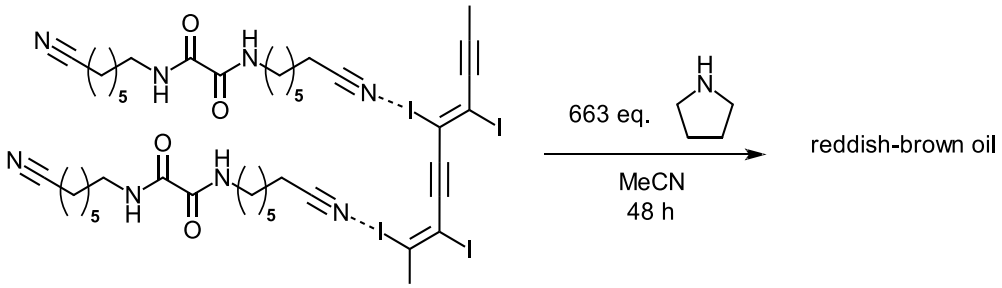

Scheme 3.3. Reaction of PIDA cocrystals with pyrrolidine in MeCN

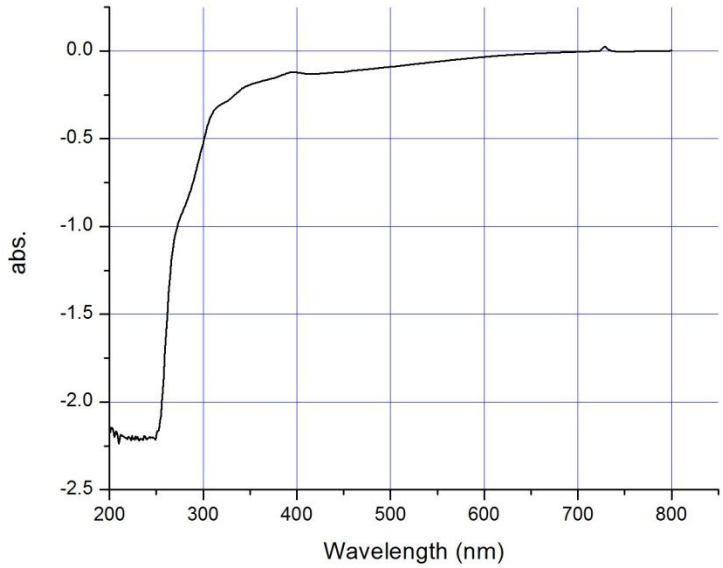

Figure 3.9. UV-vis analysis of deiodinated PIDA cocrystals in MeCN

NMR analysis of the oil was attempted, but a lock on the sample could not be obtained. One potential explanation for the failure to lock is paramagnetic species interfering with the magnetic field. The reddish-brown oil was also subjected to IR analysis (**Figure 3.10**).

The broad peak in the IR spectrum of the neat sample from about 3700-3000 cm^{-1} is potentially the N-H stretch. The diluted IR spectrum of the oil in dichloromethane does not show the same broad stretch from 3700-3000 cm^{-1}. Dichloromethane itself has IR peaks at 3049, 2985, 1433, 1429, 1265, and 896 cm^{-1}. The diluted spectrum shows peaks in addition to the ones for dichloromethane, but these features do not reveal much about the oil. Raman spectroscopy of the reddish-brown oil deposited as a thin-film on a quartz slide was also attempted. **Figure 3.11** shows the optical image of the thin film formed from the oil in dichloromethane, and its Raman spectrum. The thin film does not appear to have any Raman-active structural features.

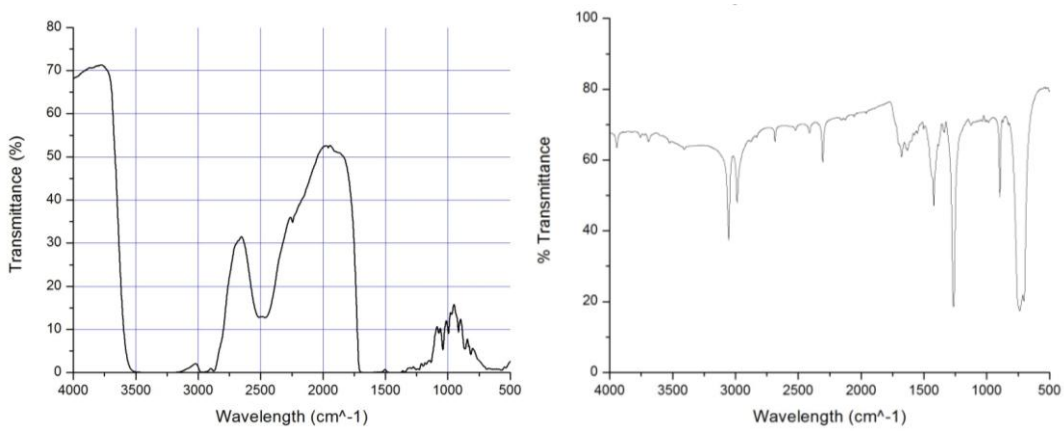

Figure 3.10. IR analysis of the reddish-brown oil both neat (left) and in CH_2Cl_2 (right) from pyrrolidine induced deiodination of PIDA cocrystals

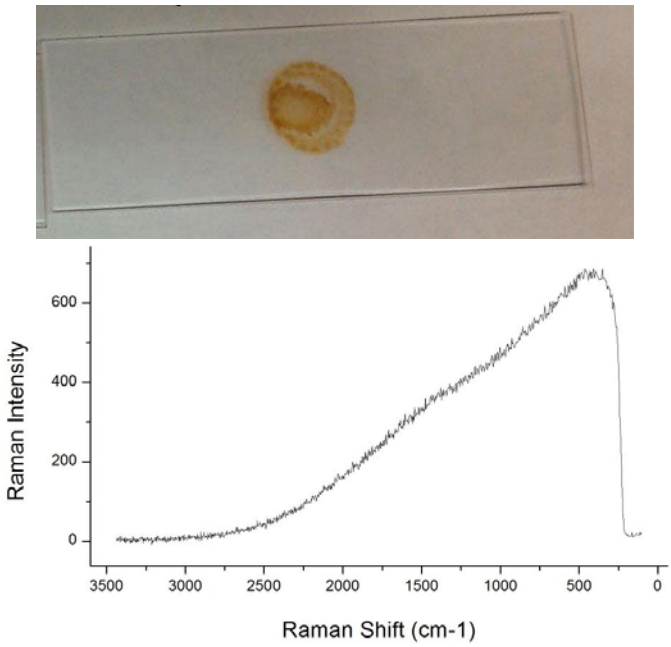

Figure 3.11. Top: Optical image of the thin film of the product of pyrrolidine-induced deiodination of PIDA cocrystals in MeCN; Bottom: Raman spectra of the thin film.

3.4 Studying the Reaction of Iodide and Bromide Anions with PIDA cocrystals

The preliminary results of the reaction between pyrrolidine and PIDA cocrystals encouraged investigation into other reagents for deiodination. Numerous literature reports of iodide salt-induced dehalogenation were found for dibromoalkanes discussed in greater detail in **Chapter 4**. Those reports encouraged the use of an iodide salt to deiodinate small molecule models. The successful deiodination of the small molecule models made promising the use of iodide to deiodinate PIDA. One of the advantages of using a halide salt to induce elimination is water solubility of the salt species. This makes purifying the final product easier, as the salt can be washed away with water. Tetrabutylammonium iodide (TBAI) was chosen as an iodide source since it is soluble in both water and most polar organic solvents. **Scheme 3.4** summarizes the initial attempts to deiodinate PIDA cocrystals with TBAI.

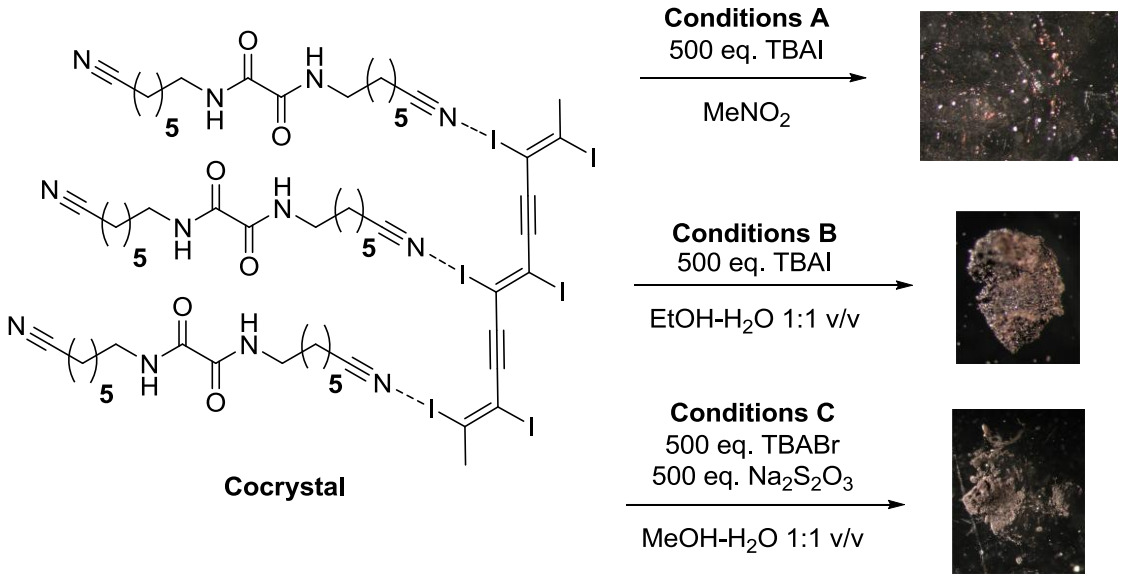

Scheme 3.4. Reaction of PIDA cocrystal under several sets of conditions

Nitromethane (b.p. 100°C) was chosen as a solvent for Conditions A because it had the best solubility of TBAI for the lowest boiling point. TBAI has excellent solubility in DMF and DMSO but these solvents have boiling points much higher than nitromethane. The high boiling point of these solvents makes their removal more difficult. The product under Conditions A in **Scheme 3.4** has been characterized by SEM imaging and Raman spectroscopy. The SEM image of TBAI-treated PIDA co-crystal in nitromethane reveals particles that are slightly larger than the pyrrolidine-treated co-crystals. The whiter-looking particles are rich in iodine, as per the EDS spectra in **Figure 3.12**. Similar results were observed with the pyrrolidine-treated samples. The greyer looking particles in **Figure 3.12** appear to be contamination of a fluoropolymer as these spots were rich in fluorine. It is possible that Teflon from the vial caps contaminated the sample. EDS spectroscopy is not quantitative, so using peak intensity to judge the amount of iodine is not appropriate here. Also, EDS techniques only penetrate the sample about 10 nm so they do not represent the sample as a whole. Raman analysis indicates an amorphous graphite-like carbon (AGLC) structure is present, though the signal-to-noise ratio is poor.

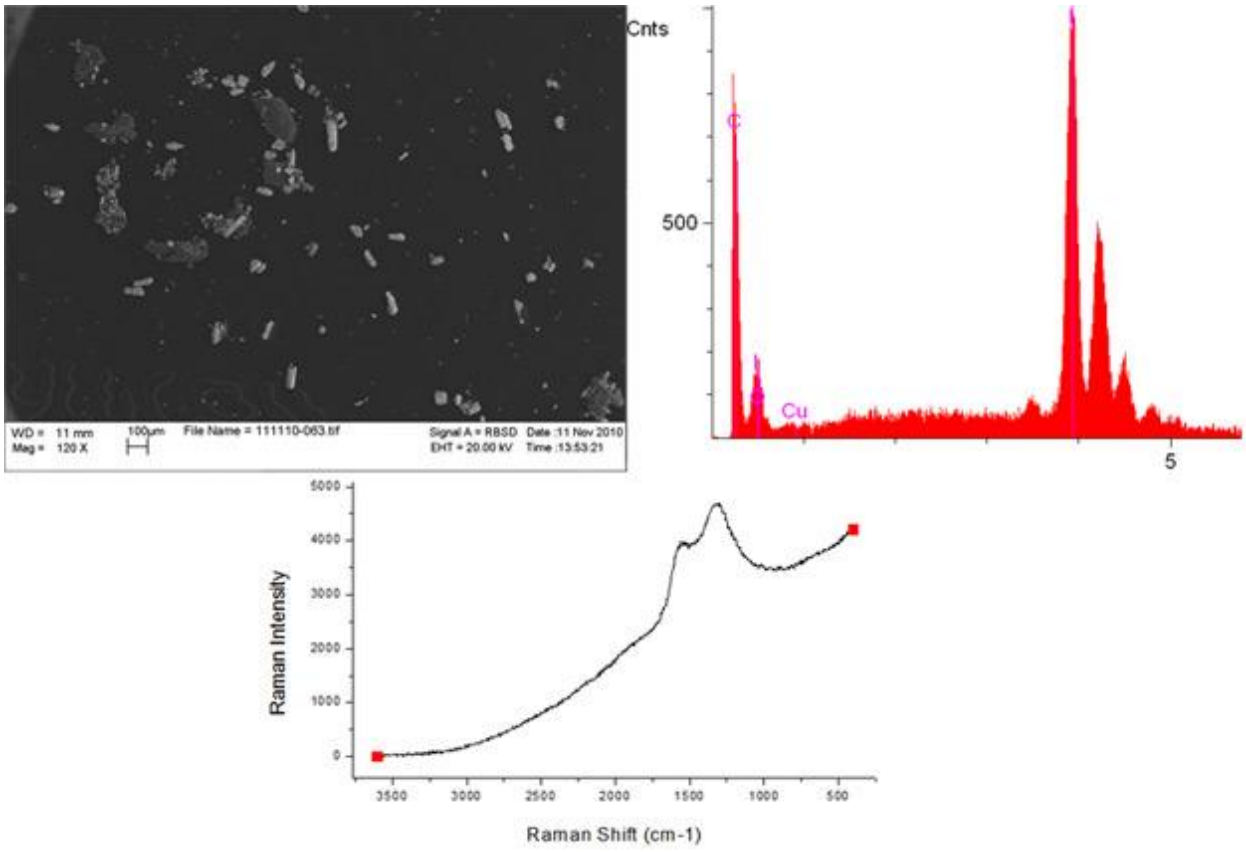

Figure 3.12. Upper-left: SEM image of the product of PIDA cocrystal deiodinated by TBAI; Upper-right: EDS spectrum; Bottom: Raman spectrum

Under conditions B (**Scheme 3.4**), TBAI is still used as the eliminating agent but a different solvent system is employed. The ethanol / water solvent system is chosen to ensure slow dissolution of host **13b**. Host **13b** is not soluble in water but has good solubility in ethanol. Slow dissolution of the host allows exfoliated PIDA strands more time to undergo deiodination before aggregation. The PIDA cocrystals treated in ethanol / water produced orange and black colored products much like the pyrrolidine treated cocrystals. Raman spectra of both products are of poor quality and the signal-to-noise ratio is low. Instead of targeting a lone spot for EDS analysis, an elemental surface profile was obtained. The red areas in **Figure 3.13** are carbon. The background carbon is from the conductive tape the sample is mounted on. The source of the silicon is not entirely clear. The most interesting feature is the location of the iodine (green). The

iodine covers most of the particles in the profile image. It is unclear as to how deep the iodine goes because EDS is limited to 10 nm. This surface profile ultimately reveals that iodine is still present in some form.

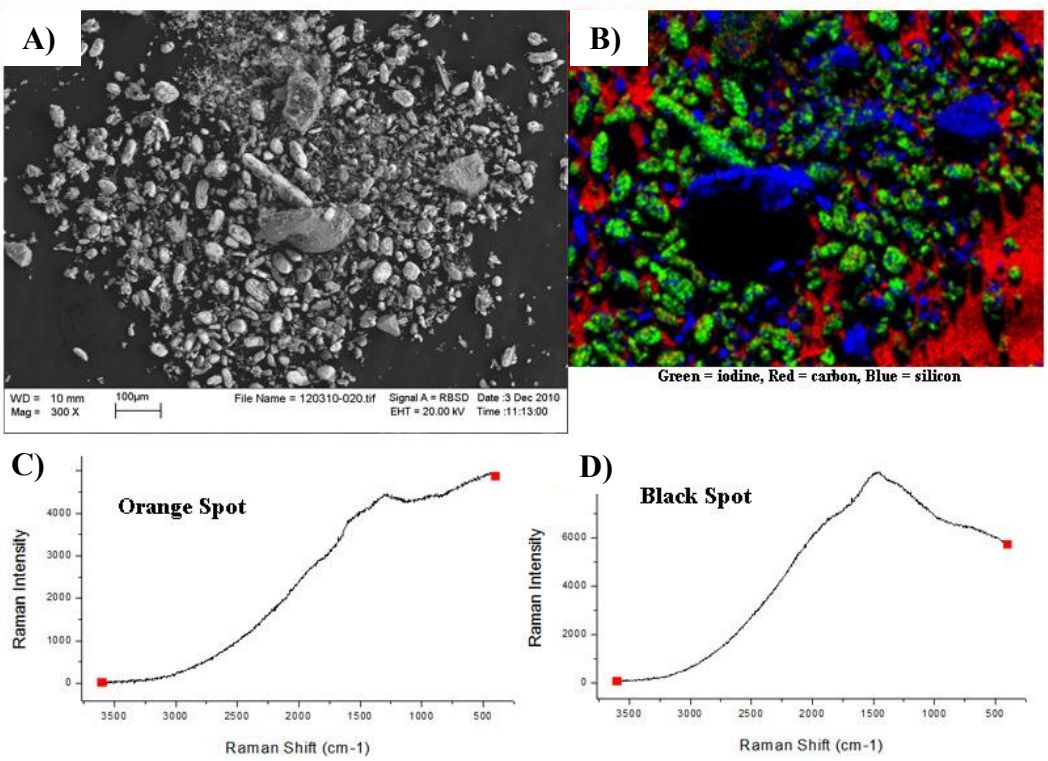

Figure 3.13. A) SEM image of the product obtained from reaction of polymerized **4e**·**5** with 500 eq. TBAI in 1:1 EtOH:H_2O; B) EDS map of iodine (green), carbon (red), and silicon (blue); C and D) Raman spectra of colored particles.

The reaction under the conditions C in **Scheme 3.4** uses an entirely different reagent and solvent. TBAI was replaced with tetrabutylammonium bromide (TBABr). The reason for using the bromide anion was to eliminate the possibility of introducing another iodine source aside from PIDA. Sodium thiosulfate was also used to reduce any diatomic halogen species to soluble halide anions. There difference between methanol and ethanol is not expected to have a major effect on the reaction, however host **4e** is slightly more soluble in methanol than ethanol. The Raman spectra in **Figure 3.14** indicate amorphous graphite-like carbon as was seen in previous experiments. SEM imaging however reveals a more fibrous looking material. The fibers vary

greatly in size with a heterogenous distribution of elements. The presence of sulfur is found in the EDS spectrum. It is possible that sodium thiosulfate was left behind or adsorbed on the carbon species. One can also see that iodine has been completely removed. There is some residual bromide, which is likely from TBABr. The EDS spectrum also indicates the presence of silicon. Silicon contamination could come from 2 sources. These sources include the glue on the carbon sticky tape that is used to mount the sample in the microscope. Another source is glass. When the glass rbf in which the reaction is conducted is subjected to sonication, bits of glass can contaminate the sample.

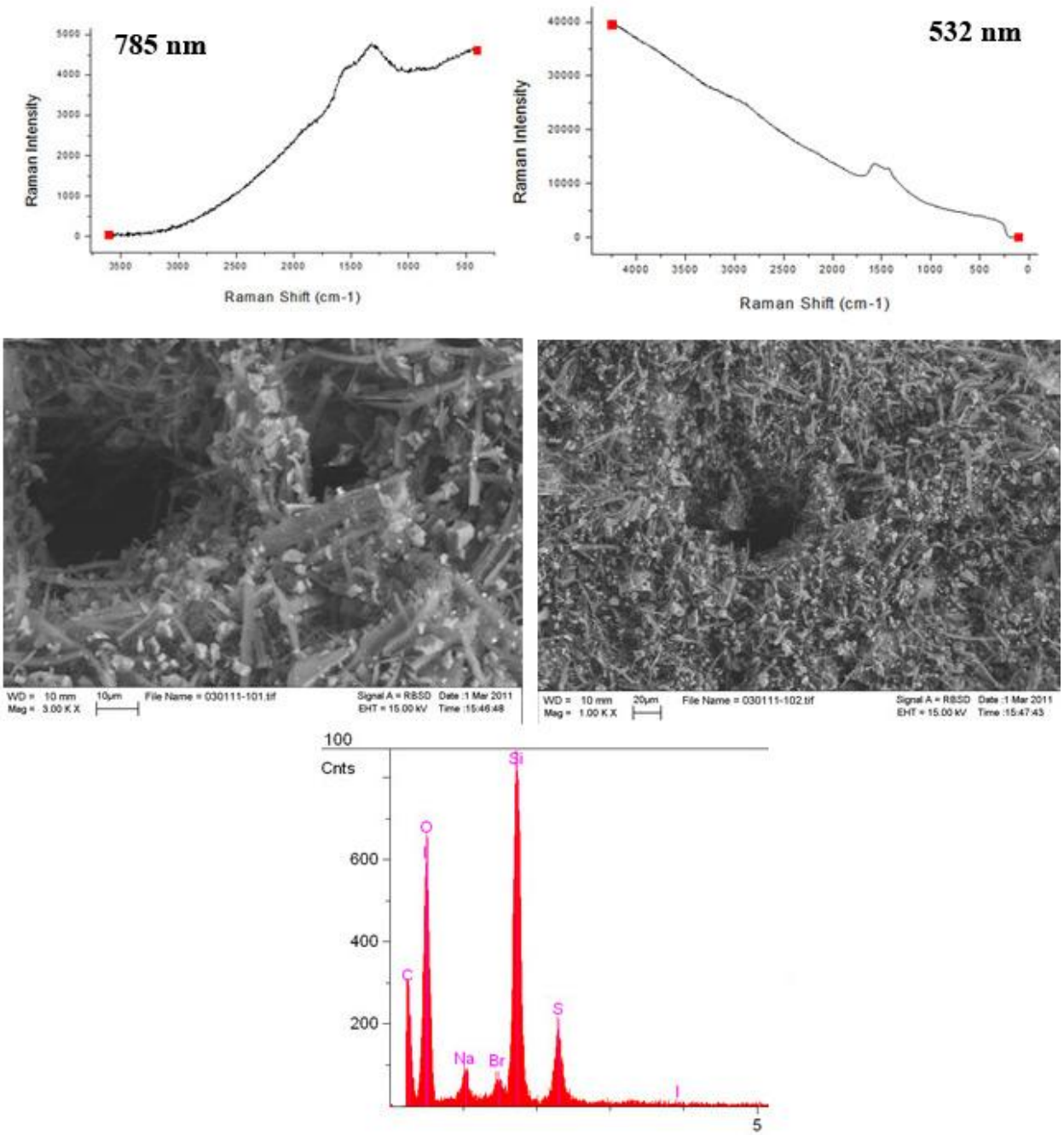

Figure 3.14. Top: Raman spectra of the product from the reaction of polymerized **4e·5** with 500 eq. TBABr and 500 eq. $Na_2S_2O_3$ in 1:1 MeOH:H_2O; Middle: SEM images; Bottom: EDS analysis

For complete iodine elimination from PIDA, the reaction media consisting of 500 eq. of TBABr and 500 eq. $Na_2S_2O_3$ in 1:1 MeOH:H_2O shows great promise. Bulk elemental analysis (**Table 3.2**) of the product obtained from Conditions C revealed that iodine has been completely removed but other non-carbon elements were still present. The data in **Table 3.2** show 74.4% of

the elemental composition of the sample is accounted for. The remaining mass is likely to be sulfur and sodium, as per the EDS data in **Figure 3.14**. These results show that it is possible to completely deiodinate PIDA, but heteroatoms are incorporated in the process.

Table 3.2. Bulk elemental analysis of deiodinated PIDA cocrystals by TBABr and $Na_2S_2O_3$

Element	Percent Composition
C	45.48
H	4.66
N	2.37
O	19.91
I	2

Results of bulk elemental analysis of the product from the reaction of polymerized **4e·5** with 500 eq. of TBABr and 500 eq. $Na_2S_2O_3$ in 1:1 MeOH:H_2O

The undesired inclusion of sulfur into the deiodinated PIDA product prompted a further investigation into reactions without a sulfur-based reducing agent. Iodide is commonly known to complex with I_2 to form the triiodide complex. It was thus thought that using just TBAI in MeCN was plausible for completely deiodinating PIDA cocrystals without incorporating any additional elements (**Scheme 3.5**). Based on the model studies in **Chapter 4**, the conditions in **Scheme 3.5** are optimal for achieving fast deiodination. The product of the reaction in **Scheme 3.5** however, still contained iodine at least at the surface level (**Figure 3.15**) based on the EDS analysis. The Raman spectrum in **Figure 3.15** is consistent with amporphous graphite-like carbon (AGLC), but the signal-to-noise is poor. The IR spectrum in **Figure 3.15** does not contain any identifiable peaks. Despite finding optimal conditions for deiodinating the model system in **Chapter 4.4**, the deiodination of the polymer was not as successful under the same conditions.

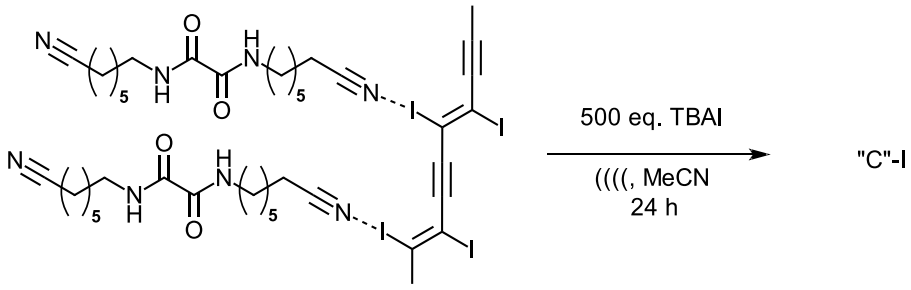

Scheme 3.5. Deiodination of PIDA cocrystals using TBAI in MeCN

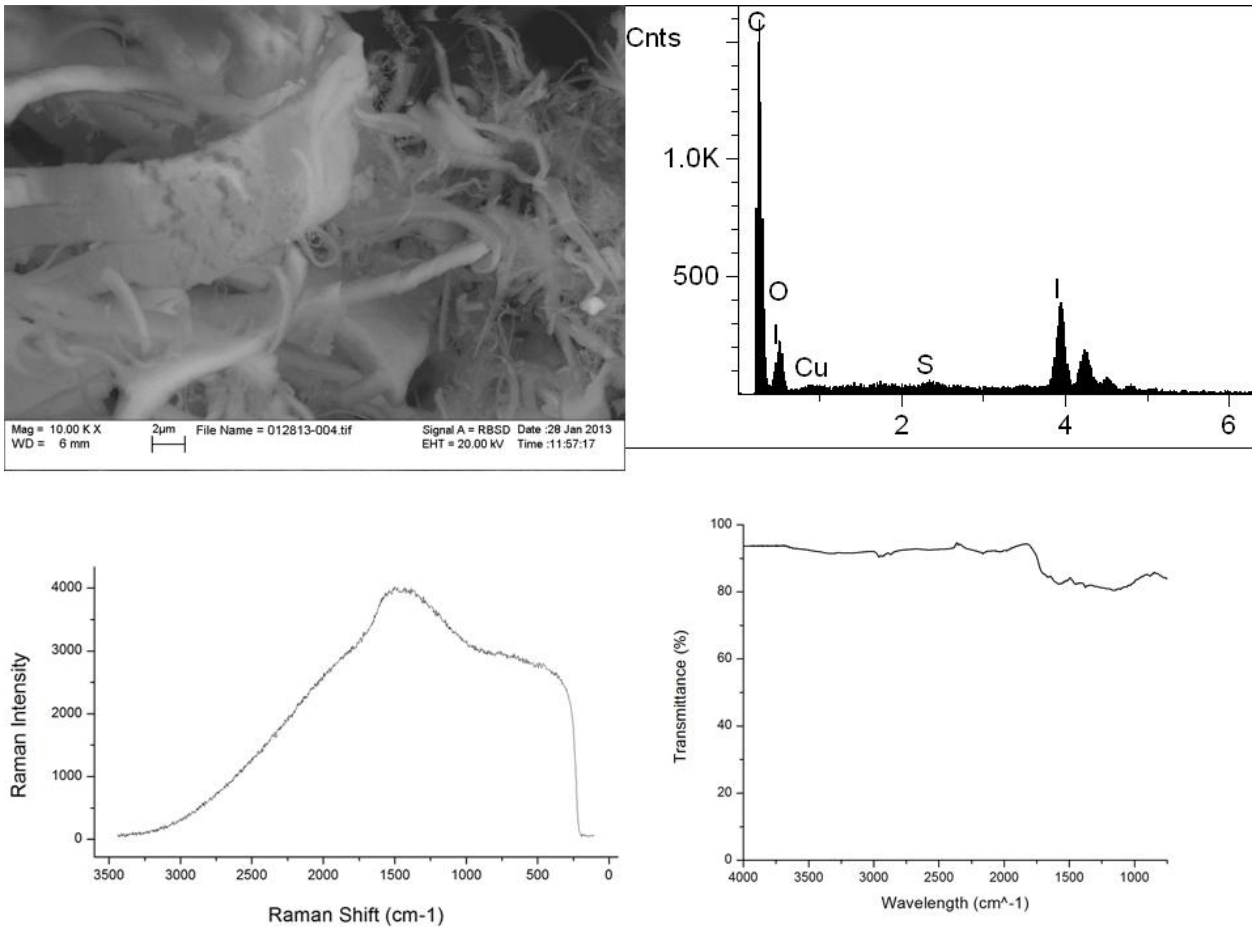

Figure 3.15. Top left: SEM image of the deiodinated PIDA cocrystal with TBAI in MeCN; Top right: EDS analysis; Bottom left: Raman spectra; Bottom right: IR spectra

One of the simplest reagents reported to induce dehalogenation is KI.[8] KI is also known to complex with iodine according to the well known triiodide equilibrium. The use of KI as a reagent for inducing deiodination is advantageous because its water solubility makes it easy to wash out. PIDA cocrystals have thus been subjected to deiodination induced by KI (**Scheme 3.6**). KI is moderately soluble in MeCN and did not completely dissolve. Deiodination was observed, however, as the solution changed from colorless to a dark reddish-brown. This observation is consistent with formation of triiodide by complexation of iodide with iodine. **Figure 3.16** shows that iodine is still present in the product of KI-treated PIDA cocrystals. The iodine present is not from KI as the potassium peak in the EDS spectrum is not prevalent. Raman

spectroscopy shows amorphous graphite-like carbon is once again obtained. The poor signal-to-noise in the Raman spectrum suggests a low degree of order in the structure.

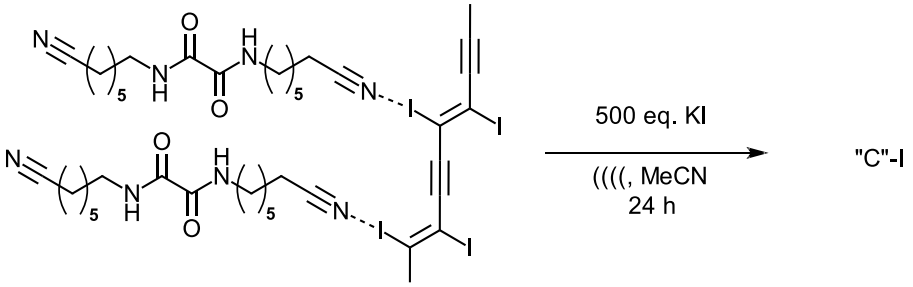

Scheme 3.6. Deiodination of PIDA cocrystals using KI

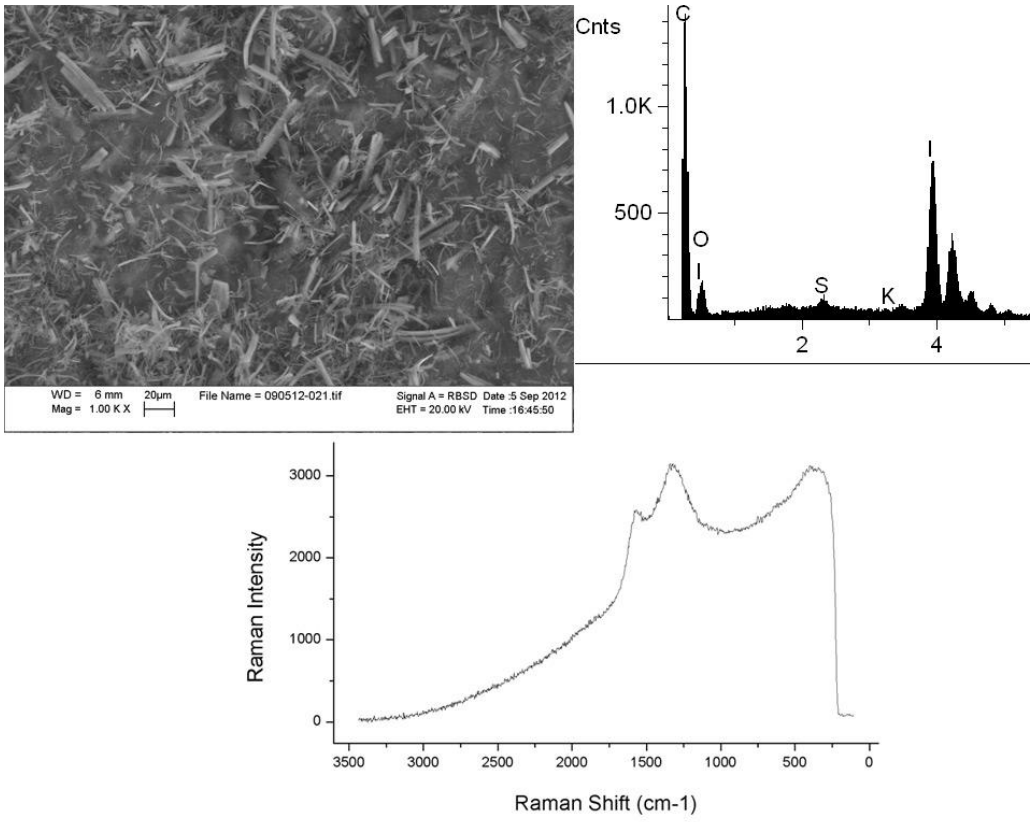

Figure 3.16. Top left: SEM image of polymerized **4e·5** deiodinated by KI in MeCN; Top right: EDS analysis; Bottom: Raman spectrum of polymerized **4e·5** deiodinated by KI in MeCN

The experiments conducted thus far showed that, in the presence of a reducing agent, full iodine elimination is observed, but the reducing agent itself gets incorporated into the product. A biphasic reaction was thus tested to see if having the reagents in separate phases could minimize exposure of the polymer to the reducing agent (**Scheme 3.7**). The rationale behind the conditions

in **Scheme 3.7** was to minimize the exposure of the polymer to sodium bisulfite, to make incorporation of sulfur into the final product more difficult. Nitromethane is immiscible with water and favors the elimination reaction. The results of the experiment show residual levels of iodine, but sulfur is still present (**Figure 3.17**). The fibrous morphology is similar to products obtained from all previous experiments in which a tetrabutylammonium salt was used as a deiodinating reagent. The Raman spectrum is consistent with amorphous graphite-like carbon, but the signal-to-noise in the Raman spectrum is quite poor. The IR spectrum does not show anything significant, which indicates there are no organic compounds adsorbed into the product.

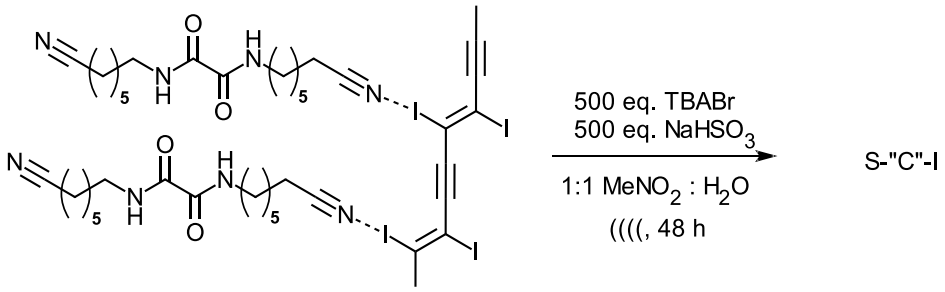

Scheme 3.7. Deiodination of PIDA cocrystal under biphasic conditions

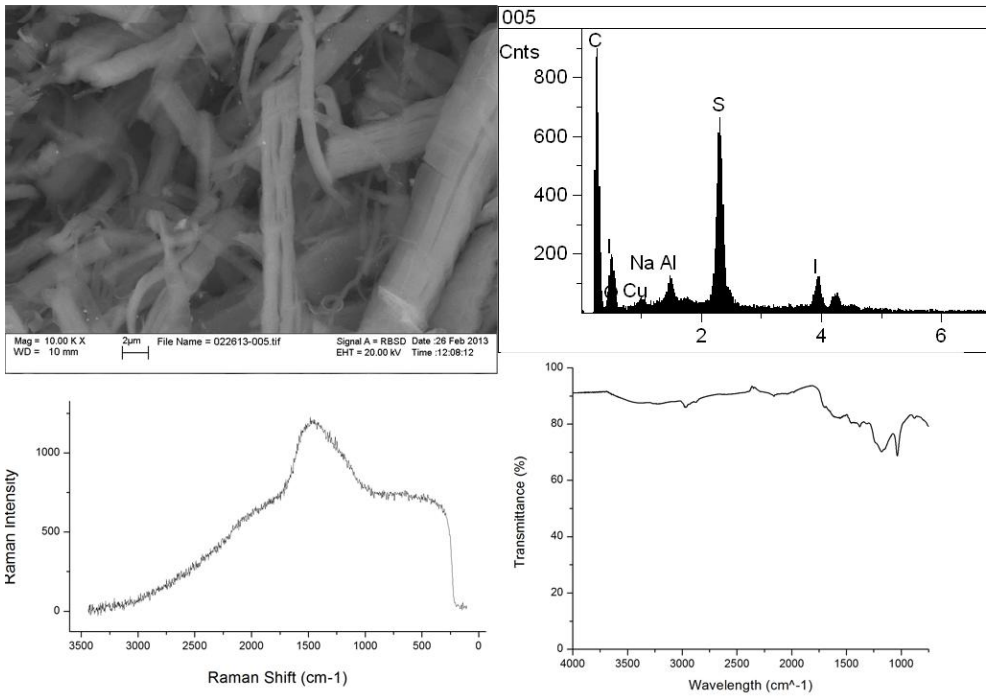

Figure 3.17. Top left: SEM image of the product in **Scheme 3.7**; Top right: EDS analysis; Bottom left: Raman spectra; Bottom right: IR spectra

It appears sulfur inclusion into the final product is unavoidable when a sulfur-based reducing agent is used. Deiodination in the absence of a reducing agent is thus desirable. Tetrabutylammonium bromide (TBABr) can induce deiodination, albeit at a much slower rate than TBAI, as per **Chapter 4**. TBABr is also a better choice for inducing deiodination, since it cannot contaminate the final product with iodine, as was possible with the conditions in **Scheme 3.5**. Another particular concern for these deiodination reactions is the heat generated by the sonicator. Prolonged periods of sonication result in appreciable heating of the reaction mixture. This heating can have an effect on the reaction, and may even result in the decomposition of PIDA. As a result, the sonicator was cooled using ice. **Scheme 3.8** shows the conditions used for the elimination reaction in an ice-cooled sonicator bath. The reaction was only carried out during the day such that the sonicator bath could be iced. The reaction vessel was safely stored in a -7°C freezer when not in the sonicator bath. A black compound is obtained from the reaction in **Scheme 3.8**. The SEM image shows similar product morphology as was seen in previous efforts. The EDS spectra shows iodine is still present in addition to a trace amount of bromine. The Raman spectrum in **Figure 3.18** shows polymer, which indicates the reaction did not go to completion. This observation is the reason for the large iodine peaks observed in the EDS spectrum. One possibility is that icing the sonicator bath slowed or disfavored the elimination reaction.

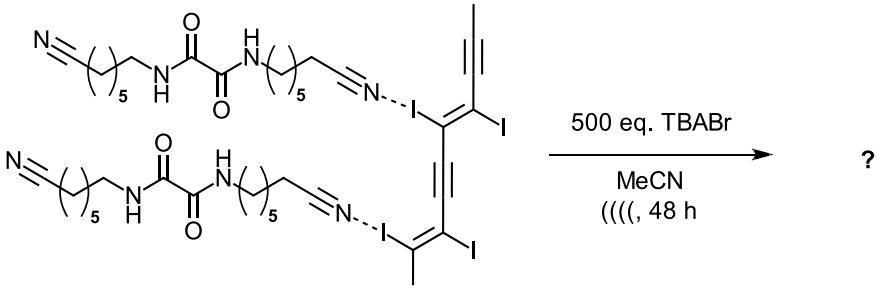

Scheme 3.8. Conditions for the deiodination of PIDA cocrystals using only TBABr

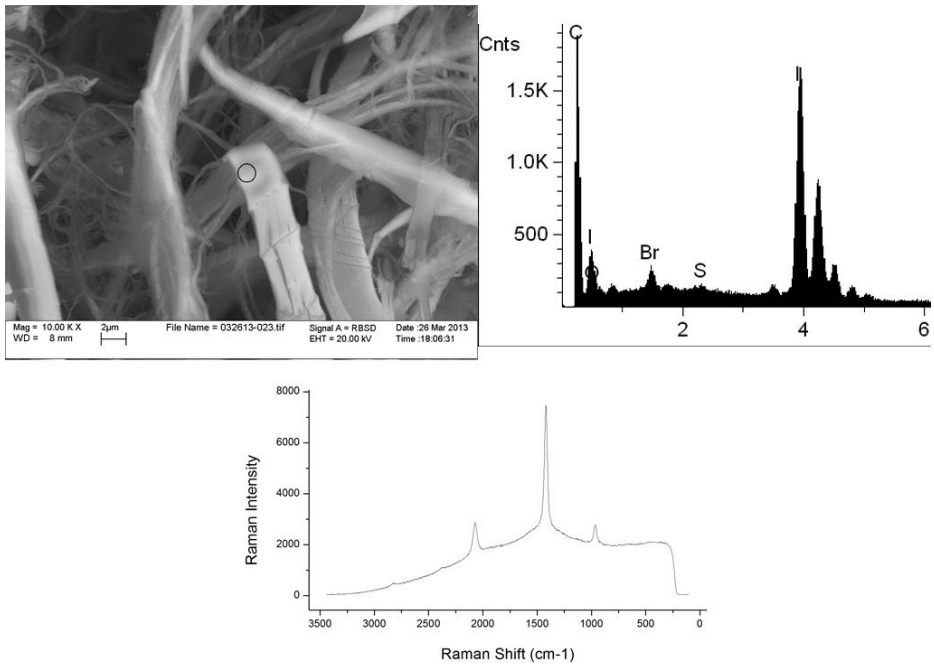

Figure 3.18. Top left: SEM image of deiodinated product obtained from the reaction of polymerized **4e**·**5** with 500 eq. TBABr in MeCN; Top right: EDS analysis; Bottom: Raman spectra show PIDA cocrystals are still present

Regardless of the conditions used, each of the aforementioned experiments gave similar results. If any sulfur reducing agent was present, it became incorporating into the final product. If a reducing agent is not used, the product still contains iodine after workup. These observations suggest complete deiodination of PIDA requires some additional reagent to take the place of iodine in the polymer.

3.5 Deiodination of PIDA Using Triphenylphosphine and Thiourea

Reagents aside from pyrrolidine and halides can induce dehalogenation. Yasui and coworkers reported that trivalent phosphorus compounds can debrominate vicinal dibromoalkanes.[9] The conditions employed by Yasui and coworkers were modified to include an excess of PPh_3 to favor rapid deiodination of PIDA cocrystals. Yasui's conditions also have the benefit of converting iodine into MeI and HI (**Scheme 3.9**). PIDA cocrystals were not fully deiodinated with 250 eq. of PPh_3 in 10:1 MeCN:H_2O. The EDS analysis in **Figure 3.19** shows both iodine and phosphorus have been incorporated into the product. One difference between the

product from the conditions in **Scheme 3.9** and past reaction with thiosulfate or bisulfite is that the PPh_3-treated sample does not form a suspension in water. The phenyl groups in PPh_3 appear to impart a hydrophobic character into the product. The Raman spectrum of the product of the TPP-treated PIDA cocrystals shows that the product is amorphous graphite-like carbon. The signal in the Raman spectrum is very poor and cannot be used to make any other claims definitively.

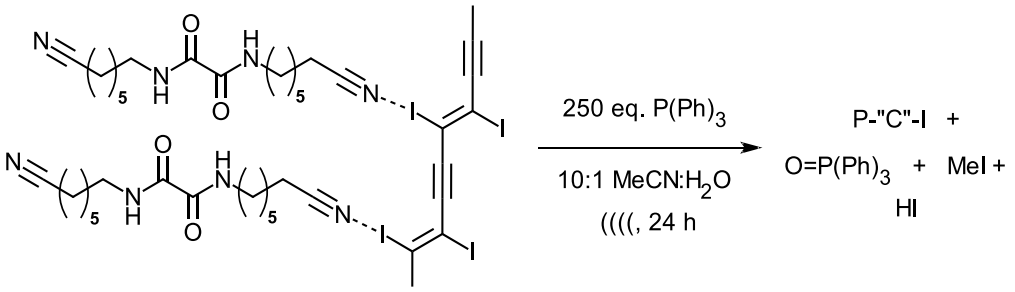

Scheme 3.9. Reaction of PIDA cocrystals with triphenylphosphine

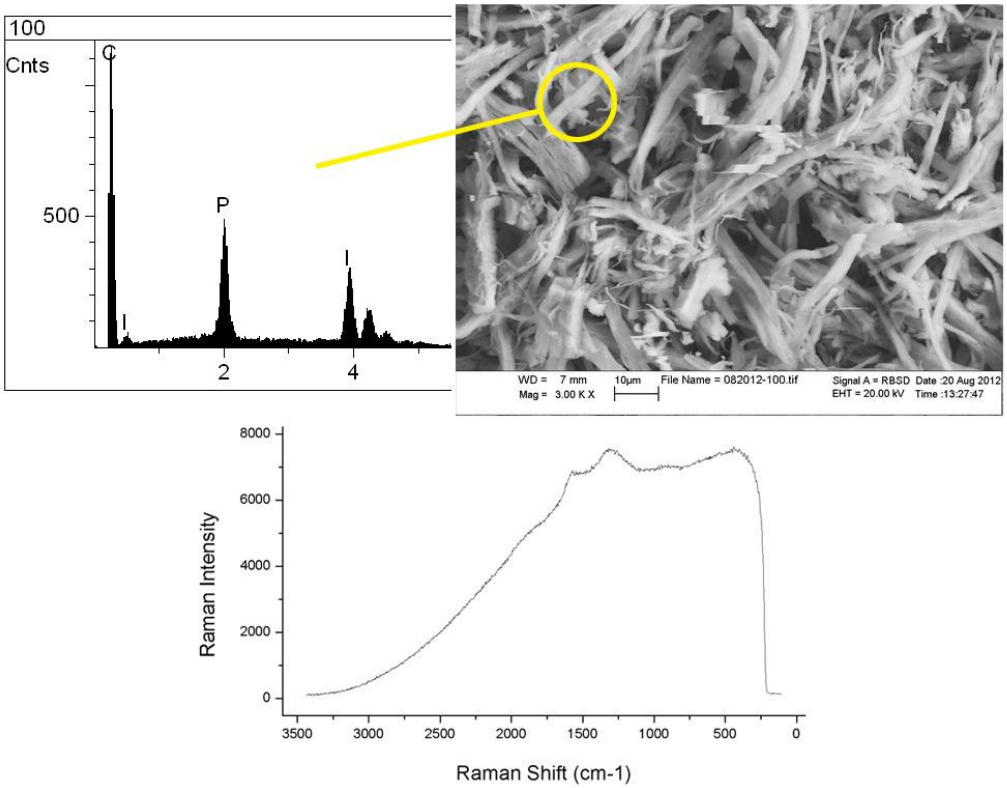

Figure 3.19. Top right: SEM graphical image of the product of polymerized **4e·5** after reaction with 250 eq. of TPP in 10:1 MeCN:H_2O; Top left: EDS analysis; Bottom: Raman spectrum

Thiourea is another reducing agent known to form a complex with free iodine.[10] It is about as fast as iodine at inducing dehalogenation in dibromoalkanes, according to Baciocchi.[11] Unlike thiosulfate and bisulfite, thiourea does not have any oxygen groups that could be included in the final product. Despite the moderate solubility of thiourea, deiodination was observed. The reaction mixture changed from colorless to a dark reddish-brown, indicating the PIDA cocrystals were undergoing deiodination. **Figure 3.20** shows that the product of thiourea-treated PIDA cocrystals still has iodine present in some form. Sulfur is still incorporated into the product, as was seen with thiosulfate and bisulfite. Interestingly, the final product also forms brown suspensions reasonably well in water. The Raman spectrum shows poor signal to noise but suggests amorphous graphite-like carbon.

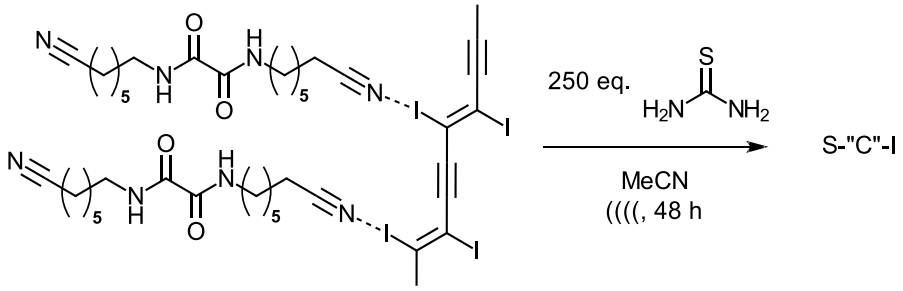

Scheme 3.10. Reaction between PIDA cocrystals and thiourea in MeCN

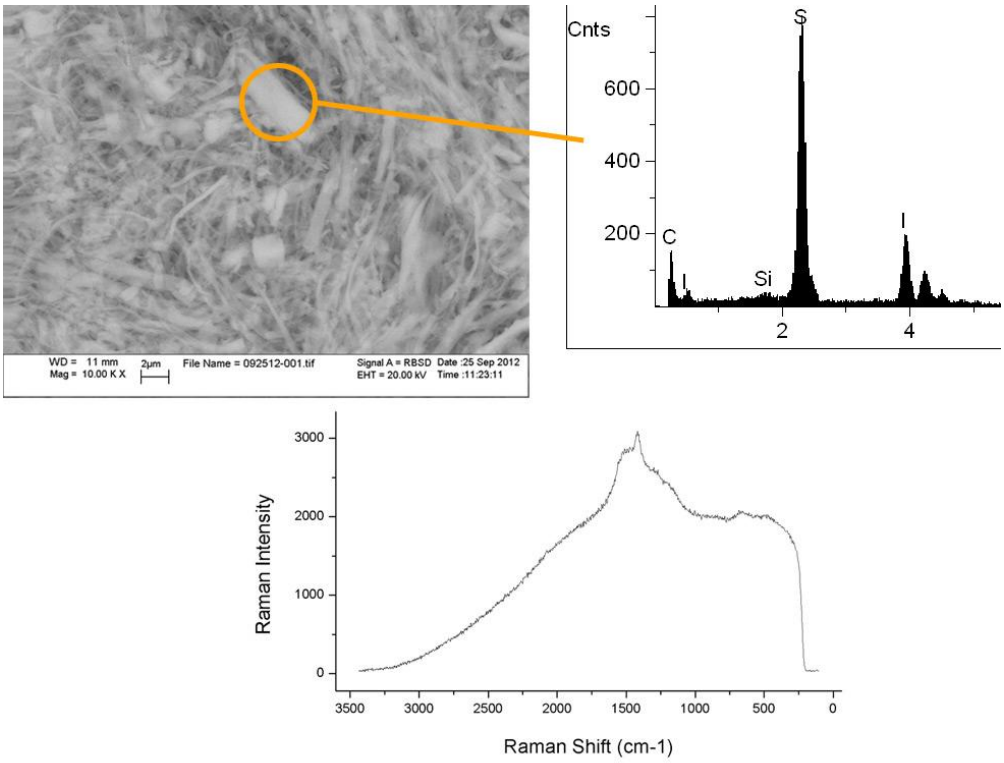

Figure 3.20. Top left: SEM graphical image of the product from the reaction of polymerized **4e·5** with thiourea in MeCN; Top right: EDS analysis; Bottom: Raman spectrum

The results of the TPP and thiourea-treated samples are consistent with the halide ion induced deiodination. The final product is amorphous graphite-like carbon with the incorporation of either sulfur or phosphorus. The mechanism by which these atoms are incorporated is unknown. Heteroatoms may be covalently bonded, trapped in, or adsorbed onto the amorphous graphite-like carbon material.

3.6. Conclusion

The pyrrolidine-induced deiodination of PIDA cocrystals in MeCN appears to give the most promising results. Under these conditions, sonication is not necessary thus eliminating the possibility ultrasonic-induced chemistry. The stirred solution of pyrrolidine in MeCN also yields an oil as opposed to the solid obtained under the other reaction conditions discussed here. Future efforts can be given to forming better quality thin films for analysis. Such analysis may give insight as to what becomes of the carbon-rich material after the polymerized cocrystals react with

pyrrolidine. ESR spectroscopy would be useful in determining if there are any unpaired electrons in the product making NMR analysis difficult.

The tetrabutylammonium salt-treated PIDA cocrystals all show similar results regardless of reaction conditions. Consistently, when a reducing agent is used, heteroatoms are incorporated into the final product. If a reducing agent is not used, the final product still contains iodine. This could be the result of iodide acting as a reducing agent, however. Future effort can be given to forming water suspensions of the sulfur-functionalized material. It would be ideal if thin films can be formed from this material for further Raman, IR, and UV analysis. X-ray Photoelectron Spectroscopy (XPS) is a technique that can be used to determine whether a C-S bond exists or not. This technique can also be used determine the oxidation state of sulfur, which gives insight as to the functionality in the material. This material could potentially serve as a catalyst support.

3.7 Experimental

All reagents and solvents were used from the stock bottles without further purification unless otherwise stated. All reactions were conducted under an argon atmosphere by bubbling argon through the headspace and finally removing all needles from the septum. The septum sealed flask was then transferred to the sonicator. The reactions carried out under sonication were run in a 2.8 L Branson Ultrasonic cleaner at 40-kHz. SEM imaging was run by a LEO1550 from Zeiss. The EDS analysis was conducted on an EDAX Phoenix/Sapphire with software and electronics from iXRF. The samples for SEM/EDS analysis were mounted onto conductive carbon adhesive tape. IR spectra were obtained on a Nicolet iS10 with an ATR attachment for solid state analysis. Raman spectra were collected using a 785-nm Class I laser on a Thermo Nicolet Almega dispersive Raman spectrometer coupled with an infinity-corrected, confocal design microscope. The data were collected in reflection mode of the microscope with a slit width of 25 μm. UV-vis spectra were obtained on a Cary-100 UV/Visible Scan

Spectrophotometer in a quartz cuvette. All data were analyzed using the Origin Pro 8 Pro Software (OriginLab Corporation, USA). Stoichiometric calculations for all elimination reactions were based on the amount of monomer used to prepare the PIDA cocrystals. For safety purposes, no more than 100 mg of PIDA cocrystals are used for any experiment.

Pyrrolidine I_2 Elimination (Scheme 3.2): In an argon flushed rbf, 3 mL of pyrrolidine and 3 mL of deionized water were mixed into solution. Polymerized PIDA cocrystals (25.3 mg) of host **4e** were then added to the reaction mixture and sonicated for 24 h. The reaction mixture was then divided in equal volume amongst 4 glass centrifuge tubes. The tubes were subject to centrifugation at 3000 rpm for 40 min. Each tube was then decanted, and the liquid was saved for NMR analysis. Acetone (3 mL per tube) was added to wash away residual organics, and the mixture was sonicated for an additional hour followed by centrifugation for 40 min. The supernatant was decanted, saved for further analysis, and fresh acetone was added. This process was repeated for a total of 5 times. The sample was then stored in a -8°C freezer in 3 mL of acetone.

Pyrrolidine PIDA Co-crystal Treatment in MeCN (Scheme 3.3): In an argon-flushed flask with 20 mL of MeCN, PIDA cocrystal (50.5 mg, 0.052 mmol) were added. Pyrrolidine (2.8 mL, 2.4536 g, 34.5 mmol) was then added to the system. The reaction was stirred at room temperature for 48 h. An aliquot of the reaction mixture was extracted and diluted to perform UV analysis. The remaining reaction mixture was then divided equally between 4 polypropylene centrifuge tubes. The tubes were subject to centrifugation at 3000 rpm for 20 min. The supernatant from each tube was then decanted, and combined. Some material was lost due to spillage while combining the supernatant from one of the tubes. The remaining residue in the centrifuge tubes was dissolved in acetone (25 mL) and stored in the freezer for future analysis.

The acetonitrile from the reaction mixture was evaporated from the combined supernatant solutions to give a dark colored reddish-brown oil of mass 0.0392 g. Before analysis, the oil was subjected to high vacuum for 30 min. The reddish-brown oil was subjected to NMR and IR analysis to confirm removal of host **4e**.

TBAI I_2 Elimination in Nitromethane (Scheme 3.4): In an argon-flushed rbf with 20 mL of nitromethane, polymerized cocrystals (20.2 mg, 0.022 mmol) of the host **4e** were added. Tetrabutylammonium iodide (4.10 g, 11.1 mmol) was then added to the system. The reaction was sonicated for 24 h before being divided equally among 4 glass centrifuge tubes. The tubes were subjected to centrifugation at 3000 rpm for 40 min. Each tube was then decanted, and the liquid was saved for IR analysis. Acetone (3 mL per tube) was added and subjected to sonication for an additional hour followed by centrifugation for 40 min. The supernatant was decanted, saved, and fresh acetone was added. This process was repeated for a total of 5 times. An additional 3 mL of acetone was then added before 5 min of sonication. The sample was then stored in a -8°C freezer. IR analysis of the final wash solution confirmed the complete removal of the host.

TBAI I_2 Elimination in EtOH / Water (Scheme 3.4): In an argon-flushed rbf with 20 mL of 1:1 EtOH:H_2O, polymerized cocrystals (20.5 mg, 0.022 mmol) of host **4e** were added. Tetrabutylammonium iodide (4.11 g, 11.1 mmol) was then added to the system. The reaction was sonicated for 24 h before being divided equally among 4 glass centrifuge tubes. The tubes were subjected to centrifugation at 3000 rpm for 40 min. Each tube was then decanted, and the liquid was saved for IR analysis. Acetone (3 mL per tube) was added and subjected to sonicated for an additional hour followed by centrifugation for 40 minutes. The supernatant was decanted, saved, and fresh acetone was added. This process was repeated for a total of 5 times. An additional 3

mL of acetone was then added before 5 min of sonication. The sample was then stored in a -8°C freezer. IR analysis of the final wash solution confirmed complete host removal.

TBABr I_2 Elimination in MeOH / Water (Scheme 3.4): In an argon-flushed rbf with 20 mL of 1:1 MeOH:H_2O, polymerized cocrystals (20.2 mg, 0.022 mmol) of host **4e** were added. Tetrabutylammonium bromide (3.58 g, 11.1 mmol) and sodium thiosulfate (2.75 g, 11.1 mmol) was then added to the system. The reaction was subjected to sonication for 48 h before being divided equally among 4 glass centrifuge tubes. The tubes were subjected to centrifugation at 3000 rpm for 40 min. Each tube was then decanted and the liquid was saved for IR analysis. Water (5 mL) was then added to each tube and subjected to sonication for 30 min. The tubes were subjected to centrifugation at 3000 rpm for 15 min and the liquid was decanted. The samples were subjected to 3 water washes. Acetone (3 mL per tube) was added and sonicated for an additional hour followed by centrifugation for 40 min. The supernatant was decanted, saved, and fresh acetone was added. This process was repeated for a total of 5 times. An additional 3 mL of acetone was then added before 5 min of sonication. The sample was then stored in a -8°C freezer. IR analysis of the final wash confirmed the complete removal of the host.

TBAI PIDA Co-crystal Treatment in MeCN (Scheme 3.5): In an argon-flushed flask with 80 mL of MeCN, PIDA cocrystals (51.1 mg, 0.055 mmol) and tetrabutylammonium iodide (10.1578 g, 27.5 mmol) were added. The reaction was subjected to sonication for 24 h before being divided equally among 4 polypropylene centrifuge tubes. The tubes were subjected to centrifugation at 3000 rpm for 20 min. Each tube was then decanted, and the liquid was combined. Water (20 mL) was added to each tube and the mixture was subjected to sonication for 30 minutes before centrifugation. The water was decanted, and the process repeated 4 times. Acetone (20 mL) was then added to each tube, and the mixture was subjected to sonication for

30 min before centrifugation. The liquid was decanted, and the process repeated 4 times. After the decanting the final wash, 2 mL of acetone was used to wash the contents of the centrifuge tubes into a 20 mL glass vial. The solvent was then removed under reduced pressure and then subjected to high vacuum for 1 hour. IR analysis of the final wash solution confirmed the complete host removal. The black solid was obtained in a mass of 0.0125 g.

KI Treated PIDA Co-crystal Treatment in MeCN (Scheme 3.6): In an argon-flushed flask with 80 mL of MeCN, PIDA cocrystals (51.0 mg, 0.055 mmol) and KI (3.6011 g, 13.7 mmol) were added. The reaction was subjected to sonication for 48 h before being divided equally among 4 polypropylene centrifuge tubes. The tubes were subjected to centrifugation at 3000 rpm for 20 min. Each tube was then decanted, and the liquid was combined. Water (20 mL) was added to each tube, and the mixture was subjected to sonication for 30 min before centrifugation. The liquid was decanted, and the process repeated 4 times. Acetone (20 mL) was added to each tube, and the mixture was subjected to sonication for 30 min before centrifugation. The liquid was decanted and the process repeated 4 times. After the decanting the final wash, 2 mL of acetone was used to wash the contents of the centrifuge tubes into a 20 mL glass vial. The solvent was then removed under reduced pressure and then subjected to high vacuum for 1 hour. IR analysis of the final wash solution confirmed the complete host removal. The black solid was obtained in a mass of 0.0105 g.

TBABr / $NaHSO_3$ Biphasic Solvent System (Scheme 3.7): In an argon-flushed flask with 80 mL of 1:1 $MeNO_2$:H_2O, PIDA cocrystals (50.1 mg, 0.050 mmol) were added. Tetrabutylammonium bromide (8.8605 g, 27.6 mmol) and sodium bisulfite (1.4301 g, 27.6 mmol) were then added to the system. The reaction was subjected to sonication for 48 h before being divided equally among 4 polypropylene centrifuge tubes. The tubes were subjected to

centrifugation at 3000 rpm for 20 min. Each tube was then decanted and the liquid was combined. Water (20 mL) was added to each tube and the mixture was sonicated for 30 min before centrifugation. The liquid was decanted, and the process repeated 4 times. Acetone (20 mL) was added to each tube, and the mixture was subjected to sonication for 30 min before centrifugation. The liquid was decanted, and the process repeated 4 times. The centrifuge tubes were allowed to evaporate to dryness after which the black solid was scraped out into a 20 mL vial. Prior to analysis, the sample was subjected to high vacuum for 1 hour. IR analysis of the final wash solution confirmed the complete host removal. The black solid was obtained in a mass of 0.0203 g.

TBABr PIDA Co-crystal Treatment in MeCN (Iced Sonicator Bath) (Scheme 3.8): In an argon-flushed flask with 80 mL of MeCN, PIDA cocrystals (50.8 mg, 0.050 mmol) were added. Tetrabutylammonium bromide (8.8601 g, 27.5 mmol) was then added to the system. The reaction was subjected to sonication for 48 h before being divided equally among 4 polypropylene centrifuge tubes. The tubes were subjected to centrifugation at 3000 rpm for 20 min. Each tube was then decanted, and the liquid was combined. Water (20 mL) was added to each tube and the mixture was subjected to sonication for 30 min before centrifugation. The liquid was decanted, and the process repeated 4 times. Acetone (20 mL) was added to each tube and the mixture was subjected to sonication for 30 min before centrifugation. The liquid was decanted and the process repeated 4 times. The centrifuge tubes were allowed to evaporate to dryness after which the black solid was scraped out into a 20 mL vial. Prior to analysis, the sample was subjected to high vacuum for 1 hour. IR analysis of the final wash solution confirmed the complete host removal. The black solid was obtained in a mass of 0.0392 g.

Triphenylphosphine Treated PIDA Co-crystals in MeCN (Scheme 3.9): In an argon-flushed flask with 80 mL of 10:1 MeCN:MeOH, PIDA cocrystals (50.8 mg, 0.055 mmol), and triphenylphosphine (3.6011 g, 13.7 mmol) were added. The reaction was sonicated for 48 h before being divided equally among 4 polypropylene centrifuge tubes. The tubes were subjected to centrifugation at 3000 rpm for 20 min. Each tube was then decanted, and the liquid was combined. Water (20 mL) was added to each tube, and the mixture was subjected to sonication for 30 minutes before centrifugation. The liquid was decanted, and the process repeated 4 times. Acetone (20 mL) was added to each tube, and the mixture was sonicated for 30 min before centrifugation. The liquid was decanted, and the process repeated 4 times. The centrifuge tubes were allowed to evaporate to dryness after which the black solid was scraped out into a 20 mL vial. Prior to analysis, the sample was subjected to high vacuum for 1 hour. IR analysis of the final wash solution confirmed the complete host removal. The black solid was obtained in a mass of 0.0421 g.

Thiourea Treated PIDA Co-crystals in MeCN (Scheme 3.10): In an argon-flushed flask with 80 mL of MeCN, PIDA cocrystal (50.2 mg, 0.055 mmol) and thiourea (1.0451 g, 13.7 mmol) were added. The reaction was subjected to sonication for 48 h before being divided equally among 4 polypropylene centrifuge tubes. The tubes were subjected to centrifugation at 3000 rpm for 20 min. Each tube was then decanted, and the liquid was combined. Water (20 mL) was added to each tube, and the mixture was subjected to sonication for 30 min before centrifugation. The liquid was decanted, and the process repeated 4 times. Acetone (20 mL) was added to each tube and the mixture was sonicated for 30 minutes before centrifugation. The liquid was decanted and the process repeated 4 times. The centrifuge tubes were allowed to evaporate to dryness after which the black solid was scraped out into a 20 mL vial. Prior to analysis, the

sample was subjected to high vacuum for 1 hour. IR analysis of the final wash solution confirmed the complete host removal. The black solid was obtained in a mass of 0.0346 g.

3.8 References

1. Chalifoux, W. A.; Tykwinski, R. R., Synthesis of polyynes to model the sp-carbon allotrope carbyne. *Nature Chemistry* **2010,** *2*, 967-971.
2. (a) Glaser, C., Beiträge zur Kenntniss des Acetenylbenzols. *Ber. Dtsch. Chem. Ges.* **1869,** *2*, 422-424; (b) Hay, A. S., Oxidative Coupling of Acetylenes. *J. Org. Chem.* **1962,** *27*, 3320-3321; (c) Eglinton, G.; Galbraith, A. R., 182. Macrocyclic acetylenic compounds. Part I. Cyclotetradeca-1 :3-diyne and related compounds. *J. Chem. Soc.* **1959,** *0*, 889-896.
3. Luo, L.; Wilhelm, C.; Young, C. N.; Grey, C. P.; Halada, G. P.; Xiao, K.; Ivanov, I. N.; Howe, J. Y.; Geohegan, D. B.; Goroff, N. S., Characterization and Carbonization of Highly Oriented Poly(diiododiacetylene) Nanofibers. *Macromolecules* **2011,** *44*, 2626-2631.
4. Luo, L.; Resch, D.; Wilhelm, C.; Young, C. N.; Halada, G. P.; Gambino, R. J.; Grey, C. P.; Goroff, N. S., Room-Temperature Carbonization of Poly(diiododiacetylene) by Reaction with Lewis Bases. *J. Am. Chem. Soc.* **2011,** *133*, 19274-19277.
5. Luo, L. Preparation and Comprehensive Characterization of Poly(diiododiacetylene) and Spectroscopic Studies of Its Reactions with Lewis Bases. Stony Brook University, Stony Brook, NY, 2009.
6. Luo, L.; Wilhelm, C.; Sun, A.; Grey, C. P.; Lauher, J. W.; Goroff, N. S., Poly(diiododiacetylene): Preparation, Isolation, and Full Characterization of a Very Simple Poly(diacetylene). *J. Am. Chem. Soc.* **2008,** *130*, 7702-7709.
7. (a) Krishna, C. M.; Kondo, T.; Riesz, P., Sonochemistry of Alcohol-Water Mixtures - Spin -Trapping Evidence for Thermal-Decomposition and Isotope-Exchange Reactions. *J. Phys. Chem.* **1989,** *93*, 5166-5172; (b) Okitsu, K.; Nakamura, H.; Takenaka, N.; Bandow, H.; Maeda, Y.; Nagata, Y., Sonochemical reactions occurring in organic solvents: reaction kinetics and reaction site of radical trapping with 1,1-diphenyl-2-picrylhydrazyl. *Res. Chem. Intermediat.* **2004,** *30*, 763-774; (c) Forney, M. W.; Poler, J. C., Sonochemical Formation of Methyl Hydroperoxide in Polar Aprotic Solvents and Its Effect on Single-Walled Carbon Nanotube Dispersion Stability. *J. Am. Chem. Soc.* **2010,** *132*, 791-797.
8. (a) Winstein, S.; Pressman, D.; Young, W. G., Investigations on the Stereoisomerism of Unsaturated Compounds. V. A Mechanism for the Formation of Butenes from 2,3-Dibromobutanes by the Action of Iodide Ion. *J. Am. Chem. Soc.* **1939,** *61*, 1645-1647; (b) Miller, S. I.; Noyes, R. M., Iodide-ion Catalysis of the Elimination of Iodine from trans-Diiodoethylene and of the Addition of Iodine to Acetylene. *J. Am. Chem. Soc.* **1952,** *74*, 3403-3406.
9. Yasui, S.; Itoh, K.; Ohno, A., Kinetic study on debromination of vic-dibromides with trivalent phosphorus compounds. *Heteroat. Chem.* **2001,** *12*, 217-222.
10. de Faria, D. L. A.; Gonçalves, N. S.; Santos, P. S., Vibrational spectra of iodine and bromine thiourea complexes. *Spectrochim. Acta A* **1989,** *45*, 643-647.
11. Baciocchi, E.; Lillocci, C., Dehalogenation reactions of vicinal dihalides. Part III. Dehalogenations of 1-chloro-2-iodo-1,2-diphenylethane induced by a variety of nucleophiles. The nucleophilic reactivity towards iodine. *J. Chem. Soc., Perkin Trans. 2* **1973**, 38-41.

Chapter 4: Probing the Mechanism of Iodine Elimination with Small Molecules

4.1 Small Molecule Modeling

Understanding the mechanism by which iodine is eliminated from PIDA is an important aspect of this project. An understanding of the fundamental chemistry can give insight as to how the reaction could be exploited. Studying the mechanism using PIDA, however is time consuming, expensive, and limited in terms of the methods available for characterization. The product obtained from the deiodination of PIDA is insoluble in organic solvents, though suspensions can be formed in water. The poor solubility and disorder of the product limits structural characterization to methods such as X-ray crystallography and solid-state NMR. Solid state NMR would be challenging since the deiodinated product lacks protons, and would require long relaxation times. The long relaxation times will have a negative impact on the signal-to-noise ratio. Another issue is the conductive nature of the material. Luo and coworkers found the deiodinated product would not spin.[1] One possible explanation for the apparent lack of spinning is eddy currents.

The limits of probing the mechanism of deiodination using the polymer can be overcome by using an appropriate small molecule model system. The advantage of a small molecule model system is that it can be readily synthesized from common organic building blocks. Small molecules can be studied using solution-state NMR and possibly X-ray crystallography. A small molecule model will also make screening reaction conditions possible, since such compounds can be prepared on a larger scale than PIDA.

4.2 Proposing and Synthesizing a Small Molecule Model for PIDA

PIDA possess 2 main structural groups. These groups include an *E*-diiodoalkene moiety and a conjugated pi system. This functionality was taken into consideration for the design of a model (compound **10, Figure 4.1**) for PIDA. Compound **10** features a single repeat unit of

PIDA. Phenyl groups were chosen to model continuous conjugation. **Scheme 4.1** below details the synthetic route initially proposed to synthesize enediyne **10**. Iodination of triple bonds is relatively difficult because molecular iodine is not always sufficiently electrophilic. For successful iodination, the iodine is usually activated with a Lewis acid. Activation of molecular iodine to convert diol **11** into diol **12** was achieved by using conditions from Luidhardt and coworkers in a solvent system that can dissolve diol **11**.[2] The conversion of diol **12** to enediyne **13** could not be carried out successfully. After workup a white solid was obtained in nearly quantitative yield that has a melting point range from 72°C-74°C. NMR analysis and the melting point data indicated the products of the reaction were exclusively homocoupled phenylacetylene and diol **11**. Interestingly and unexpectedly, iodine was eliminated from **12** under relatively mild conditions.

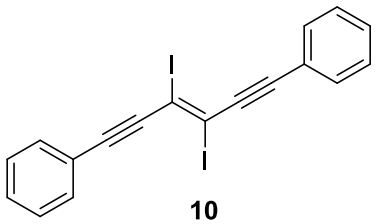

Figure 4.1. Proposed small molecule model for PIDA

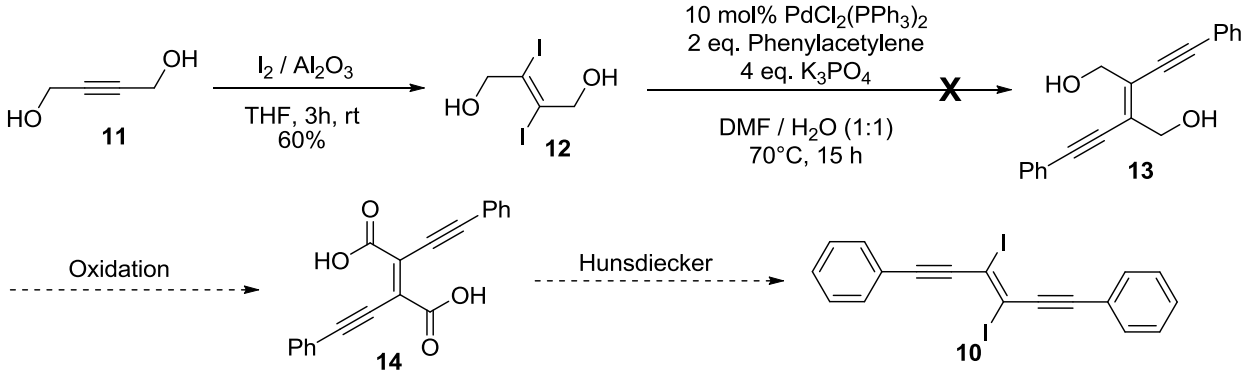

Scheme 4.1. Proposed synthesis of model compound **10**

Other Sonogashira conditions (**Table 4.1**) were tested to continue with the synthesis of the small molecule model but iodine elimination was found to be the favored reaction. Each of

the reaction conditions in **Table 4.1** resulted in homocoupled alkyne and the elimination of iodine to afford diol **11**. When inorganic bases were used, such as K_3PO_4 or Cs_2CO_3, no elimination occurred until the reaction was heated. The results of these experiments seem to parallel the iodine elimination behavior of PIDA, but further investigation was carried out to confirm this observation. Diol **12** was subjected to Suzuki coupling (**Scheme 4.2**) conditions to further explore the reactivity of the *E*-diiodoalkene functional group. Attempted Suzuki coupling of diol **12** also resulted in the elimination of iodine and homocoupling of the boronic acid. The mechanisms of the Sonogashira and Suzuki couplings are slightly different, but both reactions resulted in iodine elimination. This observation indicates that, at least in the presence of Pd, iodine elimination may in fact be general to *E*-diiodoalkenes.

Table 4.1. Sonogashira condition screening.

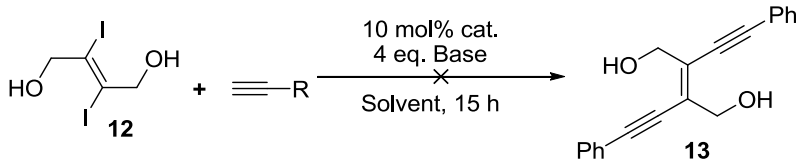

Alkyne	Base	Cat.	CuI	Solvent	T °C
R = Ph	DBU	$PdCl_2(PPh_3)_2$	0	A	70
R = Ph	K_3PO_4	$PdCl_2(PPh_3)_2$	0	A	70
R = Ph	Cs_2CO_3	$Pd_2(dba)_2$	0.2	B	rt->70
R = TIPS	DBU	$PdCl_2(PPh_3)_2$	0.2	A	rt
R = TIPS	K_3PO_4	$PdCl_2(PPh_3)_2$	0.2	A	rt->70
R = TIPS	DBU	$PdCl_2(PPh_3)_2$	0.2	B	0
R = TIPS	Cs_2CO_3	$PdCl_2(PPh_3)_2$	0.2	B	rt->70

Solvents: A) H_2O / i-PrOH (1:1) B) THF

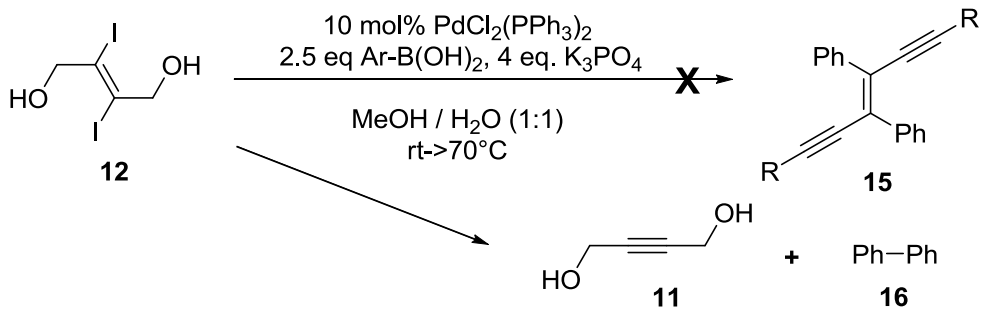

Scheme 4.2. Suzuki coupling of **12**

The elimination of iodine from diol **12** comes unexpectedly and prompted a detailed literature search for comparable reports of this reactivity. Literature references for coupling specifically with an *E*-diiodoalkene were not found, but Sonogashira couplings involving similar substrates have been reported. **Scheme 4.3** shows the coupling of an iodobromoalkene with trimethylsilyl acetylene, reported by Soscia.[3] Soscia did not use an *E*-diiodoalkene but rather a *Z*-iodobromoalkene. The elimination of IBr was not reported, and the desired product was formed in good yield. It is possible electronics may play a role since the ester group on Soscia's system in **Scheme 4.3** is electron-withdrawing.

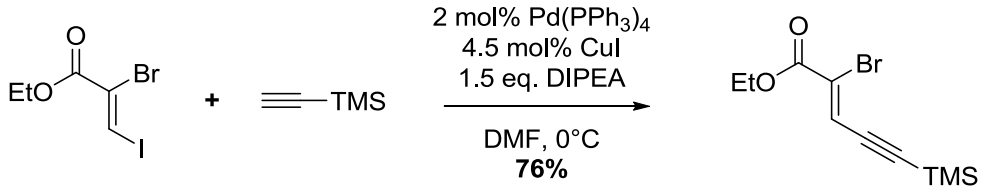

Scheme 4.3. Coupling of an iodobromoalkene under Sonogashira conditions[3]

Akita and Ozawa carried out the reaction in **Scheme 4.4** on tetraiodoethylene, which has some similarity to diol **12**.[4] It is not clear, however, that tetriodoethylene has the same reactivity as diol **12** since it does have additional iodo groups. No elimination was reported for this reaction, though the yield is moderate. The lower yield, however may be attributed to the presence of 4 possible reaction sites as opposed to just 1.

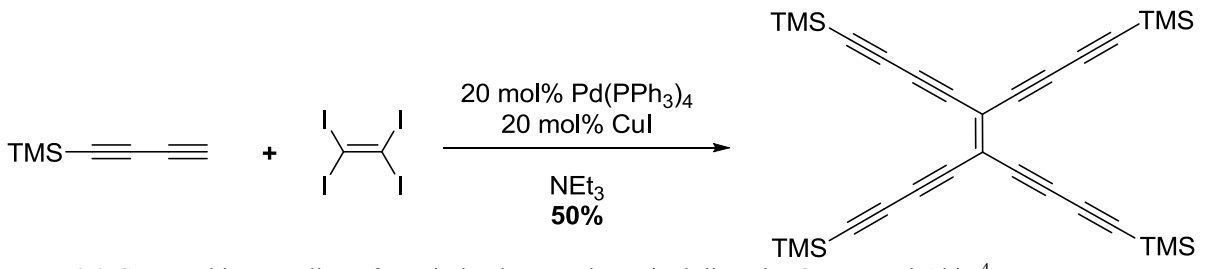

Scheme 4.4. Sonogashira coupling of tetraiodoethene and terminal diyne by Ozawa and Akita[4]

Baxendale and coworkers reported successful coupling of an *E*-dichloroalkene (**Scheme 4.5**), but chlorine is much worse of a leaving group than iodine.[5] Baxendale and coworkers do not report any elimination products, although such compounds may not be detected since they are gasses. Formation of Cl_2 under these conditions is also unlikely. The conditions in **Schemes 4.3-4.5** offer some precedent for the coupling of *E*-dihaloalkenes with terminal acetylenes, but diol **12** was only observed to undergo elimination.

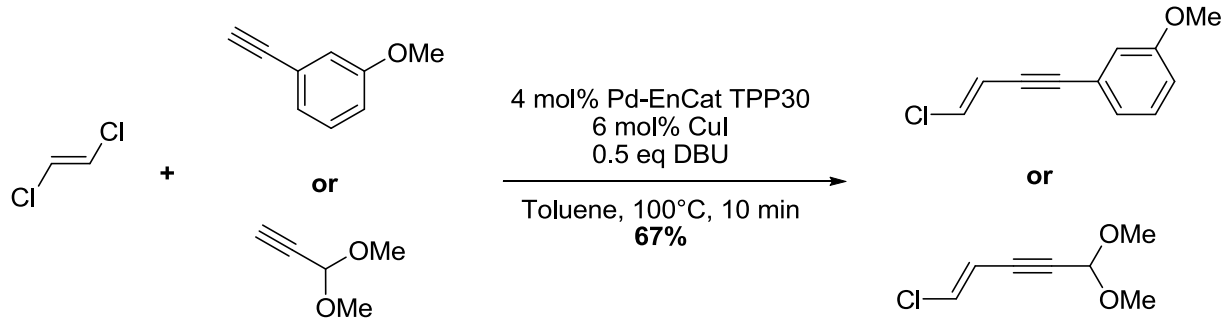

Scheme 4.5. Coupling of an E-dichloroalkene with terminal acetylenes. Pd-EnCat TPP30 = Palladium acetate and triphenylphosphine, microencapsulated in polyurea matrix[5]

A more detailed literature investigation revealed that, Chattopadhyay and Ranu reported conditions in which elimination may play a role in the synthesis of enynes (**Scheme 4.6**) from an *E*-diiodoalkene and simple vinyl substrate.[6] These conditions are similar to Sonogashira and Suzuki coupling conditions, so Chattopadhyay and Ranu provide precedence for elimination of iodine under such conditions. Chattopadhyay and Ranu propose a mechanism for this reaction as seen in **Figure 4.2**. Theoretically there are two possible routes in which an *E*-diiodoalkene can undergo elimination under the conditions reported by Chattopadhyay and Ranu. Route 1

maintains that HI is first eliminated in a syn fashion to form an iodoalkyne. The iodoalkyne then couples to a terminal alkene. This route was discredited by withholding the terminal alkene in an effort to try and isolate the iodoalkyne. Formation of the iodoalkyne was not observed thus route 1 was ruled out. Route 2 suggests that a Heck-type mechanism is involved followed by either a syn elimination (Route 2A) or E2 elimination (Route 2B). Theoretical calculations showed that route 2A is energetically more favorable by 0.3 kcal/mol.[6] Chattopadhyay and Ranu concluded that syn elimination according to route 2A is responsible for the formation of the enyne. Direct elimination of iodine from the *E*-diiodoalkene group in water by Na_2CO_3 was not observed.

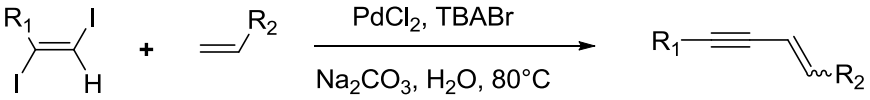

R_1 = alkyl, aryl
R_2 = CO_2Me, CO_2Bu, CN

Scheme 4.6. Coupling of a tri-substituted *E*-diiodoalkene with a mono-substituted alkene[6]

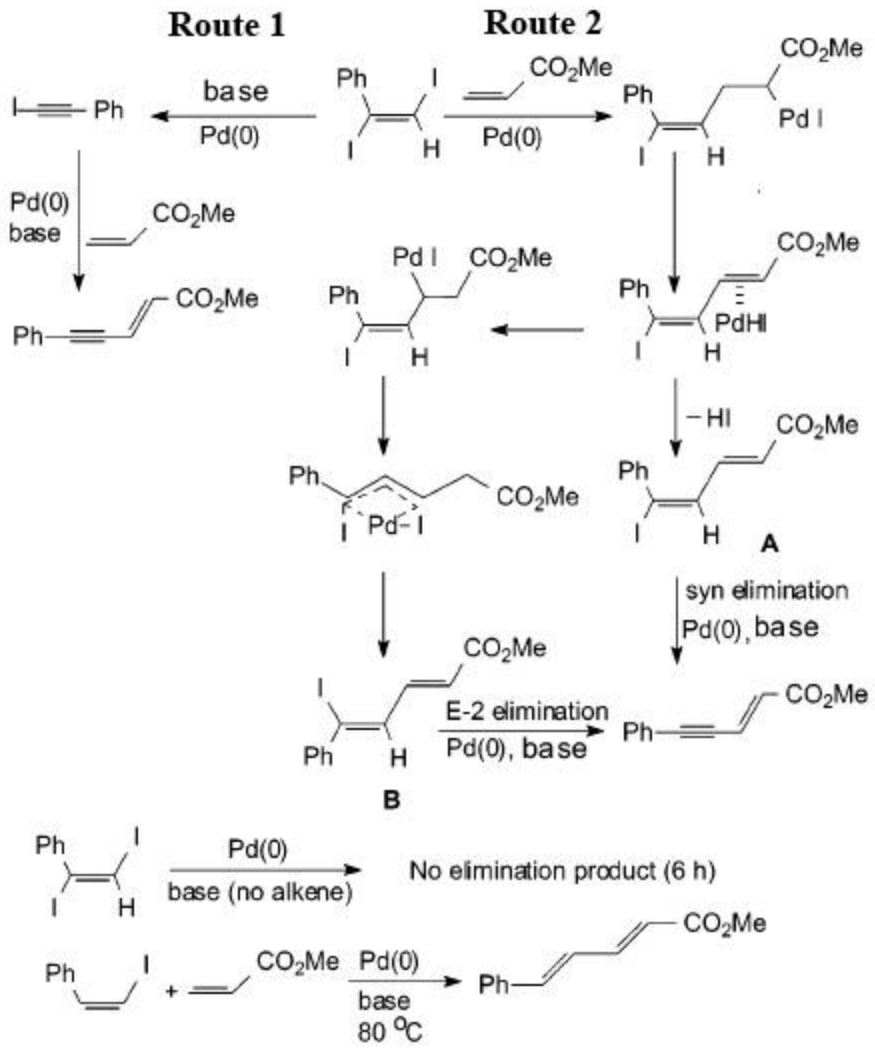

Figure 4.2. Mechanism proposed by Chattopadhyay and Ranu for coupling with *E*-diiodoalkenes. Reprinted with permission from Ref. 6. Copyright (2007) American Chemical Society.

The observed iodine elimination from diol **12** suggested that a conjugated system as found in enediyne **10** may not be necessary for model studies. As a result, simpler models were prepared from readily available alkynes that could easily be iodinated (**Figure 4.3**).

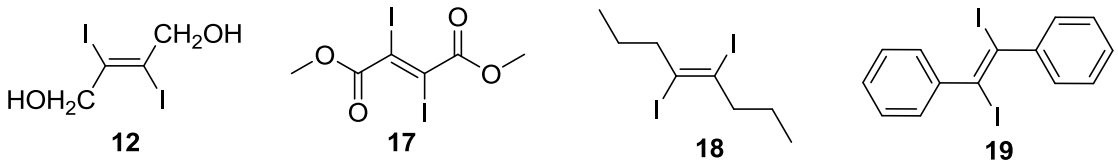

Figure 4.3. Model compounds with *E*-diiodoalkene functional group

Compounds **17-19** were iodinated (**Scheme 4.7**) using a procedure by Nikishin and co-workers.[7] Nikishin's procedure is simpler to work with than the procedure by Luidhardt and coworkers,[2] which required preparation of activated acid alumina, so it is the preferred method for making the model compounds. Despite the ease of Nikishin's method, compound **19** was difficult to work with due to very poor solubility in organic solvents. The literature melting point of 192 °C for diiododiphenylethene **19** corresponded well to the observed range of 188-191 °C. The poor solubility of **19** makes it a poor candidate for the mechanistic studies, so this compound was not used extensively. Wright and co-workers report a ^{1}H NMR spectrum [$CDCl_3$ – δ 7.45-7.30 (m)] of compound **19** in chloroform, and also cite poor solubility in organic solvents.[8] A ^{13}C NMR spectrum could not be obtained or found in the literature, as the poor solubility makes such analysis extremely difficult.

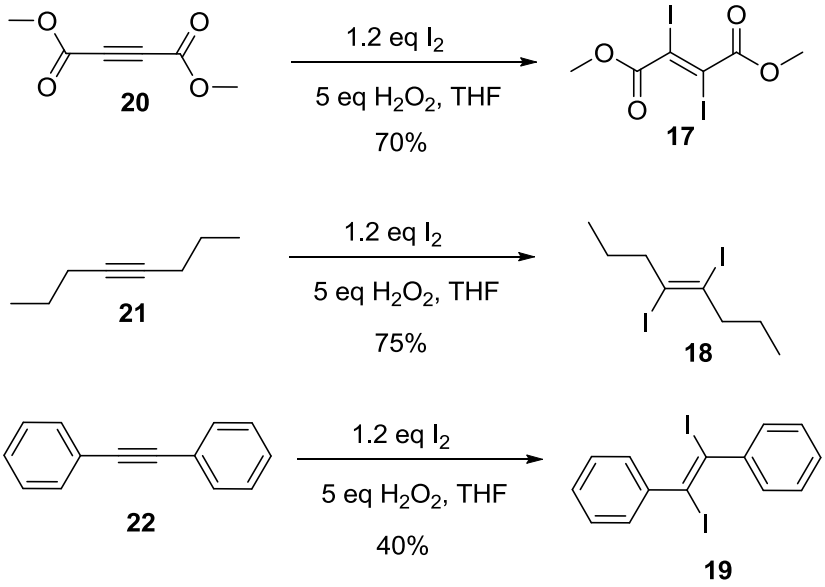

Scheme 4.7. Synthesis of model compounds **17-19.**

4.3 Evaluating the Model Systems

The model compounds in **Figure 4.3** were evaluated on the basis of whether or not each compound would eliminate iodine when allowed to react with pyrrolidine. Initial studies focused on pyrrolidine as the base, as Luo found that pyrrolidine induced deiodination occurs more

rapidly than other amines the tested.[1] Iodine is eliminated from compounds **12, 17, 18,** and **19** to afford the respective alkyne. The reaction mixtures each changed color from colorless to reddish-brown and the corresponding alkyne peaks were observed in the ^{13}C-NMR spectrum. It is worth mentioning that compound **19** has excellent solubility in pure pyrrolidine. The facile dissolution of compound **19** in pyrrolidine could be attributed to halogen bonding between the Lewis-basic nitrogen of the base and the Lewis acidic iodine.

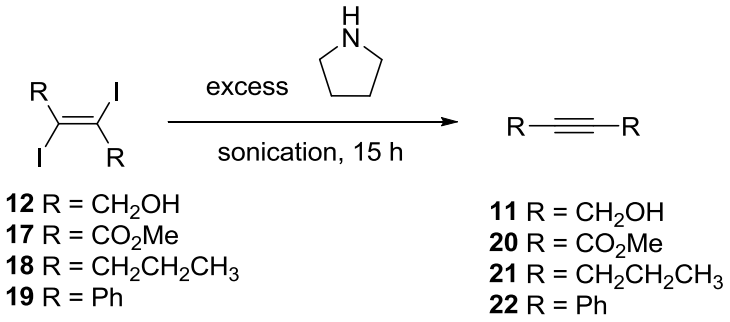

Scheme 4.8. Conditions for evaluating the model systems

Compound **18** was selected for further studies, since it can be distinguished from the corresponding alkyne **21** by ^{1}H-NMR. Another advantage of using compound **18** is that it does not contain any functional groups that could react with nucleophiles or bases, aside from the *E*-diiodoalkene group. Experimental work was carried out to determine the appropriate stoichiometry for achieving complete deiodination (**Scheme 4.9**). The conversion of compound **18** into alkyne **21** was carried out successfully, as judged by the disappearance of the peak at 102.1 ppm, which corresponds to the C-I carbon in the ^{13}C spectrum. The same carbon in the alkyne appears at 80.2 ppm. A preliminary investigation to determine the stoichiometry was reported as having required 1 eq of pyrrolidine.[9] It was later discovered that a mathematical error was made and 2 eq of pyrrolidine was actually used. The results of using 1 equivalent in d_5-$PhNO_2$ are depicted in more detail in **Figure 4.5**.

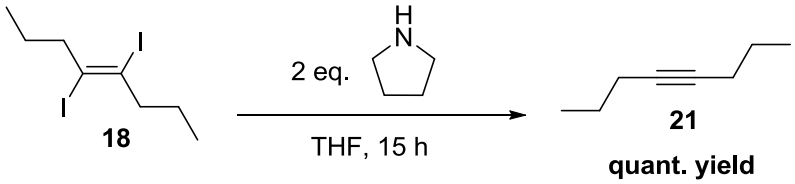

Scheme 4.9. Conditions for deiodination of **18**

The successful deiodination of model compound **18** prompted further investigation into the reaction scope. This investigation is important in determining the mechanism and proposing conditions to optimize the reaction for complete deiodination of PIDA. Solvent scope was one of the parameters to be considered in studying the reaction with pyrrolidine as the deiodination reagent (**Table 4.2**). Deiodination was not observed in nonpolar solvents such as toluene and cyclohexane. This result was interesting because the previous reactions (**Schemes 4.8** and **4.9**) only involved polar solvents, thus indicating an apparent solvent dependency. When the reaction was carried out in $CHCl_3$, an unexpected exothermic reaction occurred between pyrrolidine and $CHCl_3$. This reaction has been reported in the literature by Williams to afford N-methylated pyrrolidines.[10] The mixture of pyrrolidine in $CHCl_3$ then changed from colorless to orange upon addition of compound **18**. Iodine is pink in $CHCl_3$, but an orange color was observed. Due to the undesired reaction of pyrrolidine with $CHCl_3$, this solvent was excluded from future investigations. These preliminary solvent trials showed THF was a good solvent for further studies.

Table 4.2. Preliminary solvent trials for pyrrolidine induced deiodination.

Starting Material	Product(s)	Solvent	Time (h)
18	**18**	Toluene	48
18	**18**	Cyclohexane	48
18	**21**	THF	15
18	**?**	$CHCl_3$[a]	N/A

a) The reaction in $CHCl_3$ was problematic since pyrrolidine reacts with the solvent.

Studying reaction kinetics is one method that can be used to probe the mechanism. The application of UV-vis spectroscopy was explored by preparing a standard solution of compound

18 to obtain a UV spectrum. Compound **18** is visible in the UV spectrum, but the absorbance at 263 nm (**Figure 4.4**) poses a problem. The THF solvent peak overlaps with the peak of compound **18**, making it difficult to get reliable quantitative data. Another drawback of UV-vis spectroscopy for these experiments is the need for the analyte to be in a concentration that results in an absorbance of less than 1. The UV data in **Figure 4.4** show that this requirement is barely maintained at a diiodooctene concentration of 0.002M. Reactions that are too dilute can take extended periods of time to reach completion, depending on the mechanism. Slow reaction kinetics can be overcome by running the reaction at a higher concentration and then diluting an aliquot for analysis. Reaction mixture dilution, however adds an appreciable uncertainty into the analysis, given the time it takes to perform the dilution. As a result, NMR spectroscopy was investigated as an alternative to UV-vis spectroscopy for the pyrrolidine induced deiodination.

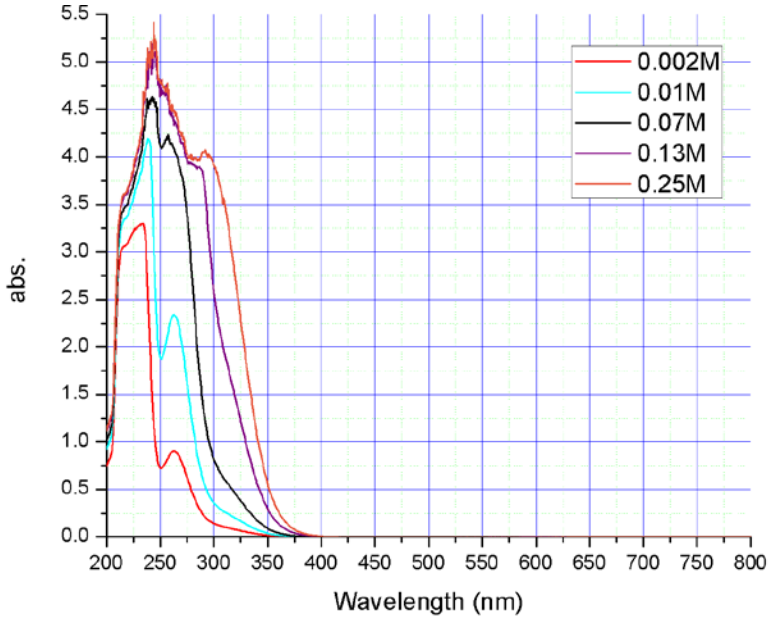

Figure 4.4. UV-vis of compound **18** at various concentrations in THF

One solvent for NMR kinetic analysis is d_5-$PhNO_2$ as the aromatic protons are far enough downfield not to interfere with the peaks of compounds **18** and **21**. Any interference will make reliable integration for quantifying the data difficult. NMR kinetic data (**Figure 4.5**) revealed

that a quaternary ammonium species (**23**) forms as the reaction between **18** and pyrrolidine progresses. The structure of quaternary ammonium species **23** is proposed in **Figure 4.5.** The ^{1}H-NMR data is consistent with the N-H proton shifting from 2.67 ppm to 6.58 ppm. The peak at 2.54 ppm corresponding to the alpha protons of the diiodoalkene functional group in compound **18** is seen to decrease. This reaction however only reaches 75% conversion in 15 hours. After 4 days the same reaction only achieves 88% conversion.

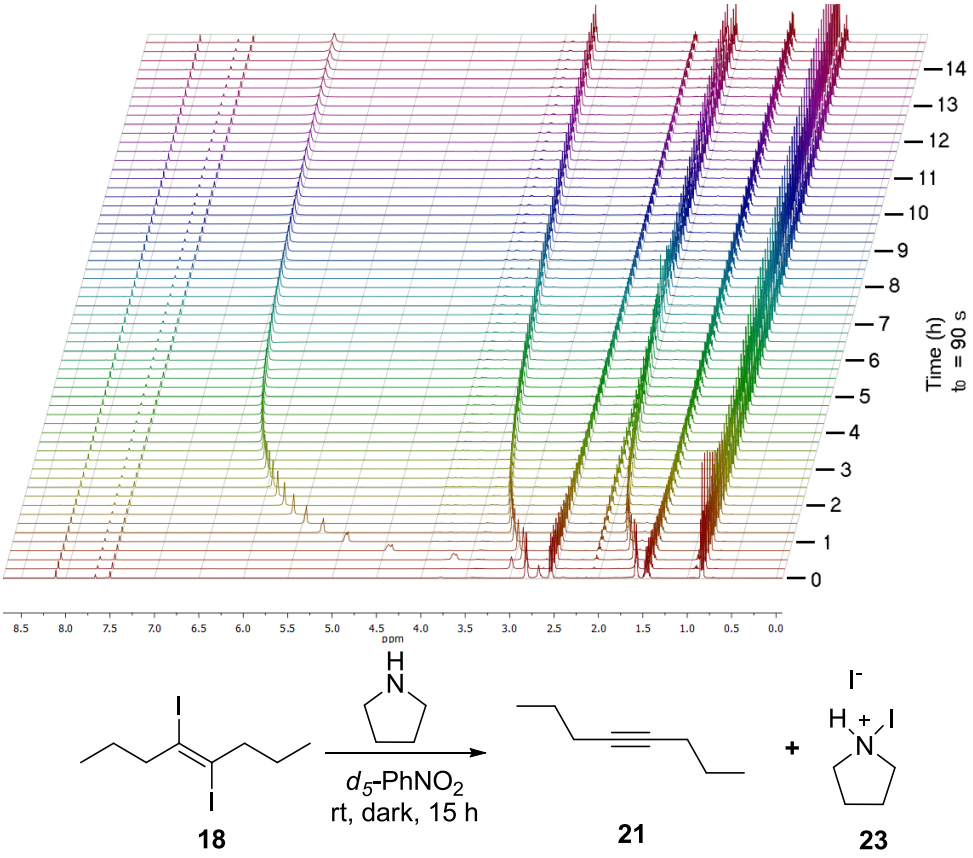

Figure 4.5. NMR kinetic profile showing formation of pyrrolidinium species and consumption of **18**.

The formation of iodopyrrolidinium iodide **23** is not surprising, as amines have been reported to complex with I_2 and ICl.[11] The reactivity of iodopyrrodinium iodide **23** was probed further by mixing iodine and pyrrolidine in d_5-nitrobenzene (**Figure 4.6**). The NMR data (**Figure 4.6**) shows that the reaction between iodine and pyrrolidine is not instantaneous. The rate of formation of iodopyrrolidinium iodide **23** is also on the timescale of the elimination reaction,

which means pyrrolidine is not necessarily consumed as it reacts with **18**. When the peak shift data for the N-H proton are plotted as a function of time it is clear that the reaction nears completion after 3 hours (**Figure 4.7**).

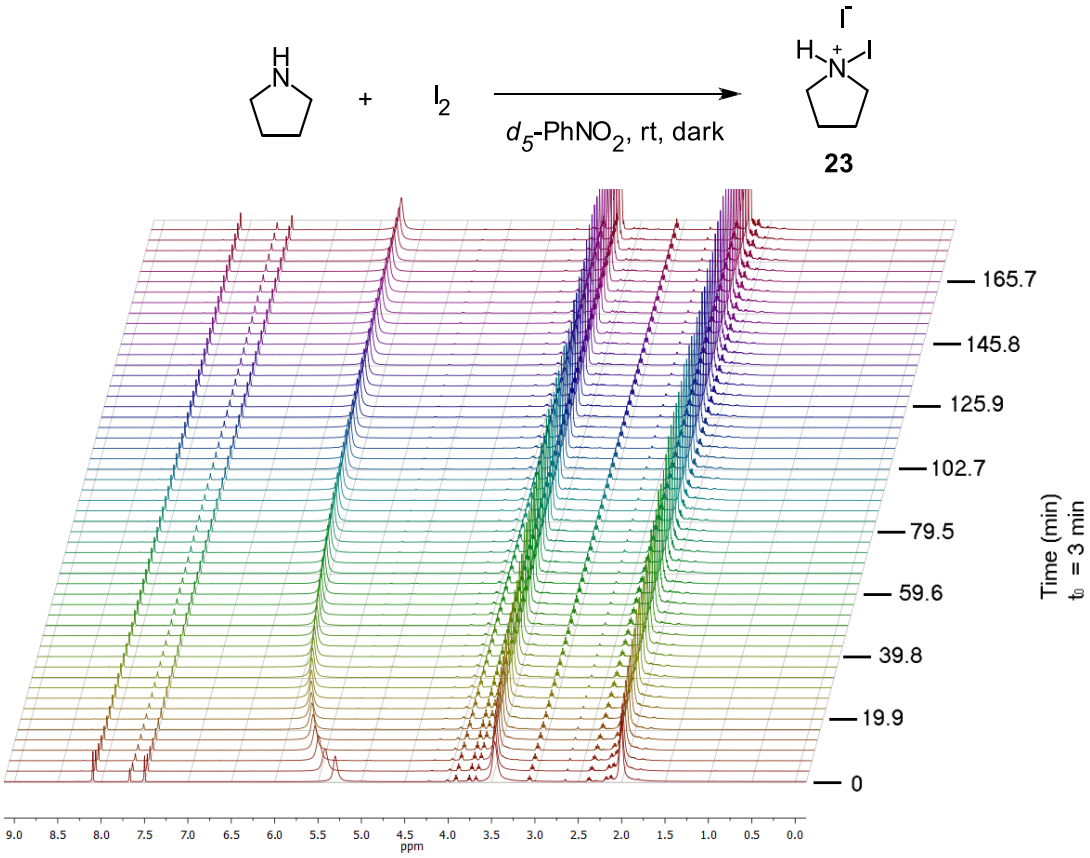

Figure 4.6. NMR kinetic profile of 0.275 M iodine reacting with 0.275 M pyrrolidine in d_5-nitrobenzene.

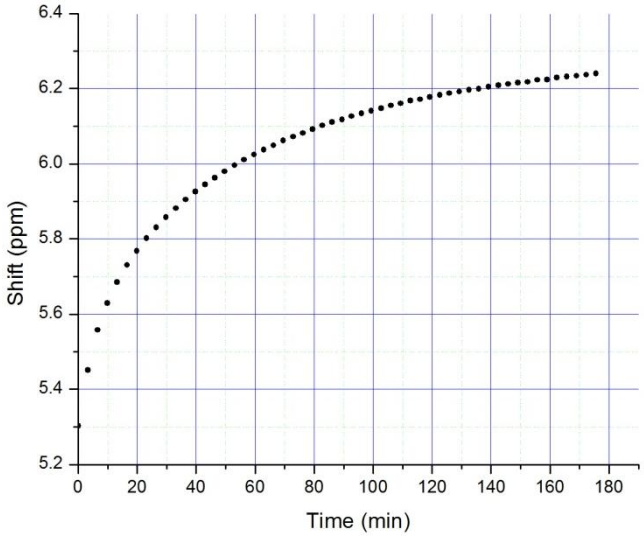

Figure 4.7. Kinetic analysis of 0.275 M iodine reacting with 0.275 M pyrrolidine in d_5-nitrobenzene. The pyrrolidinium proton shift is plotted as a function of time.

Further investigation into the reactivity of iodopyrrolidinium iodide **23** showed that it does not induce deiodination in diiodooctene **18** (**Scheme 4.10**). In these experiments, pyrrolidine was allowed to react with iodine for 24 h, at which time compound **18** was added to the mixture. It is essential to be careful when measuring the reagents in **Scheme 4.10**. Iodine has a tendency to sublime as it is weighed and transferred to the reaction vessel. If small amounts of iodine are used, a dramatic impact on the results is observed. Deiodination under the same conditions in **Scheme 4.10** was observed due to unreacted pyrrolidine from iodine sublimation. The experiment was modified such that larger quantities of iodine were used, so as to minimize the impact of sublimation.

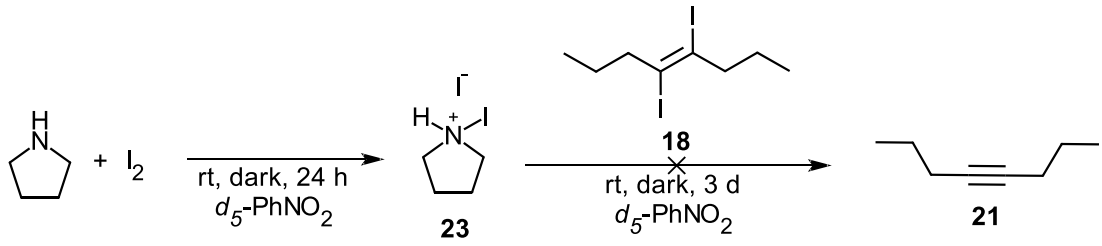

Scheme 4.10. Reaction conditions for studying the reactivity of **23**

In order to further understand the reactive species of pyrrolidine-induced deiodination, the reaction was conducted with substoichiometric quantities of base to induce elimination (**Table 4.3**). The substoichiometric experiment revealed lower concentrations of pyrrolidine gave higher turnovers per molecule of base. Interestingly, at 0.5 eq the reaction was not observed to reach completion. More than 2 turnovers per pyrrolidine were observed at 0.25 eq of base, but less than 2 were observed at 0.5 eq of base. This observation suggests that the pyrrolidinium cation and iodide do not combine instantaneously, leaving iodide free to react with another molecule of compound **18**. The pyrrolidine-induced deiodination has complicated kinetics, as a result of competing side reactions, as indicated by **Figure 4.8**.

Table 4.3. Elimination of iodine at sub-stoichiometric pyrrolidine.[a]

Days	0.25 eq.[b]	0.5 eq.[c]
0	0%	0%
1	50%	68%
2	58%	75%
3	58%	75%

a) Reagents and conditions: 0.275 M alkene **18**, d_5-$PhNO_2$, dark, rt; b) 0.137 M Pyrrolidine; c) 0.069 M Pyrrolidine

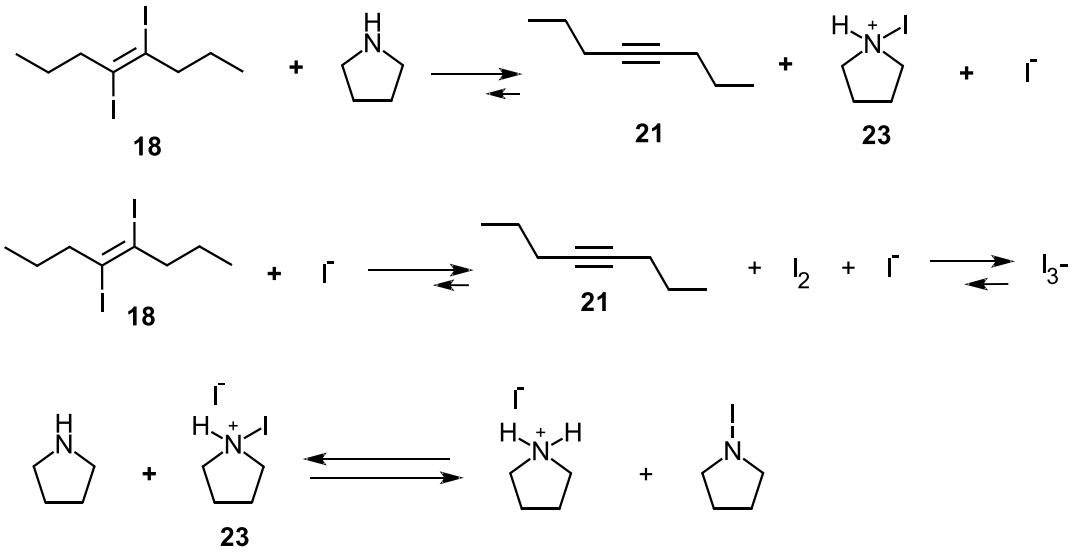

Figure 4.8. Proposed reactive species and relevant equilibria for pyrrolidine-induced deiodination

4.4 Iodide-Induced Deiodination

The pyrrolidine-induced deiodination is complicated and subject to multiple potential side reactions. These side reactions make probing the mechanism challenging and adds more

uncertainty in achieving the complete deiodination of PIDA by pyrrolidine. As a result, other deiodination agents were investigated. Miller and Noyes reported the deiodination of diiodoethene in 1952 by iodide in superheated methanol.[12] Additional literature precedent for dehalogenating *E*-dihaloalkenes was not found, but analogous elimination reactions have been reported on vicinal dihaloalkanes. Reagents such as NaI, $NaBH_4$ / cat. bis(2-thienyl)ditelluride, NaSH, and Na_2S have all been reported to induce dehalogenation.[13] Under Young's conditions, NaI was able to able to eliminate Br_2 from 2,3-dibromobutane using mild conditions.[13a] Compound **18** was thus subjected to reaction with NaI in THF (**Scheme 4.11**). The reaction shown in **Scheme 4.11** went successfully to completion in 15 hours. Reaction completion was determined by TLC, the appearance of an alkyne peak at 80.2 ppm in the ^{13}C-NMR spectrum, and the disappearance of the C-I carbon peak at 102.0 ppm the following day. When the reaction mixture was washed with sodium thiosulfate, the reddish-brown color disappeared and the solution became colorless. The color change is an indicator that iodine was reduced to give sodium iodide.

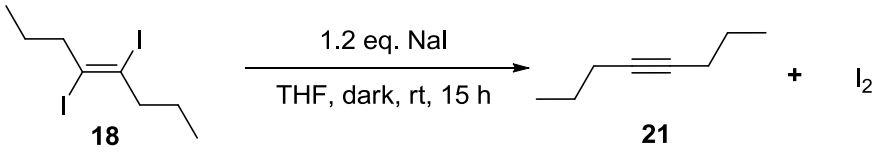

18 **21**

Scheme 4.11. Deiodination of **18** with NaI

NMR kinetic studies were conducted in an effort to probe the reaction mechanism. NaI could not be used for NMR studies, as it has poor solubility in organic solvents. This issue was easily rectified by using the organic salt tetrabutylammonium iodide (TBAI). TBAI has good solubility in polar organic solvents and water. The reaction in **Scheme 4.12** began with an almost immediate color change from colorless to a deep reddish-brown as the reaction progressed. The

TBAI showed good solubility, but at a concentration of 0.2 M TBAI it was apparent that some of the salt did not dissolve.

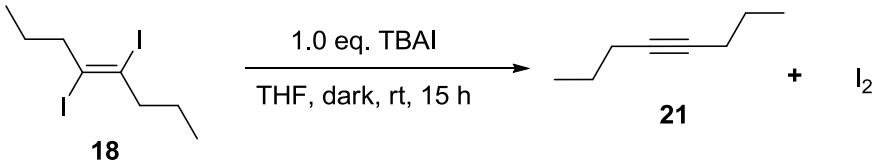

Scheme 4.12. Deiodination of **18** by TBAI

In order to probe the reaction further, solvent trials were conducted by Chang Lee (**Table 4.4**). The solvent trials revealed that polar aprotic solvents favor the deiodination reaction, whereas no deiodination is observed in nonpolar solvents. The poor solubility of TBAI in nonpolar solvents may explain the apparent stability of compound **18** in nonpolar solvents. Further investigation into the deiodination reaction in methanol showed that the reaction progresses very slowly and does not reach completion even after 5 days (**Table 4.5**). The data in **Table 4.5** are indicative of a reduced reactivity in the nucleophile. The nucleophile experiences forms hydrogen bonds with the protic solvent, which makes it less available to induce the deiodination reaction. The solvent trials are thus consistent with a polar mechanism.

Table 4.4. Solvent trials for iodide induced deiodination from **18**[a]

Solvent	Nucleophile	Elimination / Completion[f]
Acetonitrile[b,c]	I^-	Yes / 1 h
Nitromethane[c,d]	I^-	Yes / 2 h
Nitrobenzene[c]	I^-	Yes / 1 h
Methanol	I^-	Yes / No
2-Propanol	I^-	Yes / No
1,2-Dichloroethane	I^-	Yes / 3 d
Dichloromethane	I^-	Yes / 3 d
1,2-Dimethoxyethane	I^-	Yes / 3 d
Ethyl acetate	I^-	Yes / 4 d
Diethyl ether[e]	I^-	None
Cyclohexane[e]	I^-	None

a) Reagents and conditions: 0.137 M **18**, 0.164 M TBAI, rt, dark; b) See **Figure 4.10**; c) By NMR; d) Reagents and conditions: 0.275M **18**, 0.330 M TBAI, rt, dark; e) Poor solubility of TBAI; f) By TLC (silica/hexanes; R_f of **18** = 0.75 then silica/3:1 hexanes:ethyl acetate R_f of **21** = 0.65).

Table 4.5. Iodine elimination from alkene **18** in d_4-methanol.[a]

Days	Conversion of 18[a]
1	46%
2	59%
3	66%
5	75%

a) Reagents and conditions: 0.275 M **18**, 0.275 M TBAI, rt, dark

NMR spectroscopy was used to probe the kinetics of the TBAI-induced deiodination. It is possible to observe the conversion of alkene **18** to alkyne **21** by NMR, but the formation of the $TBAI_3$ complex cannot be observed. The transparency of $TBAI_3$ formation is one drawback of using NMR spectroscopy to follow this reaction. Kinetic analysis showed that TBAI completely deiodinates **18** in 1 h (**Figure 4.9**). TBAI-thus reacts much more quickly than pyrrolidine. Kinetic analysis was also carried out in acetonitrile for comparison (**Figure 4.10**). The results of the TBAI induced elimination in d_3-acetonitrile and d_5-nitrobenzene were comparable. In both solvents, the reaction goes to completion in about 1 hour. The plot of ln(C) for the reaction in either solvent is linear. This indicates the reaction is first order in **18**. An additional experiment involving double the concentration of TBAI in d_3-acetonitrile was also conducted (**Figure 4.11**). The results of the experiment in **Figure 4.11** showed that the reaction rate is doubled when the concentration of TBAI is doubled. This is consistent with first order behavior in TBAI.

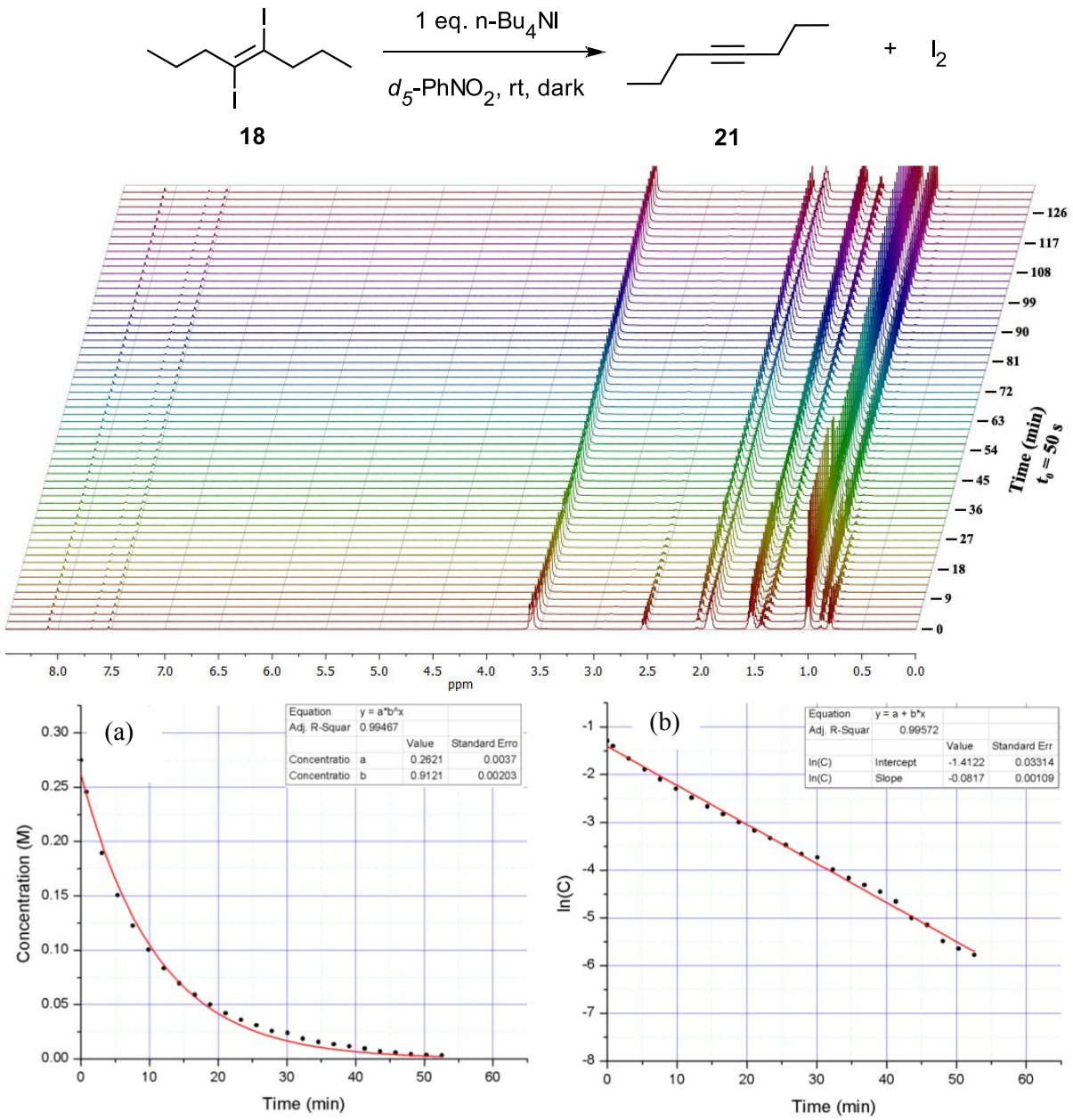

Figure 4.9. Kinetic analysis of 0.275 M alkene **18** reacting with 0.275 M n-Bu_4NI in d_5-$PhNO_2$. The protons alpha to the diiodoalkene of alkene **18** were integrated from 2.51–2.58 ppm and the protons alpha to the alkyne group in compound **21** were integrated between 2.12–2.05 ppm. Plot (a) shows concentration of compound **19** (C) as a function of time. Plot (b) shows ln(C) as a function of time.

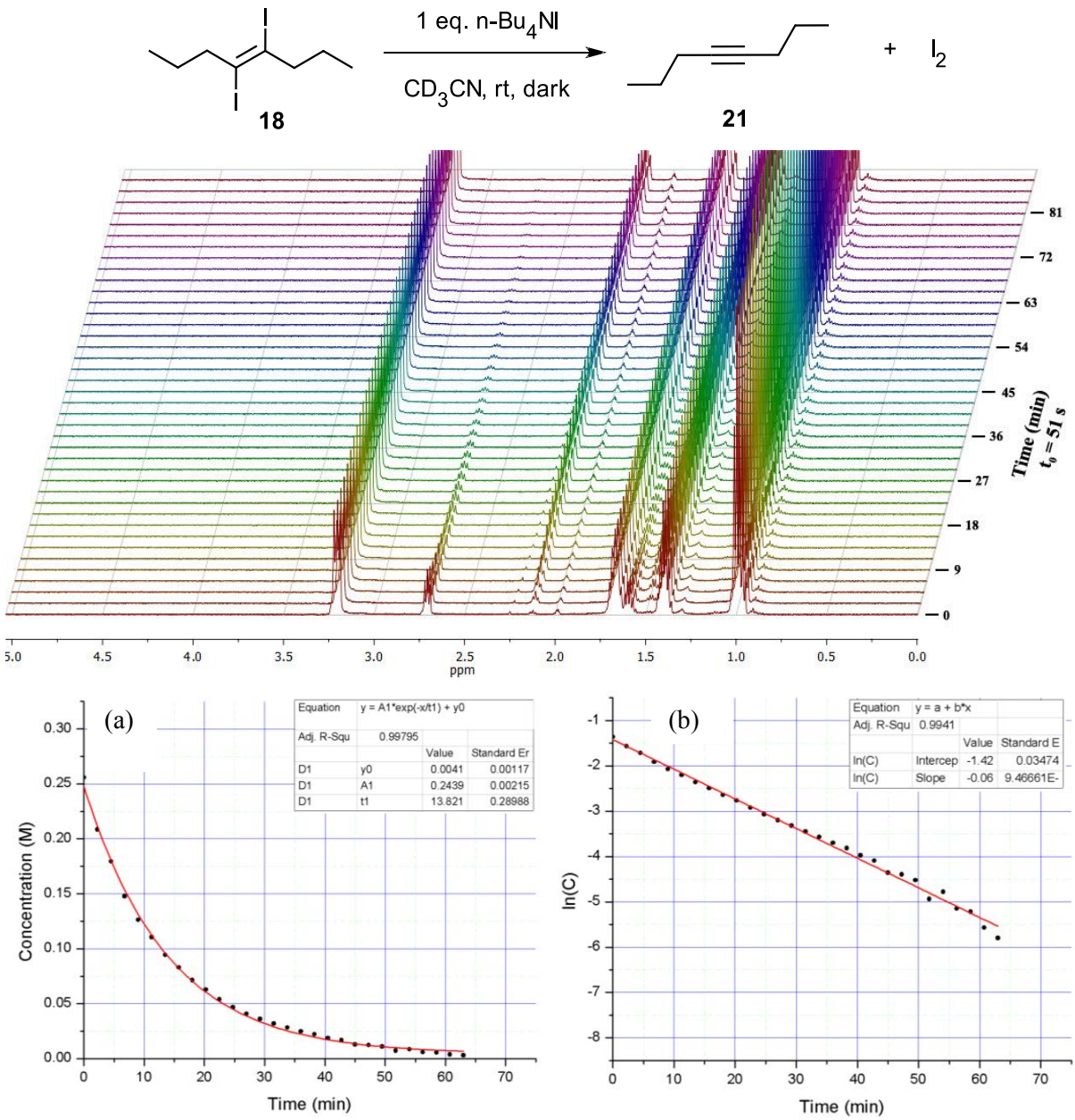

Figure 4.10. Kinetic analysis of 0.275 M alkene **18** reacting with 0.275 M n-Bu_4NI in CD_3CN. The protons alpha to the diiodoalkene of **18** were integrated from 2.51–2.58 ppm and the protons alpha to the alkyne of **21** were integrated between 2.12–2.05 ppm. Plot (a) shows concentration of compound **18** (C) as a function of time. Plot (b) shows the natural log of concentration plotted as a function of time.

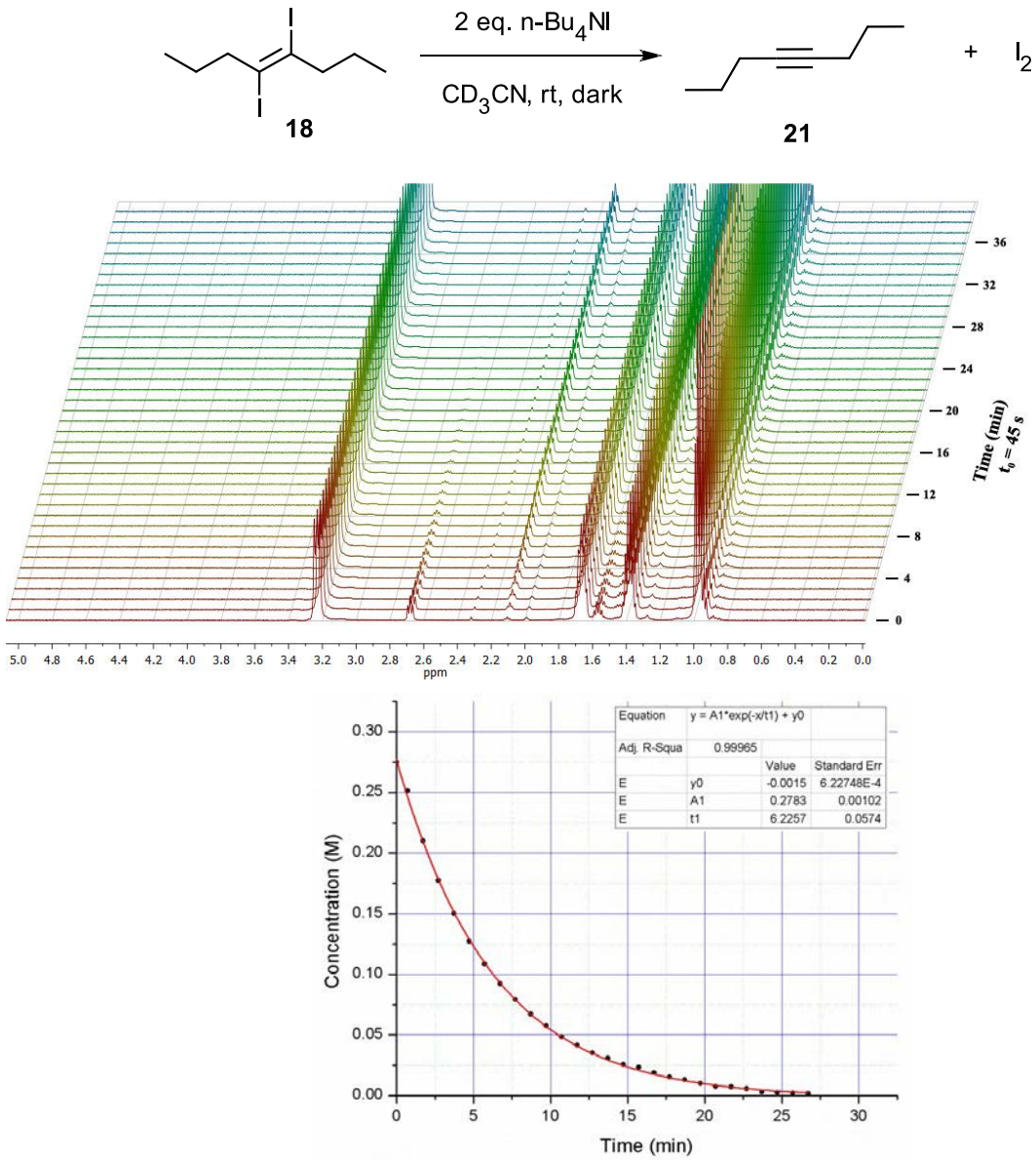

Figure 4.11. Kinetic analysis of 0.275 M Alkene **18** reacting with 0.550 M n-Bu_4NI in CD_3CN. The protons alpha to the diiodoalkene of **21** were integrated from 2.51–2.58 ppm and the protons alpha to the alkyne of **21** were integrated between 2.12–2.05 ppm. The plot shows concentration of compound **18** (C) as a function of time.

Unfortunately, one cannot observe the iodide, iodine, or triiodide complex species directly in the NMR experiments. Iodine and triiodide can be observed in the UV-vis spectrum, but due to solvent peak interference, nitrobenzene cannot be used. Acetonitrile is an excellent solvent for UV analysis, as its cutoff absorption is outside the UV range, and the reaction is strongly favored in this solvent (**Figure 4.10**). Figure **4.12** shows triiodide is formed more slowly

than alkene **23** is consumed. Consistent with Semnani and coworkers, the triiodide signal dominates the UV spectrum since is molar absorption coefficient is approximately 3-fold greater than the coefficient for iodine.[14] For this reason, iodine is more difficult to observe in **Figure 4.12**. The data corresponding to the concentration of alkene **18** were obtained by NMR whereas the concentration data for triiodide were obtained by UV-vis spectroscopy. The reaction conditions are the same in both NMR and UV-vis experiments for consistency. These results show that the iodide concentration does not change as fast as the concentration of alkene **18,** which suggests pseudo-first order behavior overall.

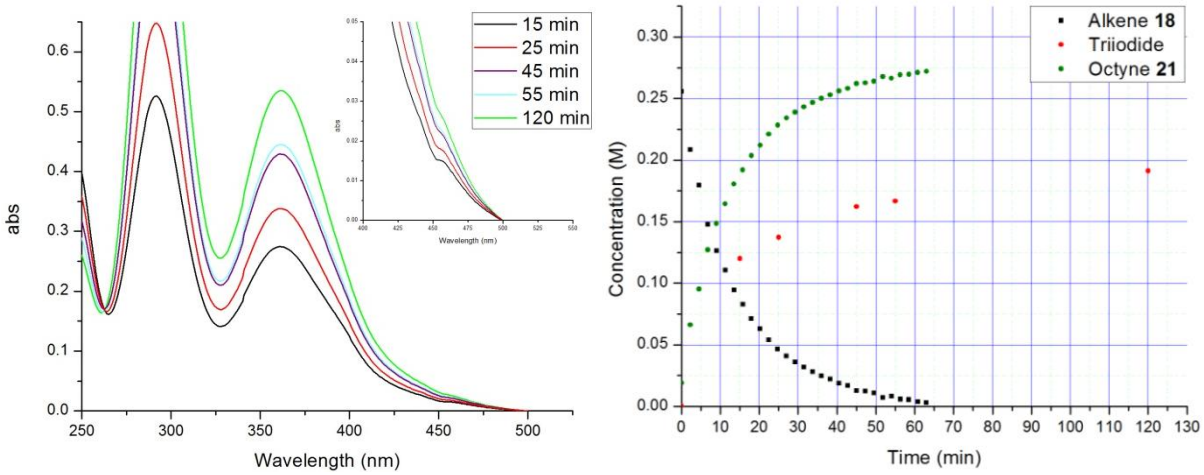

Figure 4.12. UV-vis spectra of triiodide (left) with inset showing the presence of iodine at 475 nm and concentration plot of alkene and triiodide (right)

To further understand the nature of the reactive species in the iodide-induced deiodination, the reactivity of the triiodide ion formed during the elimination was examined. $TBAI_3$ was pre-formed by mixing tetrabutylammonium iodide and molecular iodine for 10 minutes, and then alkene **18** was added to the mixture. After seven days, no deiodination of compound **18** was observed. Slator[15] found that in saturated diiodides the rate of elimination slows as iodide complexes to iodine to form triiodide. The results discussed here further confirm that triiodide does not compete with iodide for reaction with alkene **18**. An additional control

experiment, using of 1.2 eq iodine and 2.4 eq TBAI, indicates that the presence of triiodide also does not inhibit reaction (**Figure 4.13**).

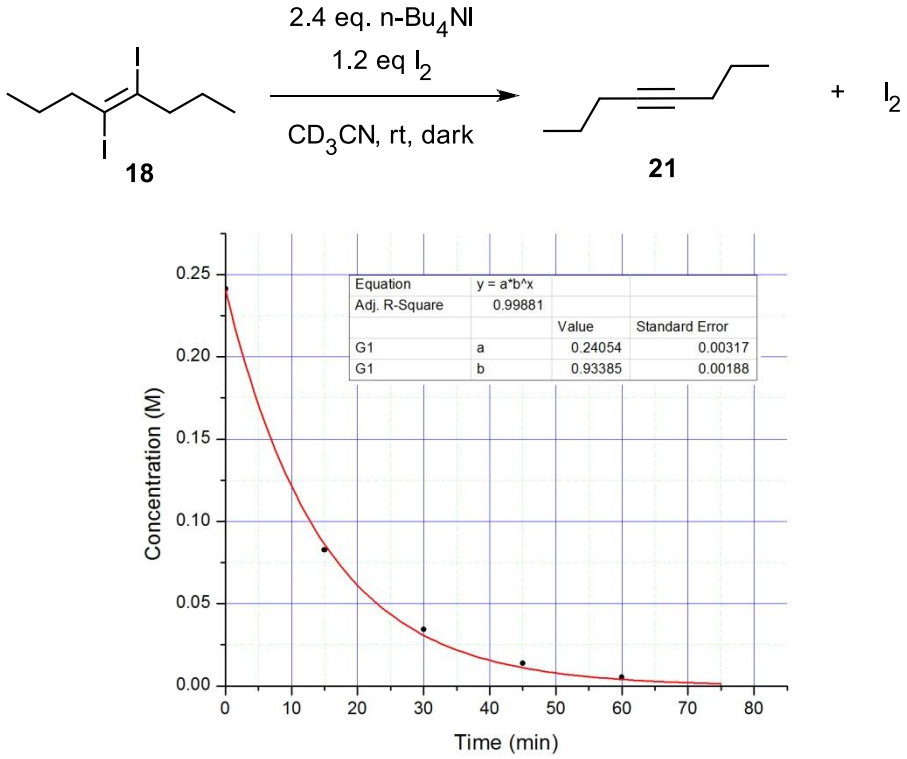

Figure 4.13. Kinetic analysis of 0.275 M alkene **18**, 0.330 M I_2, and 0.660 n-Bu_4NI. Time delay from injection of alkene **18** and collection of first data point is estimated to be about 1 minute. The plot shows concentration as a function of time.

To test the reversibility of the reaction, Chang Lee mixed TBAI with iodine and let it sit for 24 hours. Alkyne **21** was then added to the TBAI / I_2 mixture and was monitored for 3 days, but no detectable amount of diiodoalkene **18** was observed. This experiment suggests that when iodine is fully complexed as triiodide, the deiodination reaction is irreversible. In the absence of iodide, molecular iodine does react with 4-octyne under these conditions (**Scheme 4.13**). Monitoring the reaction by NMR indicated 95% conversion to alkene **18** in 12.5 hours.

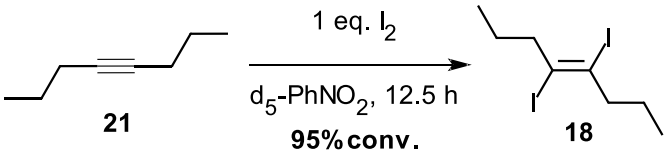

Scheme 4.13. Iodination of alkyne **21** in d_5-nitrobenzene.

The deiodination reaction was also studied under an excess of alkene **18,** to probe further the role of the iodide/triiodide equilibrium (**Table 4.6**). These studies were carried out with two different concentrations of alkene **18** (0.275 M or 0.137 M) and either ¼ or ½ equivalent of iodide. In these experiments, more than one turnover per iodide is observed, but the deiodination does not go to completion. These results are consistent with asynchronous formation of alkyne and triiodide. The more concentrated mixtures gave somewhat higher conversion percentages, suggesting increased rate of elimination relative to formation of triiodide. To test for salt effects, the non-nucleophilic salt tetrabutylammonium perchlorate was added to increase the ionic strength of the reaction mixture (**Table 4.6**). This addition had no effect on the rate or percent conversion in the deiodination of alkene **18**, consistent with Dillon's observation in the case of vicinal dibromoalkanes that neutral substrates are not susceptible to salt effects.[16] The general proposed mechanism for deiodination is summarized in Scheme **4.14**.

Table 4.6. Elimination of iodine at sub-stoichiometric TBAI.[a]

[18] (M)	[n-Bu_4NI] (M)	[n-Bu_4NClO_4] (M)	% conv.
0.275	0.069	-	32
0.275	0.103	-	61
0.275	0.138	-	86
0.137	0.034	-	26
0.137	0.069	-	57
0.137	0.034	0.034	25
0.137	0.069	0.069	60

a) Reagents and conditions: dark, rt, d_5-$PhNO_2$, 1 day

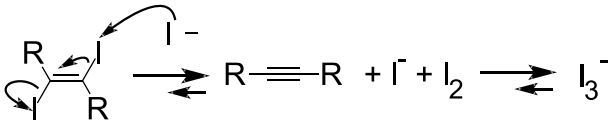

Scheme 4.14. Proposed mechanism for the deiodination of diiodoalkenes.

The overall reaction of the iodide induced deiodination is pseudo-first order and thus bimolecular. The pseudo first order behavior is observed because there is an asynchronous

complexation of iodide with I_2 and production of alkyne (**Figure 4.12**). This asynchronous behavior is likely due to the deiodination reaction occurring faster than formation of the triiodide complex. The data in **Table 4.6** show that at a higher concentration of reagents, more turnovers per iodide are observed. The solvent trials also support a polar mechanism. Overall the deiodination reaction follows an E2-like mechanism.

4.5 Investigating the Scope of the Deiodinaton Reaction

Tetrabutylammonium fluoride, chloride, and bromide, have also been observed to induce deiodination in compound **18** (**Figure 4.14**). The reaction of diiodoalkene **18** with either chloride or bromide results in the formation of mixed dihaloalkene 4-chloro-5-iodo-4-octene (**24**) or 4-bromo-5-iodo-4-octene (**25**) respectively. As compounds **24** and **25** form, a synchronous reduction in the concentration of alkyne **21** is observed. These products indicate dehalogenation is reversible, and the products are less reactive than **18**. Tetrabutylammonium fluoride-induced deiodination does not give fluoroiodoalkene, but the rate of deiodination under these conditions is much slower. The iodide ion remains the fastest for inducing deiodination of all the halides tested here.

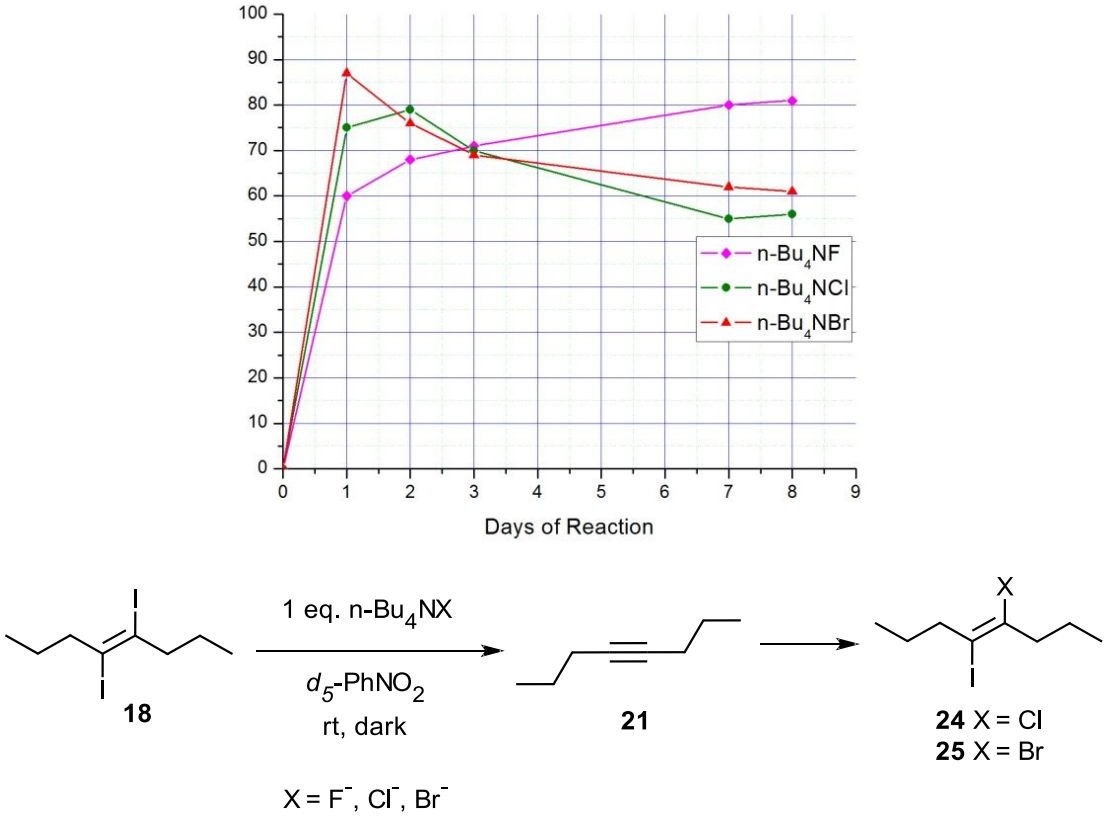

Figure 4.14. Percent of alkyne **21** by ^{1}H-NMR from fluoride, chloride, and bromide-induced deiodination

Potassium halide salts gave the same results as the tetrabutyl ammonium halides, but required 18-crown-6 to dissolve the salt. (**Table 4.7**). The non-nucleophilic salts KPF_6 and $KClO_4$ do not induce deiodination in **18**, as expected. The KOH-induced deiodination of compound **18** occurs rapidly in the presence of 18-crown-6 in d_5-nitrobenzene. Deiodination, in d_4-methanol, by KOH showed no reaction after 2 days. This result is consistent with the observations made when both pyrrolidine and tetrabutylammonium iodide were allowed to react with **18** in protic solvents.

Table 4.7. Elimination of iodine using potassium salts.[a]

Salt	Salt Equivalents	Solvent	Elimination	Completion	Time[b]
KI	1	d_5-$PhNO_2$	Yes	Yes	1 d
KI	1	Toluene	No	No	7 d[d]
KBr	1	d_5-$PhNO_2$	Yes	No	3 d[c]
KBr	1	Toluene	No	No	5 d
$KClO_4$	1.1	$MeNO_2$	No	No	7 d
KPF_6	1	$MeNO_2$	No	No	7 d
KOH	1.1	d_5-$PhNO_2$	Yes	Yes	1 d

a) Reagents and conditions: *x* eq. salt, *x* eq. 18-crown-6, rt, dark; b) By TLC (silica/hexanes; R_f of **18** = 0.75 then 3:1 silica/hexanes:ethyl acetate R_f of **21** = 0.65); c) Observation of **25** by NMR; d) Approximately half the KI remained dissolved.

Diester **17** has orthogonal functional groups with very different reactivity. Shah and co-workers[17] report selective hydrolysis of **17** in quantitative yield using an aqueous alcohol hydroxide system, without observing deiodination. This experiment was repeated by Chang Lee and the reported results were confirmed. Compound **17** can be completely deiodinated when heated with TBAI with the sole product being diester **20** (**Scheme 4.15**).

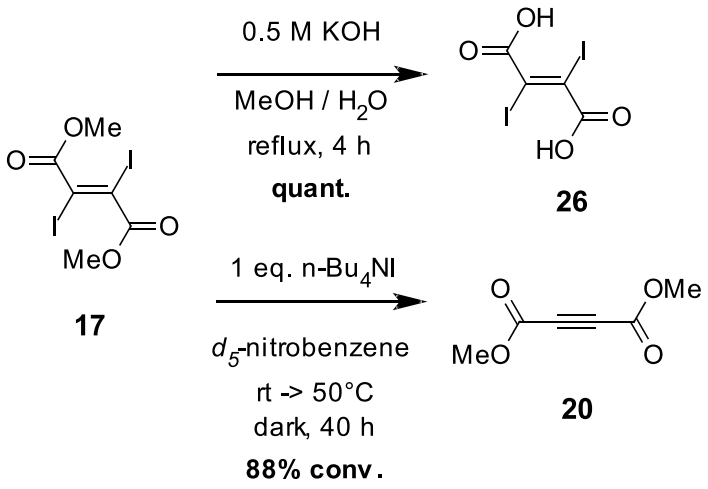

Scheme 4.15. The orthogonal reactivity of diiododiester **17**

4.6 Conclusion

The halide nucleophiles, hydroxide, and amines were all found to induce dehalogenation of the *E*-diiodoalkene functional group. The iodide ion is the fastest and mildest of all the nucleophiles tested at inducing deiodination. Compound **17** showed that iodine can be eliminated selectively in the presence of ester groups. Furthermore, the cation is merely a spectator ion in

this reaction as tetrabutylammonium and potassium give the same results. The mechanism of the deiodination reaction is an E2-like elimination.

4.7 Experimental

General Procedures. Air was purged from the NMR tubes used for the kinetic experiments by displacement with argon gas prior to the addition of any reagents. All other experiments were conducted in closed small vials or NMR tubes under atmospheric conditions. Prior to insertion in the spectrometer, the reaction mixture was kept in the dark by wrapping aluminum foil around the NMR tube. To determine the relative concentration of starting material and product, peaks corresponding to alkene **18** and alkyne **21** were integrated such that peak area overlap was not an issue. These integrals were compared and the fractions of **18** and **21** were calculated to determine the percent conversion. All solvents and reagents were used without further purification.

For kinetics studies, it is of the utmost importance to measure out the quantities of iodine and pyrrolidine carefully, given the small scale of the reactions reported here. All kinetic experiments were conducted using solutions prepared in volumetric flasks to ensure concentration could be accurately determined. Small deviations in reagent concentrations were found to markedly affect conversion percentages.

(4E)-4,5-Diiodooct-4-ene (**18**) and dimethyl (2E)-2,3-diiodo-2-butendioate (**17**) were prepared according to the procedure of Terentev and co-workers.[7] (*E*)-2,3-Diiodobut-2-ene-1,4-diol (**12**) was prepared according to the procedure of Hollins and Campos.[18] All other starting materials were used as purchased. Spectral data for 4-octyne (**21**) and dimethyl acetylenedicarboxylate (**20**) matched the corresponding spectra from the Spectral Database for Organic Compounds.[19] The NMR spectra for (*E*)-4-chloro-5-iodooct-4-ene (**24**) matched the spectral data reported by Organ, Ghasemi, and Valente.[20]

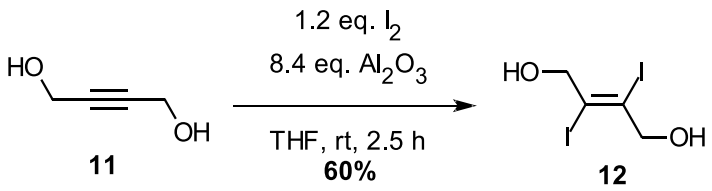

(E)-2,3-diiodobut-2-ene-1,4-diol (**12**): Acidic alumina (10.0121 g, 98.2 mmol) was dried in a vaccum oven at 200°C for 2 hours. The acidic alumina was cooled to room temperature and then put into a 500 mL rbf previously flushed with argon. Iodine (3.538 g, 13.9 mmol) was introduced into the 500 mL rbf with the acid alumina in it. Dry THF (60 mL) was added to the flask and the iodine was allowed to absorb onto the alumina for 30 minutes. Compound **11** (1.0031g, 11.7 mmol) was added to the 500 mL rbf flask and allowed to react for an additional 2.5 hours. The alumina oxide was then filtered out via vaccum filtration. THF was used to wash any product on the alumina into a vacuum flask. The solvent was then removed in vacuo. Chloroform was then used to wash out excess iodine and collect any remaining solid in a Buchner funnel. The solid was washed 4 times with 40 mL of chloroform. The solid was collected and recrystallized from hot acetone affording an off-white powdery solid (m.p. 155-157°C) in 60% yield (2.3860 g, 7.02 mmol). ^{1}H NMR (500 MHz, DMSO) δ 5.64 (s, 2H), 4.33 (s, 4H); ^{13}C NMR (126 MHz, DMSO) δ 105.1, 73.9.[18]

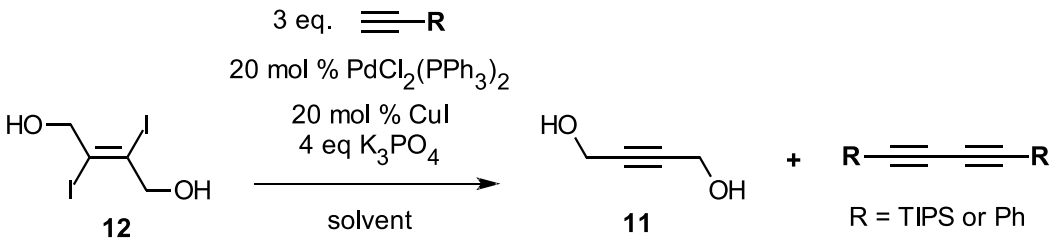

Representative Sonogashira protocol for Diol 12: Diol **12** (0.2509 g, 0.74 mmol), $PdCl_2(PPh_3)_2$ (51.8 mg, 0.15 mmol), and $K_3PO_4 \cdot H_2O$ (0.6821 g, 2.95 mmol) was introduced into a round bottom flask. The flask was then flushed with argon gas and 20 mL of solvent was introduced via syringe. The solution was allowed to stir for 15 minutes before adding TIPS-

acetylene (0.4022 g, 2.21 mmol) and CuI (0.0821 g, 0.15 mmol). The reaction was monitored via TLC and was quenched with sat. NH_4Cl solution. The resulting solution was extracted with ethyl acetate, dried with $MgSO_4$, and concentrated *in vacuo*. The resulting mixture was subjected to NMR analysis and no further purification was justified since all peaks were identified as either homocoupled alkyne or diol **11**. The homocoupled alkynes were obtained in quantitative yield. [R = Ph] – ^{1}H NMR (500 MHz, $CDCl_3$) – δ 7.37 (1H, m), 7.24 (2H, m), 7.14 (2H, m), 4.20 (4H, s), 3.71 (2H, s); ^{13}C NMR (125 MHz, $CDCl_3$) – δ 132.5, 129.1, 128.4, 121.8, 84.5, 81.6, 74.0, 50.6.[19] [R = TIPS] – ^{1}H NMR (500 MHz, $CDCl_3$) – δ 4.20 (4H, s), 3.71 (2H, s), 1.06 (42H, m); ^{13}C NMR (125 MHz, $CDCl_3$) – δ 90.3, 84.5, 81.7, 50.6, 18.6, 11.3.[19]

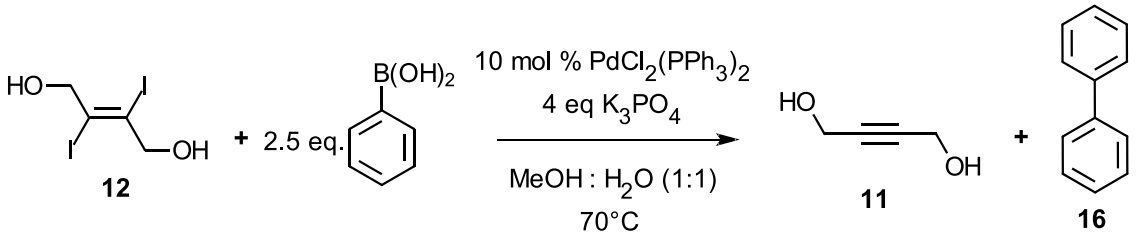

Suzuki protocol for Diol 12: Diol **12** (0.2515 g, 0.74 mmol), $PdCl_2(PPh_3)_2$ (51.8 mg, 0.15 mmol), and $K_3PO_4 \cdot H_2O$ (0.6821 g, 2.95 mmol) was introduced into a round bottom flask. The flask was then flushed with argon gas and 20 mL of solvent was introduced via syringe. The solution was allowed to stir for 15 minutes before adding phenylboronic acid (0.2255 g, 1.85 mmol). The reaction was monitored via TLC for the disappearance of **12** and was quenched with sat. NH_4Cl solution. The resulting solution was extracted with ethyl acetate, dried with $MgSO_4$, and concentrated *in vacuo*. The resulting mixture was subjected to NMR analysis and no further purification was justified since all peaks were identified as either biphenyl or diol **11**. Biphenyl and **11** were obtained in quantitative yield in a 1:1 ratio. ^{1}H NMR (500 MHz, $CDCl_3$) – δ 7.60 (2H, m), 7.44 (2H, m), 7.36 (1H, m), 4.20 (4H, s), 3.71 (2H, s); ^{13}C NMR (125 MHz, $CDCl_3$) – δ 141.0, 128.5, 126.9, 126.8, 84.5, 50.6.[19]

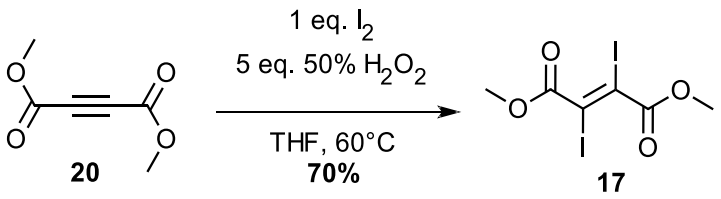

Dimethyl (2E)-2,3-diiodo-2-butendioate (**17**):[7] Dimethyl acetylenedicarboxylate (0.5019 g, 3.53 mmol) **20** was added to 15 mL of wet THF. Iodine (0.896 g, 3.53 mmol) was added to the solution followed by 50% Hydrogen peroxide solution (1.2 mL, 17.6 mmol). The reaction was heated at 60°C and monitored via TLC until completion. 15 mL of deionized water was added to the reaction followed by extraction with hexanes (40 mL x4). The extract were combined and washed with 15% Sodium Thiosulfate (40 mL x2). The organic layer was dried with anhy. $MgSO_4$ and filtered before rotary evaporation. The resulting white solid had a melting point range of 121°C-124°C (m.p. 125°C)[7] and was collected in a yield of 70% (0.9783 g, 2.35 mmol). ^{1}H NMR (500 MHz, $CDCl_3$) δ – 3.91 (s, 6H); ^{13}C NMR (126 MHz, $CDCl_3$) δ – 165.6, 88.0, 53.9.[7]

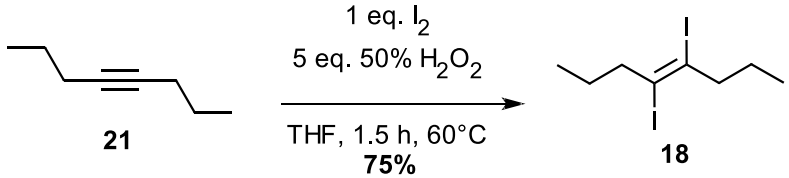

(E)-4,5-diiodooct-4-ene (**18**): 4-Octyne (1.0121 g, 9.18 mmol) **21** was added to 15 mL of wet THF. Iodine (2.8101 g, 11.02 mmol) was added to the solution followed by 50% Hydrogen peroxide solution (3.1 mL, 45.9 mmol). The reaction was heated at 60°C and monitored via TLC until completion. 15 mL of deionized water was added to the reaction followed by extraction with hexanes (40 mL x4). The extract were combined and washed with 15% Sodium Thiosulfate (40 mL x2). The organic layer was dried with anhy. $MgSO_4$ and filtered before rotary evaporation. The resulting yellow liquid was collected in a yield of 75% (2.5061 g, 6.89 mmol).

^{1}H NMR (400 MHz, C_6D_{12}) δ – 2.68 (t, 2H), 1.59 (dd, 7.4 Hz, 2H), 0.95 (t, J = 7.4 Hz, 6H); ^{13}C NMR (101 MHz, C_6D_{12}) δ – 101.9, 53.3, 22.2, 12.9.[7]

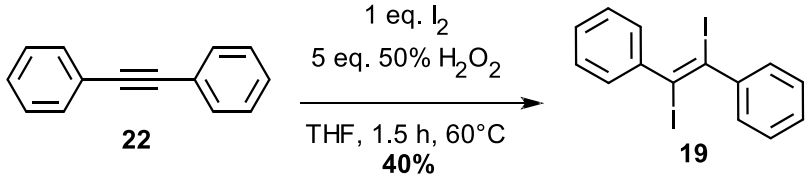

(E)-1,2-diiodo-1,2-diphenylethene (**19**): Diphenylacetylene (0.5281 g, 2.96 mmol) **22** was added to 15 mL of wet THF. Iodine (0.7520 g, 2.96 mmol) was added to the solution followed by 50% Hydrogen peroxide solution (1.0 mL, 14.8 mmol). The reaction was heated at 60°C and monitored via TLC until completion. 15 mL of deionized water was added to the reaction followed by extraction with hexanes (40 mL x4). The extract were combined and washed with 15% $Na_2S_2O_3$ (40 mL x2). The organic layer was dried with anhy. $MgSO_4$ and filtered before rotary evaporation. The resulting off-white solid had a melting point range of 196°C-200°C (m.p. 192°C)[8] and was collected in a yield of 40% (0.5115 g, 1.18 mmol). ^{1}H NMR (500 MHz, $CDCl_3$) δ 7.45-7.30 (m).[8]

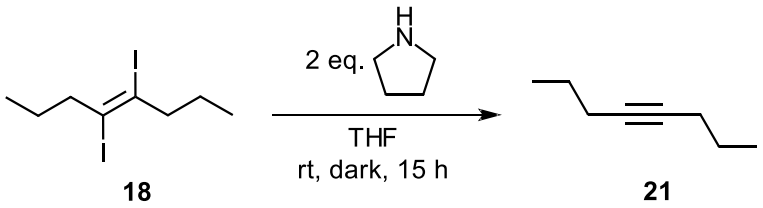

Elimination Reaction Procedure (Pyrrolidine): THF (1.13 mL, not dry) and pyrrolidine (32 mg, 0.452 mmol) were mixed in a reaction vessel with the pyrrolidine having been added from a microliter syringe. Compound **18** (82 mg, 0.226 mmol) was then added via microliter syringe to afford a 0.2M concentration. The reaction was monitored via TLC until the starting material spot had vanished. Following completion, the reaction mixture was concentrated in vacuo to remove THF. The residue was dissolved in $CDCl_3$ and subjected to NMR analysis.

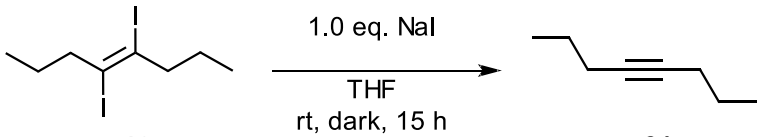

18 **21**

Elimination Reaction Procedure (Sodium Iodide): THF (1.13 mL, not dry) and sodium iodide (34 mg, 0.226 mmol) were mixed in a reaction vessel. Compound **18** (82 mg, 0.226 mmol) was then added via microliter syringe to afford a 0.2M concentration. The reaction was monitored via TLC until the starting material spot had vanished. An aliquot of 20 mL of 15% Sodium Thiosulfate solution was used to quench the reaction. The reaction mixture was the extracted with ethyl acetate (3x 30 mL) and dried with anhy. $MgSO_4$. After filtering, the solvent was removed in vacuo and the remaining material was subjected to NMR analysis. ^{1}H NMR (400 MHz, C_6D_{12}) δ 2.13 – 1.97 (m, 4H), 1.46 (dd, J = 7.0 Hz, 4H), 0.96 (td, J = 7.7, 6H); ^{13}C NMR (101 MHz, C_6D_{12}) δ 79.80, 23.23, 21.34, 13.55.

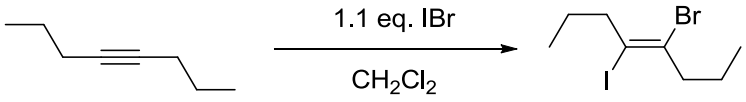

21 **25**

Preparation of (*E*)-4-Bromo-5-iodooct-4-ene (25): To an argon-flushed and aluminum foil-wrapped rbf equipped with a magnetic stir bar was added a 1 M IBr solution in CH_2Cl_2 (4.5 mL, 4.5 mmol). Compound **21** (0.60 mL, 0.4506 g, 4.09 mmol) was then added. After 1 day, 20 mL of CH_2Cl_2 was added into the solution. The organic layer was washed with 5% $Na_2S_2O_3$ (20 mL x 2) then deionized water (30 mL x 2). The organic layer was then dried with anhydrous $MgSO_4$ and filtered before rotary evaporation. A short silica plug using 100% hexanes as the eluent was used to separate alkyne **21** from the resulting clear pale yellow liquid. The product is an inseparable mixture of *cis* and *trans* isomers of alkene **25**. ^{1}H NMR (400 MHz, $CDCl_3$) δ 2.73–2.65 (m, 4H), 1.67–1.54 (m, 4H), 1.00-0.90 (m, 6H); ^{13}C NMR (101 MHz, $CDCl_3$) δ 122.7,

121.7, 102.0, 100.0, 60.3, 52.6, 47.5, 46.9, 42.5, 34.5, 21.6, 20.9, 13.0, 11.8; EI-MS (m/z) $[M]^+$ 316, 318; HRMS-EI (m/z) calcd. for $C_8H_{14}IBr$ $[M]^+$ 315.93238, found 315.93257.

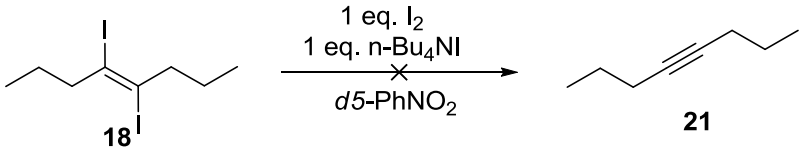

Testing for Triiodide Induced Elimination. To an aluminum foil-wrapped vial were added n-Bu_4NI (0.0510 g, 0.137 mmol) and iodine (0.0348 g, 0.137 mmol). *d_5*-Nitrobenzene (1.0 mL) was added and the vial was shaken. The mixture was subjected to sonication for 15 sec to ensure homogeneity. Compound **18** (20.1 µL, 0.0502 g, 0.137 mmol) was then added, and the vial was shaken. The contents of the vial were transferred to an NMR tube and an initial NMR was taken. The ^{1}H-NMR spectrum was measured on a daily basis for a week, but showed no change from the initial spectrum of compound **18**.

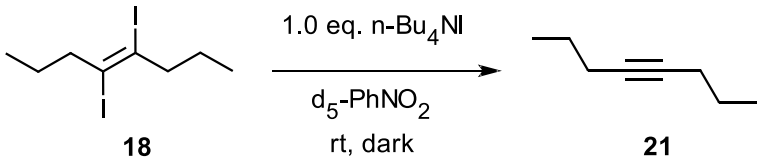

Measuring Triiodide Concentration by UV-vis. In a 1 mL volumetric flask was added n-Bu_4NI (0.1016 g, 0.275 mmol). Acetonitrile was introduced in the flask just below the mark to dissolve n-Bu_4NI followed by compound **18** (0.1002 g, 0.275 mmol). The solution was quickly diluted to the mark, shaken, and an aliquot of 36 µL was extracted as an initial data point. The aliquot was diluted in a 25 mL volumetric flask with acetonitrile for UV-vis analysis. The UV-vis experiment was setup as a double-beam experiment with an acetonitrile blank. Aliquots of 36 µL were extracted and diluted at the indicated intervals in **Figure 4.12**. A stock triiodide solution of 1 $x10^{-2}$ M was prepared by dissolving n-Bu_4NI (0.1847 g, 0.50 mmol) and I_2 (0.1269, 0.50 mmol) with acetonitrile to volume in a 50 mL volumetric flask. Working solutions were prepared from the stock solution by serial dilution (1.0 $x10^{-4}$ M, 2.0 $x10^{-4}$ M, 3.0 $x10^{-4}$ M, 4.0 $x10^{-4}$ M, 5.0

x10^{-4} M, and 8.0 x10^{-4} M). Linear regression analysis was carried out on the standard curve data, and the linear equation was used to determine the concentration of the diluted aliquots.

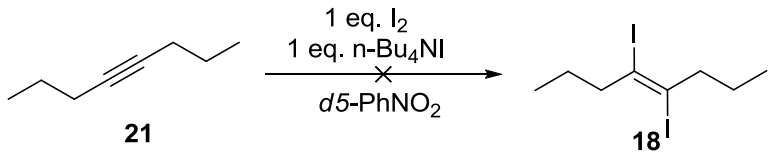

Testing for Iodination by Triiodide. To an aluminum foil-wrapped vial were added n-Bu_4NI (0.0510 g, 0.137 mmol) and iodine (0.0348 g, 0.137 mmol). d_5-Nitrobenzene (1.0 mL) was added and the vial was shaken. The mixture was subjected to sonication for 15 sec to ensure homogeneity and then allowed to sit for 24 hours. Compound **21** (20.1 μL, 0.0151 g, 0.137 mmol) was then added, and the vial was shaken. The contents of the vial were transferred to an NMR tube and an initial NMR was taken. The ^{1}H-NMR spectrum was measured on a daily basis for 3 days, but showed no change from the initial spectrum of compound **21**.

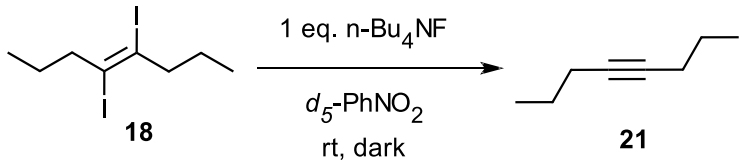

Procedure for Dehalogenation by n-Bu_4NF. To an aluminum foil wrapped vial was added TBAF hydrate (0.0358 g, 0.137 mmol). d_5-Nitrobenzene (0.5 mL) was added and the vial was shaken. The mixture was subjected to sonication for 15 sec to ensure homogeneity. Compound **18** (0.0502 g, 0.137 mmol) was then added and the vial was shaken. The contents of the vial were transferred to a NMR tube, and an initial NMR was taken. A color change from a pale yellow to a deep reddish-brown was observed. ^{13}C and ^{1}H-NMR spectra were collected on a daily basis for 8 days. The reaction mixture was then left in the NMR tube wrapped with aluminum foil. The triplet corresponding to **21** at 2.04 ppm and the multiplet corresponding to **18** from 2.45-2.50 ppm were integrated. The conversion was calculated using the integral of **21** expressed as a percentage of the total integral sum.

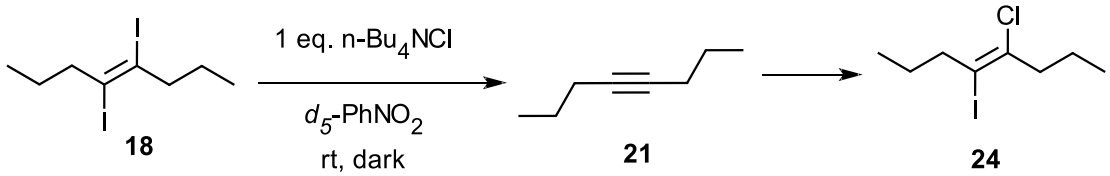

Procedure for Dehalogenation by n-Bu_4NCl. To an aluminum foil wrapped vial was added TBACl (0.0381 g, 0.137 mmol). d_5-Nitrobenzene (0.5 mL) was added and the vial was shaken. The mixture was subjected to sonication for 15 sec to ensure homogeneity. Compound **18** (0.0502 g, 0.137 mmol) was then added, and the vial was shaken. The contents of the vial were transferred to an NMR tube, and an initial NMR was taken. A color change from a pale yellow to a deep reddish-brown was observed. ^{13}C and ^{1}H-NMR spectra were collected on a daily basis for 8 days. The reaction mixture was then left in the NMR tube, wrapped with aluminum foil. The triplet corresponding to **21** at 2.04 ppm and the multiplet from 2.45-2.58 ppm, corresponding to **18** at the start of experiment, and to **24** at the end of the experiment, was integrated to determine the conversion percentage.

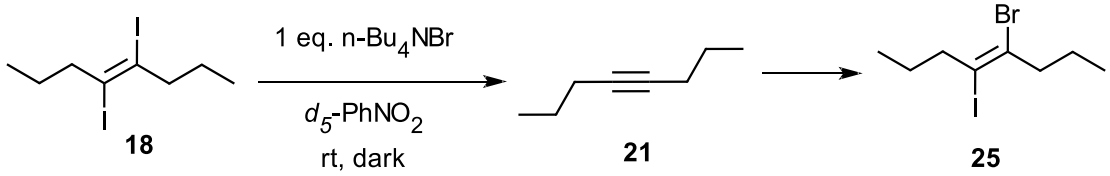

Procedure for Dehalogenation by n-Bu_4NBr. To an aluminum foil-wrapped vial was added tetrabutyl ammonium bromide (0.0442 g, 0.137 mmol). d_5-Nitrobenzene (0.5 mL) was added and the vial was shaken. The mixture was subjected to sonication for 15 sec to ensure homogeneity. Compound **18** (0.0502 g, 0.137 mmol) was then added, and the vial was shaken. The contents of the vial were transferred to a NMR tube, and an initial NMR was taken. A color change from a pale yellow to a deep reddish-brown was observed. ^{13}C and ^{1}H-NMR spectra were collected on a daily basis for 8 days. The reaction mixture was then left in the NMR tube, wrapped with aluminum foil. The triplet corresponding to **21** at 2.04 ppm and the multiplet from 2.45-2.58

ppm, corresponding initially to compound **18** and later to compound **25**, were integrated to calculate the conversion percentage.

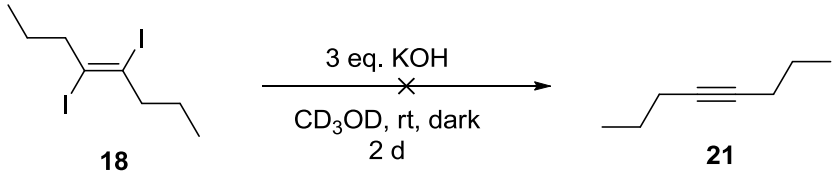

Testing for KOH Induced Elimination in *d*$_4$-MeOD. Compound **18** (20.0 µL, 0.0501 g, 0.138 mmol) was added to MeOH (0.5 mL) in a rbf equipped with a magnetic stir bar. An aqueous solution of 0.5 M KOH (0.83 mL, 0.4 mmol) was then added to the flask. After 48 hours, it was neutralized by adding an aq. 0.5 M HCl solution (0.83 mL). The solution was extracted with hexanes (1.0 mL x 3). The organic phase was washed with brine (1.0 mL x 3), then dried with $MgSO_4$. The solvent was removed in *vacuo*. The residue was dissolved in d_5-nitrobenzene for NMR analysis. Only compound **18** was observed in the ^{1}H NMR.^{1}H NMR (400 MHz, d_5-$PhNO_2$) δ 2.61 – 2.45 (m, 4H), 1.45 (m, 4H), 0.83 (t, 6H); ^{13}C NMR (101 MHz, d_5-$PhNO_2$) δ 13.0, 22.4, 53.0, 102.7.

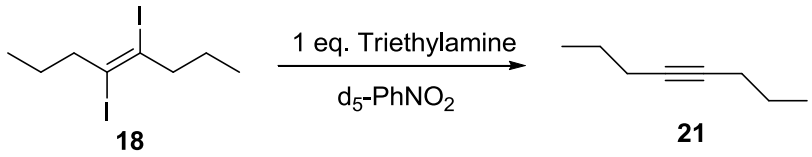

Triethylamine-Induced Elimination. Triethylamine (0.0139 g, 0.137 mmol) was placed in an aluminum foil-wrapped vial, d_5-nitrobenzene (0.5 mL) was added, and the vial was shaken. Compound **18** (0.0502 g, 0.137 mmol) was then added, and the contents of the vial were mixed by shaking. The contents of the vial were transferred to an NMR tube, and an initial NMR was taken. A ^{1}H-NMR spectrum was collected after 1 day, and only compound **21** was observed. A color change from a pale yellow to a deep reddish-brown was observed. ^{1}H NMR (500 MHz, d_5-$PhNO_2$) δ 3.43 (m, 8H), 2.14–2.00 (m, 4H), 1.59 (m, 12H), 1.43 (m, 4H), 0.92 (m, 6H).

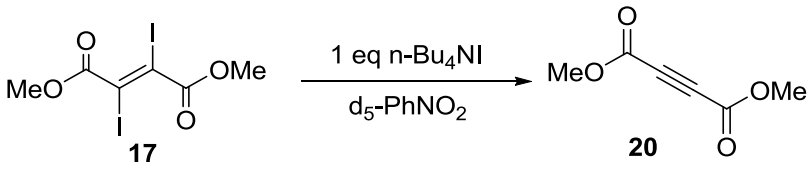

17 20

n-Bu$_4$NI-Induced Elimination from Diester (17). To an aluminum foil-wrapped vial was added n-Bu$_4$NI (0.0510 g, 0.137mmol) and d_5-PhNO$_2$ (0.5 mL). The mixture was subjected to sonication for 15 sec to ensure homogeneity. Compound **17** (0.0546 g, 0.137 mmol) was then added, and the vial was shaken. After a few minutes, a white solid precipitated out. The vial was heated to 45 °C to enhance solubility. ^{1}H NMR analysis was conducted after 40 hours, and showed compound **20** with a trace amount of **17**. ^{1}H NMR (400 MHz, d_5-PhNO$_2$) δ 3.86 (m, 6H), 3.61–3.27 (m, 8H), 1.90 (m, 8H), 1.56 (m, 8H), 1.04 (m, 12H); ^{13}C NMR (101 MHz, C_6D_6) δ 13.2, 19.6, 23.7, 52.9, 53.1, 58.8, 74.0, 93.6, 151.6, 165.9.

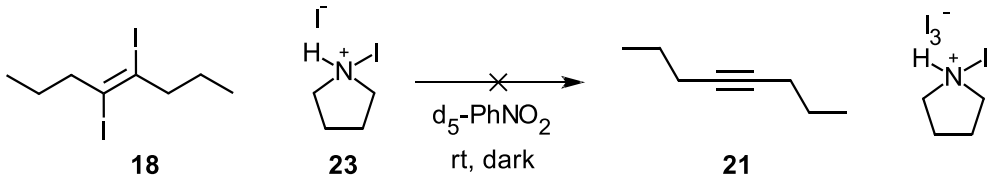

18 23 21

Testing for Iodopyrrolidinium (23) Induced Elimination. In a 1-mL volumetric flask, iodine (0.140 g, 0.550 mmol) was mixed with pyrrolidine (45.2 µL, 0.0391 g, 0.550 mmol), and d_5-nitrobenzene. This solution was allowed to sit at room temperature in the dark for 24 h to ensure complete reaction of iodine and pyrrolidine. An aliquot of 0.50 mL of this stock solution was placed into a clean 1-mL volumetric flask, followed by addition of compound **18** (40.0 µL, 0.1000 g, 0.275 mmol). The solution was diluted with d_5-nitrobenzene, immediately transferred to an NMR tube, and an initial spectrum was collected after 15 min. The mixture was observed by ^{1}H- and ^{13}C-NMR for 3 days. Compound **18** was found to remain stable over the 3-day period.

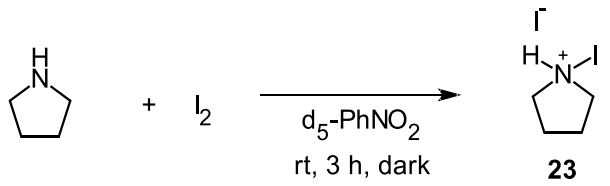

Kinetic Investigation of the Reaction Between Iodine and Pyrrolidine. In a 2-mL volumetric flask, iodine (0.1396 g, 0.550 mmol) was dissolved in d_5-nitrobenzene. A 1.0-mL aliquot of the 0.275 M solution was transferred into an NMR tube. Pyrrolidine (22.6 µL, 0.0196 g, 0.275 mmol) was then added to the NMR tube, and the tube was shaken. The time elapsed between addition of pyrrolidine and collection of the first ^{1}H spectra was 3 min. A total of 55 spectra were collected at 3.3 minute intervals to obtain a kinetic profile. A color change from a pale yellow to a deep reddish-brown was observed.

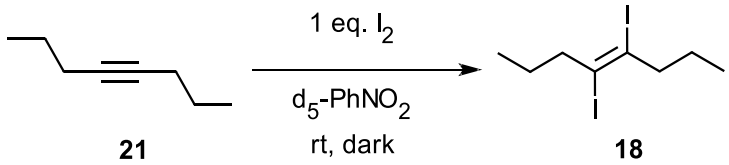

Reaction of Compound 21 and Iodine. To an aluminum foil-wrapped vial were added d_5-nitrobenzene (0.6 mL) and iodine (0.0350 g, 0.138 mmol). The mixture was subjected to sonication for 30 min to ensure homogeneity. Compound **21** (0.0151 g, 0.137 mmol) was then added, and the vial was shaken. The contents of the vial were transferred to an NMR tube and an initial NMR spectrum was collected. The time elapsed between mixing of reagents and collection of the initial spectra was 7 minutes. The ^{1}H-NMR spectrum was measured every 15 min for 12.5 hours. At 12.5 h the reaction showed 95% conversion of compound **21** to compound **18**.

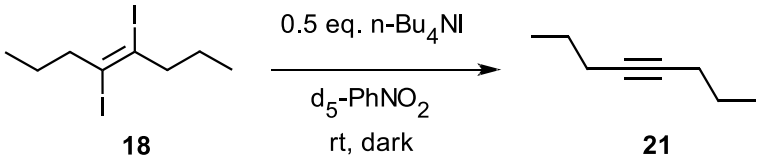

Representative Procedure for Experiments with Sub-Stoichiometric n-Bu$_4$NI. N-Bu$_4$NI (0.0442 g, 0.137 mmol) was added to a 1-mL volumetric flask and diluted with d_5-nitrobenzene. The solution was thoroughly shaken and then subjected to sonication for 15 sec to ensure homogeneity. An aliquot (0.5 mL) of this solution was then added to an NMR tube. The sample was inserted into the NMR instrument for locking and shimming, then ejected so that compound **18** (20.0 µL, 0.0501 g, 0.137 mmol) could be added to the tube. The spectrum was measured initially, and after 24 h. The triplets at 2.53 ppm corresponding to **18** and 2.06 ppm corresponding to **21** were integrated to calculate the conversion percentage. A color change from a pale yellow to a deep reddish-brown was observed.

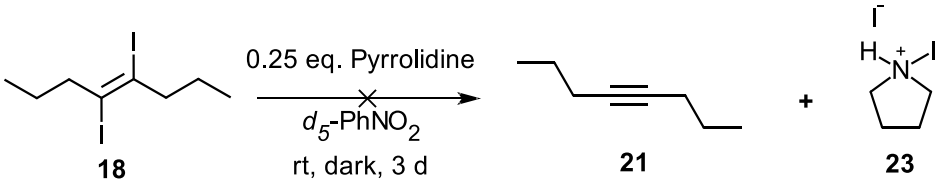

Representative Procedure for Experiments with Sub-Stoichiometric Pyrrolidine. Pyrrolidine (22.6 µL, 0.0196 g, 0.275 mmol) was added to a 1-mL volumetric flask and diluted with d_5-nitrobenzene. The solution was thoroughly shaken and then subjected to sonication for 15 seconds to ensure homogeneity. A 1-mL syringe was used to extract 0.50 mL of the solution, and it was diluted in another 1-mL volumetric flask to make a stock solution with concentration of 0.14 M. An aliquot of 0.50 mL was then extracted from the diluted solution and introduced into an NMR tube. Compound **18** (0.0501 g, 0.137 mmol) was then added by syringe into the NMR tube, and an initial spectrum was taken. The ^{1}H-NMR spectrum was measured on a daily

basis for 3 days. In between, the reaction mixture was kept in the NMR tube, covered with aluminum foil. The triplets at 0.83 ppm corresponding to alkene **18** and 0.92 ppm corresponding to alkyne **21** were integrated to determine the percentage of compound **21**. A color change from a pale yellow to a deep reddish-brown was observed.

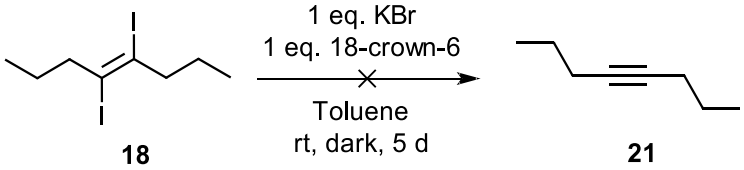

Representative Procedure for Iodine Elimination by Potassium Salts. To an aluminum foil-wrapped vial were added KBr (0.0160 g, 0.137 mmol) and 18-crown-6 (36.1 mg, 0.137 mmol). Toluene (1 mL) was added and the vial was shaken. The mixture was subjected to sonication for 1 min to ensure homogeneity. Compound **18** (0.0501 g, 0.137 mmol) was then added and the vial was shaken. The reaction was monitored by TLC (SiO_2/hexanes) for 5 d, with no observed change. (Compound **18** has $R_f = 0.7$, while compound **21** has $R_f = 0$ under these conditions.) In addition, there was no observed color change.

4.8 References

1. Luo, L. Preparation and Comprehensive Characterization of Poly(diiododiacetylene) and Spectroscopic Studies of Its Reactions with Lewis Bases. Stony Brook University, Stony Brook, NY, 2009.
2. Pagni, R. M.; Kabalka, G. W.; Boothe, R.; Gaetano, K.; Stewart, L. J.; Conaway, R.; Dial, C.; Gray, D.; Larson, S.; Luidhardt, T., Reactions of Unsaturated-Compounds With Iodine and Bromine on Gamma-Alumina. *J. Org. Chem.* **1988,** *53*, 4477-4482.
3. Soscia, M., Palladium catalysed coupling of a vinyl iodide with a terminal alkyne (Sonogashira coupling); enynes. *SyntheticPages* **2001**, 106.
4. Ozawa, T.; Akita, M., Tetrakis(trimethylsilylbutadiynyl)ethene, C18(SiMe3)4: An Extended Two-Dimensional π-Conjugated System Consisting of Eighteen Carbon Atoms. *Chem. Lett.* **2004,** *33*, 1180-1181.
5. Sedelmeier, J.; Ley, S. V.; Lange, H.; Baxendale, I. R., Pd-EnCatTM TPP30 as a Catalyst for the Generation of Highly Functionalized Aryl- and Alkenyl-Substituted Acetylenes via Microwave-Assisted Sonogashira Type Reactions. *Eur. J. Org. Chem.* **2009,** *2009*, 4412-4420.
6. Ranu, B. C.; Chattopadhyay, K., A new route to the synthesis of (E)- and (Z)-2-alkene-4-ynoates and nitriles from vic-diiodo-(E)-alkenes catalyzed by Pd(0) nanoparticles in water. *Org. Lett.* **2007,** *9*, 2409-2412.
7. Terentev, A. O.; Borisov, D. A.; Krylov, I. B.; Nikishin, G. I., Facile Synthesis of E-Diiodoalkenes: H2O2-Activated Reaction of Alkynes with Iodine. *Syn. Comm.* **2007,** *37*, 3151–3164.
8. Wright, M. E.; Lowe-Ma, C. K., Bis(2-pyridyl)silane ligands. 2. Structural characterization and catalytic applications of palladium complexes in organostannane cross-coupling reactions. *Organometallics* **1990,** *9*, 347-352.
9. Luo, L.; Resch, D.; Wilhelm, C.; Young, C. N.; Halada, G. P.; Gambino, R. J.; Grey, C. P.; Goroff, N. S., Room-Temperature Carbonization of Poly(diiododiacetylene) by Reaction with Lewis Bases. *J. Am. Chem. Soc.* **2011,** *133*, 19274-19277.
10. Williams, H., An Investigation into the Action of Bases on Chloroform. *J. Pharm. Pharmacol.* **1959,** *11*, 400-410.
11. (a) Baciocchi, E.; Lillocci, C., Dehalogenation reactions of vicinal dihalides. Part IV. Kinetics of amine-promoted eliminations of 1-chloro-2-iodo-1,2-diphenylethane in aqueous dioxan. *J. Chem. Soc., Perkin Trans. 2* **1975**, 802-804; (b) Tassaing, T.; Besnard, M., Ionization Reaction in Iodine/Pyridine Solutions: What Can We Learn from Conductivity Measurements, Far-Infrared Spectroscopy, and Raman Scattering? *J. Phys. Chem. A* **1997,** *101*, 2803-2808.
12. Miller, S. I.; Noyes, R. M., Iodide-ion Catalysis of the Elimination of Iodine from trans-Diiodoethylene and of the Addition of Iodine to Acetylene. *J. Am. Chem. Soc.* **1952,** *74*, 3403-3406.
13. (a) Winstein, S.; Pressman, D.; Young, W. G., Investigations on the Stereoisomerism of Unsaturated Compounds. V. A Mechanism for the Formation of Butenes from 2,3-Dibromobutanes by the Action of Iodide Ion. *J. Am. Chem. Soc.* **1939,** *61*, 1645-1647; (b) Engman, L., Catalytic Debromination of Vicinal Dibromides. *Tet. Lett.* **1982,** *23*, 3601-3602; (c) Nakayama, J.; Machida, H.; Hoshino, M., A new reduction system: combination of sodium sulfide (sodium hydrosulfide) with phase transfer agent in a two-phase mixture. Reductive debromination ofvic-dibromides to olefins. *Tet. Lett.* **1983,** *24*, 3001-3004.

14. Semnani, A. P., H.R.; Keshavarz, M.H., Spectrophotometric Study of the Interaction between Tetraethylammonium Halides and Aza-15-crown-5 with I2 and ICl in Acetonitrile Solution. *Bull. Korean Chem. Soc.* **2006,** *27*, 886-892.
15. Slator, A., The Decomposition of Ethylene Iodide under the Influence of the Iodide Ion. *J. Chem. Soc., Trans.* **1904,** *85*, 1697-1708.
16. Dillon, R. T., The Reaction Rate of Potassium Iodide with Dibromides of the Ethylene Bromide Type. *J. Am. Chem. Soc.* **1932,** *54* (3), 952-960.
17. Shah, A.-u.-H. A.; Khan, Z. A.; Choudhary, N.; Lohölter, C.; Schäfer, S.; Marie, G. P. L.; Farooq, U.; Witulski, B.; Wirth, T., Iodoxolone-Based Hypervalent Iodine Reagents. *Org. Lett.* **2009,** *11*, 3578-3581.
18. Hollins, R. A.; Campos, M. P. A., *J. Org. Chem.* **1979,** *44*, 3931-3934.
19. SDBSWeb: http://riodb01.ibase.aist.go.jp/sdbs/ (National Institute of Advanced Industrial Science and Technology, June 6, 2012).
20. Organ, M. G.; Ghasemi, H.; Valente, C., The effect of vicinyl olefinic halogens on cross-coupling reactions using Pd(0) catalysis. *Tetrahedron* **2004,** *60*, 9453-9461.

Chapter 1 References

1. Kirk-Othmer, In *Encyclopedia of Chemical Technology*, John Wiley & Sons, Inc.: New York, 1985.
2. The DOE Bioethanol Pilot Plant: A Tool for Commercialization. http://www.nrel.gov/docs/fy00osti/28397.pdf (accessed April 25, 2011).
3. Kowarik, S.; Gerlach, A.; Schreiber, F., Organic molecular beam deposition: fundamentals, growth dynamics, and in situ studies. *J. Phys-Condens. Mat.* **2008,** *20*, 184005.
4. Inzelt, G.; Scholz, F., *Conducting Polymers: A New Era in Electrochemistry*. Springer: Leipzig, Germany, 2008.
5. Yakuphanoglu, F.; Basaran, E.; Şenkal, B. F.; Sezer, E., Electrical and Optical Properties of an Organic Semiconductor Based on Polyaniline Prepared by Emulsion Polymerization and Fabrication of Ag/Polyaniline/n-Si Schottky Diode. *J. Phys. Chem. B* **2006,** *110*, 16908-16913.
6. Klauk, H., *Organic Electronics*. 1st ed.; Wiley VCH Verlag GmbH & Co.: Strauss GmbH, Morlenbach, 2006.
7. McGinnes.J; Corry, P.; Proctor, P., Amorphous Semiconductor Switching in Melanins. *Science* **1974,** *183*, 853-855.
8. (a) Reynolds, J. R.; Ruiz, J. P.; Child, A. D.; Nayak, K.; Marynick, D. S., Electrically conducting polymers containing alternating substituted phenylenes and bithiophene repeat units. *Macromolecules* **1991,** *24*, 678-687; (b) Eley, D. D., Phthalocyanines as Semiconductors. *Nature* **1948,** *162*, 819-819; (c) Chiang, C. K.; Fincher, C. R., Jr.; Park, Y. W.; Heeger, A. J.; Shirakawa, H.; Louis, E. J.; Gau, S. C.; MacDiarmid, A. G., Electrical Conductivity in Doped Polyacetylene. *Phys. Rev. Lett.* **1977,** *39*, 1098-1101; (d) Gundlach, D. J.; Lin, Y. Y.; Jackson, T. N.; Nelson, S. F.; Schlom, D. G., Pentacene organic thin-film transistors - Molecular ordering and mobility. *IEEE Electr. Device L.* **1997,** *18*, 87-89.
9. (a) Huheey, J. E. K., E.A.; Keiter, R.L.;, *Inorganic Chemistry: Principles of Structure and Reactivity*. 4th ed.; HarperCollins College Publishers: New York, NY, 1993; (b) Anslyn, E. V.; Dougherty, D. A., Electronic organic materials. In *Mordern Physical Organic Chemistry*, University Science Books: Sausalito, California, 2004; pp 1001-1046.
10. Huang, X.; Zhai, H. J.; Kiran, B.; Wang, L. S., Observation of d-orbital aromaticity. *Angew. Chem. Int. Ed.* **2005,** *44*, 7251-7254.
11. Brutting, W., *Physics of Organic Semiconductors*. 1st ed.; Wiley-VCH Verlag GmbH &Co. LGaA: Strauss GmbH, Morlenbach, 2005.
12. Odonnell, K. P.; Chen, X., Temperature-Dependence of Semiconductor Band-Gaps. *Appl. Phys. Lett.* **1991,** *58*, 2924-2926.
13. Podesta, M. d., *Understanding the Properties of Matter*. 2nd ed.; Taylor and Francis Inc.: New York, NY, 2002.
14. Kahn, A.; Koch, N.; Gao, W., Electronic structure and electrical properties of interfaces between metals and π-conjugated molecular films. *J. Polym. Sci. Pol. Phys.* **2003,** *41*, 2529-2548.
15. Birendra, T. S.; Sariciftci, N. S., Progress in Plastic Electronics Devices. *Annu. Rev. Mater. Res.* **2006,** *36*, 199–230.
16. Dutta, A. K., Electrical Conductivity of Single Crystals of Graphite. *Phys. Rev.* **1953,** *90*, 187.
17. IUPAC. Compendium of Chemical Terminology, 2nd ed. (the "Gold Book"). Compiled by A. D. McNaught and A. Wilkinson. Blackwell Scientific Publications, Oxford (1997). XML

on-line corrected version: http://goldbook.iupac.org (2006-) created by M. Nic, J. Jirat, B. Kosata; updates compiled by A. Jenkins. ISBN 0-9678550-9-8. doi:10.1351/goldbook.
18. Amano, Y.; Cheng, Q., Detection of influenza virus: traditional approaches and development of biosensors. *Anal Bioanal Chem* **2005,** *381*, 156-164.
19. (a) Reichert, A.; Nagy, J. O.; Spevak, W.; Charych, D., Polydiacetylene Liposomes Functionalized with Sialic Acid Bind and Colorimetrically Detect Influenza Virus. *J. Am. Chem. Soc.* **1995,** *117*, 829-830; (b) Charych, D. H.; Nagy, J. O.; Spevak, W.; Bednarski, M. D., Direct colorimetric detection of a receptor-ligand interaction by a polymerized bilayer assembly. *Science* **1993,** *261*, 585-588.
20. Filhol, J.-S. b.; Deschamps, J. r. m.; Dutremez, S. G.; Boury, B.; Barisien, T.; Legrand, L.; Schott, M., Polymorphs and Colors of Polydiacetylenes: A First Principles Study. *J. Am. Chem. Soc.* **2009,** *131*, 6976-6988.
21. Boyd, R. W., *Nonlinear Optics (Third Edition)*. 3rd ed.; Elsevier Inc.: Burlington, MA, 2008.
22. Franken, P. A.; Weinreich, G.; Peters, C. W.; Hill, A. E., Generation of Optical Harmonics. *Phys. Rev. Lett.* **1961,** *7*, 118-119.
23. (a) Greene, B. I.; Mueller, J. F.; Orenstein, J.; Rapkine, D. H.; Schmittrink, S.; Thakur, M., Phonon-Mediated Optical Nonlinearity in Polydiacetylene. *Phys. Rev. Lett.* **1988,** *61*, 325-328; (b) Bolger, J.; Harvey, T. G.; Ji, W.; Kar, A. K.; Molyneux, S.; Wherrett, B. S.; Bloor, D.; Norman, P., Near-resonant third-order optical nonlinearities in p-toluene sulfonate polydiacetylene. *J. Opt. Soc. Am. B* **1992,** *9*, 1552-1557; (c) Yoshino, F.; Polyakov, S.; Stegeman, G. I., All-optical multiphoton absorption figures of merit: Polydiacetylene poly (bis para-toluene sulfonate) of 2,4-hexadiyne-1,6 diol. *Appl. Phys. Lett.* **2004,** *84*, 5362-5364.
24. Thakur, M.; Meyler, S., Growth of large-area thin-film single crystals of poly(diacetylenes). *Macromolecules* **1985,** *18*, 2341-2344.
25. Polyakov, S.; Yoshino, F.; Liu, M.; Stegeman, G. In *Effects of self-focusing on multiphoton absorption processes in polymer bis-paratoluene sulfonate (PTS)*, Quantum Electronics and Laser Science Conference, 2000. (QELS 2000). Technical Digest, 12-12 May 2000; 2000; pp 169-170.
26. (a) Abdeldayem, H.; Frazier, D. O.; Paley, M. S., An all-optical picosecond switch in polydiacetylene. *App. Phys. Lett.* **2003,** *82*, 1120-1122; (b) Paley, M. S.; Frazier, D. O.; Abdeldayem, H.; McManus, S. P., Photodeposition of Thin Polydiacetylene Films from Solution That Exhibit Large Third-Order Optical Nonlinearities. *Chem. Mater.* **1994,** *6*, 2213-2215.
27. Hossin Abdeldayem; Donald. O. Frazier; Mark S. Paley; Witherow, W. K. Now, Just A Blinkin' Picosecond! http://science.nasa.gov/headlines/y2000/ast28apr_1m.htm (accessed August 12, 2013).
28. (a) Green, P. E., *Fiber Optic Networks*. Prentice Hall: Upper Saddle River, NJ, 1993; (b) Palais, J. C., *Fiber Optic Communications*. 4th ed.; Prentice Hall: Upper Saddle River, NJ, 1998.
29. Bosch, M.; Fischer, C.; Linkatas, I.; Bosshard, C.; Gunter, P. In *Photochemical stability of highly nonlinear optical chromophores for electro-optic applications*, Lasers and Electro-Optics Europe, 2000. Conference Digest., 10-15 Sep 2000.
30. Charlier, J. C.; Gonze, X.; Michenaud, J.-P., Graphite Interplanar Bonding: Electronic Delocalization and van der Waals Interaction. *Europhys. Lett.* **1994,** *28*, 403.
31. Boehm, H. P.; Clauss, A.; Fischer, G. O.; Hofmann, U., Das Adsorptionsverhalten sehr dünner Kohlenstoff-Folien. *Z. Anorg. Allg. Chem.* **1962,** *316*, 119-127.

32. Novoselov, K. S.; Geim, A. K.; Morozov, S. V.; Jiang, D.; Zhang, Y.; Dubonos, S. V.; Grigorieva, I. V.; Firsov, A. A., Electric field effect in atomically thin carbon films. *Science* **2004,** *306*, 666-669.
33. (a) Geim, A. K., Graphene: Status and Prospects. *Science* **2009,** *324*, 1530-1534; (b) Geim, A. K.; Novoselov, K. S., The rise of graphene. *Nat Mater* **2007,** *6*, 183-191.
34. Lin, Y. M.; Dimitrakopoulos, C.; Jenkins, K. A.; Farmer, D. B.; Chiu, H. Y.; Grill, A.; Avouris, P., 100-GHz Transistors from Wafer-Scale Epitaxial Graphene. *Science* **2010,** *327*, 662-662.
35. Ryu, S.; Han, M. Y.; Maultzsch, J.; Heinz, T. F.; Kim, P.; Steigerwald, M. L.; Brus, L. E., Reversible Basal Plane Hydrogenation of Graphene. *Nano Lett.* **2008,** *8*, 4597-4602.
36. Du, A.; Zhu, Z.; Smith, S. C., Multifunctional Porous Graphene for Nanoelectronics and Hydrogen Storage: New Properties Revealed by First Principle Calculations. *J. Am. Chem. Soc.* **2010,** *132*, 2876-2877.
37. Langa, F.; Nierengarten, J.-F., *Fullerenes: Principles and Applications*. The Royal Society of Chemistry: Cambridge CB4 0WF, UK, 2007.
38. Pan, H.; Li, J.; Feng, Y., Carbon Nanotubes for Supercapacitor. *Nanoscale Res. Lett.* **2010,** *5*, 654 - 668.
39. Aliev, A.; Gartstein, Y.; Baughman, R. H., Mirage effect from thermally modulated transparent carbon nanotube sheets. *Nanotechnology* **2011,** *43*, 435704.
40. Kaempgen, M.; Lebert, M.; Nicoloso, N.; Roth, S., Multifunctional carbon nanotube networks for fuel cells *Appl. Phys. Lett.* **2008,** *92*, 094103.
41. Lagow, R. J.; Kampa, J. J.; Wei, H. C.; Battle, S. L.; Genge, J. W.; Laude, D. A.; Harper, C. J.; Bau, R.; Stevens, R. C.; Haw, J. F.; Munson, E., Synthesis of Linear Acetylenic Carbon - The sp Carbon Allotrope. *Science* **1995,** *267*, 362-367.
42. Casari, C. S.; Li Bassi, A.; Ravagnan, L.; Siviero, F.; Lenardi, C.; Piseri, P.; Bongiorno, G.; Bottani, C. E.; Milani, P., Chemical and thermal stability of carbyne-like structures in cluster-assembled carbon films. *Phys. Rev. B* **2004,** *69*, 075422.
43. Hummers, W. S.; Offeman, R. E., Preparation of Graphitic Oxide. *J. Am. Chem. Soc.* **1958,** *80*, 1339-1339.
44. Marcano, D. C.; Kosynkin, D. V.; Berlin, J. M.; Sinitskii, A.; Sun, Z.; Slesarev, A.; Alemany, L. B.; Lu, W.; Tour, J. M., Improved Synthesis of Graphene Oxide. *ACS Nano* **2010,** *4*, 4806-4814.
45. Gao, W.; Alemany, L. B.; Ci, L.; Ajayan, P. M., New insights into the structure and reduction of graphite oxide. *Nat. Chem.* **2009,** *1*, 403-408.
46. Ismach, A.; Druzgalski, C.; Penwell, S.; Schwartzberg, A.; Zheng, M.; Javey, A.; Bokor, J.; Zhang, Y., Direct Chemical Vapor Deposition of Graphene on Dielectric Surfaces. *Nano Lett.* **2010,** *10*, 1542-1548.
47. Iijima, S., Helical Microtubules of Graphitic Carbon. *Nature* **1991,** *354*, 56-58.
48. Guo, T.; Nikolaev, P.; Rinzler, A. G.; Tomanek, D.; Colbert, D. T.; Smalley, R. E., Self-Assembly of Tubular Fullerenes. *J. Phys. Chem.* **1995,** *99*, 10694-10697.
49. Joseyacaman, M.; Mikiyoshida, M.; Rendon, L.; Santiesteban, J. G., Catalytic Growth of Carbon Microtubules with Fullerene Structure. *Appl. Phys. Lett.* **1993,** *62*, 657-659.
50. Scott, L. T.; Boorum, M. M.; McMahon, B. J.; Hagen, S.; Mack, J.; Blank, J.; Wegner, H.; de Meijere, A., A rational chemical synthesis of C-60. *Science* **2002,** *295*, 1500-1503.
51. Fowler, F. W.; Lauher, J. W., A rational design of molecular materials. *J. Phys. Org. Chem.* **2000,** *13*, 850-857.

52. (a) Baughman, R. H., Solid-State Synthesis of Large Polymer Single Crystals. *J. Polym. Sci., Part B: Polym. Phys.* **1974,** *12*, 1511-1535; (b) Wegner, G., Topochemical polymerization of monomers with conjugated triple bonds. *Macromol. Chem. Phys.* **1972,** *154*, 35-48; (c) Wegner, G., Topochemical reactions of monomers with conjugated triple-bonds. IV. Polymerization of bis-(p-toluene sulfonate) of 2.4-hexadiin-1.6-diol. *Macromol. Chem. Phys.* **1971,** *145*, 85-94.
53. (a) Kim, J.-M.; Lee, Y. B.; Yang, D. H.; Lee, J.-S.; Lee, G. S.; Ahn, D. J., A Polydiacetylene-Based Fluorescent Sensor Chip. *J. Am. Chem. Soc.* **2005,** *127*, 17580-17581; (b) Ahn, D. J.; Chae, E.-H.; Lee, G. S.; Shim, H.-Y.; Chang, T.-E.; Ahn, K.-D.; Kim, J.-M., Colorimetric Reversibility of Polydiacetylene Supramolecules Having Enhanced Hydrogen-Bonding under Thermal and pH Stimuli. *J. Am. Chem. Soc.* **2003,** *125*, 8976-8977; (c) Fujita, N.; Sakamoto, Y.; Shirakawa, M.; Ojima, M.; Fujii, A.; Ozaki, M.; Shinkai, S., Polydiacetylene Nanofibers Created in Low-Molecular-Weight Gels by Post Modification: Control of Blue and Red Phases by the Odd−Even Effect in Alkyl Chains. *J. Am. Chem. Soc.* **2007,** *129*, 4134-4135.
54. Wilhelm, C.; Boyd, S. A.; Chawda, S.; Fowler, F. W.; Goroff, N. S.; Halada, G. P.; Grey, C. P.; Lauher, J. W.; Luo, L.; Martin, C. D.; Parise, J. B.; Tarabrella, C.; Webb, J. A., Pressure-Induced Polymerization of Diiodobutadiyne in Assembled Cocrystals. *J. Am. Chem. Soc.* **2008,** *130*, 4415-4420.
55. (a) Sun, A. W.; Lauher, J. W.; Goroff, N. S., Preparation of poly(diiododiacetylene), an ordered conjugated polymer of carbon and iodine. *Science* **2006,** *312*, 1030-1034; (b) Lauher, J. W.; Fowler, F. W.; Goroff, N. S., Single-Crystal-to-Single-Crystal Topochemical Polymerizations by Design. *Acc. Chem. Res.* **2008,** *41*, 1215-1229.
56. Goroff, N. S.; Curtis, S. M.; Webb, J. A.; Fowler, F. W.; Lauher, J. W., Designed Cocrystals Based on the Pyridine−Iodoalkyne Halogen Bond. *Org. Lett.* **2005,** *7*, 1891-1893.
57. Luo, L.; Wilhelm, C.; Sun, A.; Grey, C. P.; Lauher, J. W.; Goroff, N. S., Poly(diiododiacetylene): Preparation, Isolation, and Full Characterization of a Very Simple Poly(diacetylene). *J. Am. Chem. Soc.* **2008,** *130*, 7702-7709.
58. Luo, L. Preparation and Comprehensive Characterization of Poly(diiododiacetylene) and Spectroscopic Studies of Its Reactions with Lewis Bases. Stony Brook University, Stony Brook, NY, 2009.
59. Luo, L.; Wilhelm, C.; Young, C. N.; Grey, C. P.; Halada, G. P.; Xiao, K.; Ivanov, I. N.; Howe, J. Y.; Geohegan, D. B.; Goroff, N. S., Characterization and Carbonization of Highly Oriented Poly(diiododiacetylene) Nanofibers. *Macromolecules* **2011,** *44*, 2626-2631.
60. Luo, L.; Resch, D.; Wilhelm, C.; Young, C. N.; Halada, G. P.; Gambino, R. J.; Grey, C. P.; Goroff, N. S., Room-Temperature Carbonization of Poly(diiododiacetylene) by Reaction with Lewis Bases. *J. Am. Chem. Soc.* **2011,** *133*, 19274-19277.

Chapter 2 References

1. Sun, A. W.; Lauher, J. W.; Goroff, N. S., Preparation of poly(diiododiacetylene), an ordered conjugated polymer of carbon and iodine. *Science* **2006,** *312*, 1030-1034.
2. Luo, L.; Wilhelm, C.; Sun, A.; Grey, C. P.; Lauher, J. W.; Goroff, N. S., Poly(diiododiacetylene): Preparation, Isolation, and Full Characterization of a Very Simple Poly(diacetylene). *J. Am. Chem. Soc.* **2008,** *130*, 7702-7709.
3. Luo, L. Preparation and Comprehensive Characterization of Poly(diiododiacetylene) and Spectroscopic Studies of Its Reactions with Lewis Bases. Stony Brook University, Stony Brook, NY, 2009.
4. Fringuelli, F.; Pizzo, F.; Vaccaro, L., Cobalt(II) Chloride-Catalyzed Chemoselective Sodium Borohydride Reduction of Azides in Water. *Synthesis* **2000,** *2000*, 646-650.
5. Osby, J. O.; Heinzman, S. W.; Ganem, B., Studies on the mechanism of transition-metal-assisted sodium borohydride and lithium aluminum hydride reductions. *J. Am. Chem. Soc.* **1986,** *108*, 67-72.

Chapter 3 References

1. Chalifoux, W. A.; Tykwinski, R. R., Synthesis of polyynes to model the sp-carbon allotrope carbyne. *Nature Chemistry* **2010,** *2*, 967-971.
2. (a) Glaser, C., Beiträge zur Kenntniss des Acetenylbenzols. *Ber. Dtsch. Chem. Ges.* **1869,** *2*, 422-424; (b) Hay, A. S., Oxidative Coupling of Acetylenes. *J. Org. Chem.* **1962,** *27*, 3320-3321; (c) Eglinton, G.; Galbraith, A. R., 182. Macrocyclic acetylenic compounds. Part I. Cyclotetradeca-1 :3-diyne and related compounds. *J. Chem. Soc.* **1959,** *0*, 889-896.
3. Luo, L.; Wilhelm, C.; Young, C. N.; Grey, C. P.; Halada, G. P.; Xiao, K.; Ivanov, I. N.; Howe, J. Y.; Geohegan, D. B.; Goroff, N. S., Characterization and Carbonization of Highly Oriented Poly(diiododiacetylene) Nanofibers. *Macromolecules* **2011,** *44*, 2626-2631.
4. Luo, L.; Resch, D.; Wilhelm, C.; Young, C. N.; Halada, G. P.; Gambino, R. J.; Grey, C. P.; Goroff, N. S., Room-Temperature Carbonization of Poly(diiododiacetylene) by Reaction with Lewis Bases. *J. Am. Chem. Soc.* **2011,** *133*, 19274-19277.
5. Luo, L. Preparation and Comprehensive Characterization of Poly(diiododiacetylene) and Spectroscopic Studies of Its Reactions with Lewis Bases. Stony Brook University, Stony Brook, NY, 2009.
6. Luo, L.; Wilhelm, C.; Sun, A.; Grey, C. P.; Lauher, J. W.; Goroff, N. S., Poly(diiododiacetylene): Preparation, Isolation, and Full Characterization of a Very Simple Poly(diacetylene). *J. Am. Chem. Soc.* **2008,** *130*, 7702-7709.
7. (a) Krishna, C. M.; Kondo, T.; Riesz, P., Sonochemistry of Alcohol-Water Mixtures - Spin -Trapping Evidence for Thermal-Decomposition and Isotope-Exchange Reactions. *J. Phys. Chem.* **1989,** *93*, 5166-5172; (b) Okitsu, K.; Nakamura, H.; Takenaka, N.; Bandow, H.; Maeda, Y.; Nagata, Y., Sonochemical reactions occurring in organic solvents: reaction kinetics and reaction site of radical trapping with 1,1-diphenyl-2-picrylhydrazyl. *Res. Chem. Intermediat.* **2004,** *30*, 763-774; (c) Forney, M. W.; Poler, J. C., Sonochemical Formation of Methyl Hydroperoxide in Polar Aprotic Solvents and Its Effect on Single-Walled Carbon Nanotube Dispersion Stability. *J. Am. Chem. Soc.* **2010,** *132*, 791-797.
8. (a) Winstein, S.; Pressman, D.; Young, W. G., Investigations on the Stereoisomerism of Unsaturated Compounds. V. A Mechanism for the Formation of Butenes from 2,3-Dibromobutanes by the Action of Iodide Ion. *J. Am. Chem. Soc.* **1939,** *61*, 1645-1647; (b) Miller, S. I.; Noyes, R. M., Iodide-ion Catalysis of the Elimination of Iodine from trans-Diiodoethylene and of the Addition of Iodine to Acetylene. *J. Am. Chem. Soc.* **1952,** *74*, 3403-3406.
9. Yasui, S.; Itoh, K.; Ohno, A., Kinetic study on debromination of vic-dibromides with trivalent phosphorus compounds. *Heteroat. Chem.* **2001,** *12*, 217-222.
10. de Faria, D. L. A.; Gonçalves, N. S.; Santos, P. S., Vibrational spectra of iodine and bromine thiourea complexes. *Spectrochim. Acta A* **1989,** *45*, 643-647.
11. Baciocchi, E.; Lillocci, C., Dehalogenation reactions of vicinal dihalides. Part III. Dehalogenations of 1-chloro-2-iodo-1,2-diphenylethane induced by a variety of nucleophiles. The nucleophilic reactivity towards iodine. *J. Chem. Soc., Perkin Trans. 2* **1973**, 38-41.

Chapter 4 References

1. Luo, L. Preparation and Comprehensive Characterization of Poly(diiododiacetylene) and Spectroscopic Studies of Its Reactions with Lewis Bases. Stony Brook University, Stony Brook, NY, 2009.
2. Pagni, R. M.; Kabalka, G. W.; Boothe, R.; Gaetano, K.; Stewart, L. J.; Conaway, R.; Dial, C.; Gray, D.; Larson, S.; Luidhardt, T., Reactions of Unsaturated-Compounds With Iodine and Bromine on Gamma-Alumina. *J. Org. Chem.* **1988,** *53*, 4477-4482.
3. Soscia, M., Palladium catalysed coupling of a vinyl iodide with a terminal alkyne (Sonogashira coupling); enynes. *SyntheticPages* **2001**, 106.
4. Ozawa, T.; Akita, M., Tetrakis(trimethylsilylbutadiynyl)ethene, C18(SiMe3)4: An Extended Two-Dimensional π-Conjugated System Consisting of Eighteen Carbon Atoms. *Chem. Lett.* **2004,** *33*, 1180-1181.
5. Sedelmeier, J.; Ley, S. V.; Lange, H.; Baxendale, I. R., Pd-EnCatTM TPP30 as a Catalyst for the Generation of Highly Functionalized Aryl- and Alkenyl-Substituted Acetylenes via Microwave-Assisted Sonogashira Type Reactions. *Eur. J. Org. Chem.* **2009,** *2009*, 4412-4420.
6. Ranu, B. C.; Chattopadhyay, K., A new route to the synthesis of (E)- and (Z)-2-alkene-4-ynoates and nitriles from vic-diiodo-(E)-alkenes catalyzed by Pd(0) nanoparticles in water. *Org. Lett.* **2007,** *9*, 2409-2412.
7. Terentev, A. O.; Borisov, D. A.; Krylov, I. B.; Nikishin, G. I., Facile Synthesis of E-Diiodoalkenes: H2O2-Activated Reaction of Alkynes with Iodine. *Syn. Comm.* **2007,** *37*, 3151–3164.
8. Wright, M. E.; Lowe-Ma, C. K., Bis(2-pyridyl)silane ligands. 2. Structural characterization and catalytic applications of palladium complexes in organostannane cross-coupling reactions. *Organometallics* **1990,** *9*, 347-352.
9. Luo, L.; Resch, D.; Wilhelm, C.; Young, C. N.; Halada, G. P.; Gambino, R. J.; Grey, C. P.; Goroff, N. S., Room-Temperature Carbonization of Poly(diiododiacetylene) by Reaction with Lewis Bases. *J. Am. Chem. Soc.* **2011,** *133*, 19274-19277.
10. Williams, H., An Investigation into the Action of Bases on Chloroform. *J. Pharm. Pharmacol.* **1959,** *11*, 400-410.
11. (a) Baciocchi, E.; Lillocci, C., Dehalogenation reactions of vicinal dihalides. Part IV. Kinetics of amine-promoted eliminations of 1-chloro-2-iodo-1,2-diphenylethane in aqueous dioxan. *J. Chem. Soc., Perkin Trans. 2* **1975**, 802-804; (b) Tassaing, T.; Besnard, M., Ionization Reaction in Iodine/Pyridine Solutions: What Can We Learn from Conductivity Measurements, Far-Infrared Spectroscopy, and Raman Scattering? *J. Phys. Chem. A* **1997,** *101*, 2803-2808.
12. Miller, S. I.; Noyes, R. M., Iodide-ion Catalysis of the Elimination of Iodine from trans-Diiodoethylene and of the Addition of Iodine to Acetylene. *J. Am. Chem. Soc.* **1952,** *74*, 3403-3406.
13. (a) Winstein, S.; Pressman, D.; Young, W. G., Investigations on the Stereoisomerism of Unsaturated Compounds. V. A Mechanism for the Formation of Butenes from 2,3-Dibromobutanes by the Action of Iodide Ion. *J. Am. Chem. Soc.* **1939,** *61*, 1645-1647; (b) Engman, L., Catalytic Debromination of Vicinal Dibromides. *Tet. Lett.* **1982,** *23*, 3601-3602; (c) Nakayama, J.; Machida, H.; Hoshino, M., A new reduction system: combination of sodium sulfide (sodium hydrosulfide) with phase transfer agent in a two-phase mixture. Reductive debromination ofvic-dibromides to olefins. *Tet. Lett.* **1983,** *24*, 3001-3004.

14. Semnani, A. P., H.R.; Keshavarz, M.H., Spectrophotometric Study of the Interaction between Tetraethylammonium Halides and Aza-15-crown-5 with I2 and ICl in Acetonitrile Solution. *Bull. Korean Chem. Soc.* **2006,** *27*, 886-892.
15. Slator, A., The Decomposition of Ethylene Iodide under the Influence of the Iodide Ion. *J. Chem. Soc., Trans.* **1904,** *85*, 1697-1708.
16. Dillon, R. T., The Reaction Rate of Potassium Iodide with Dibromides of the Ethylene Bromide Type. *J. Am. Chem. Soc.* **1932,** *54* (3), 952-960.
17. Shah, A.-u.-H. A.; Khan, Z. A.; Choudhary, N.; Lohölter, C.; Schäfer, S.; Marie, G. P. L.; Farooq, U.; Witulski, B.; Wirth, T., Iodoxolone-Based Hypervalent Iodine Reagents. *Org. Lett.* **2009,** *11*, 3578-3581.
18. Hollins, R. A.; Campos, M. P. A., *J. Org. Chem.* **1979,** *44*, 3931-3934.
19. SDBSWeb: http://riodb01.ibase.aist.go.jp/sdbs/ (National Institute of Advanced Industrial Science and Technology, June 6, 2012).
20. Organ, M. G.; Ghasemi, H.; Valente, C., The effect of vicinyl olefinic halogens on cross-coupling reactions using Pd(0) catalysis. *Tetrahedron* **2004,** *60*, 9453-9461.

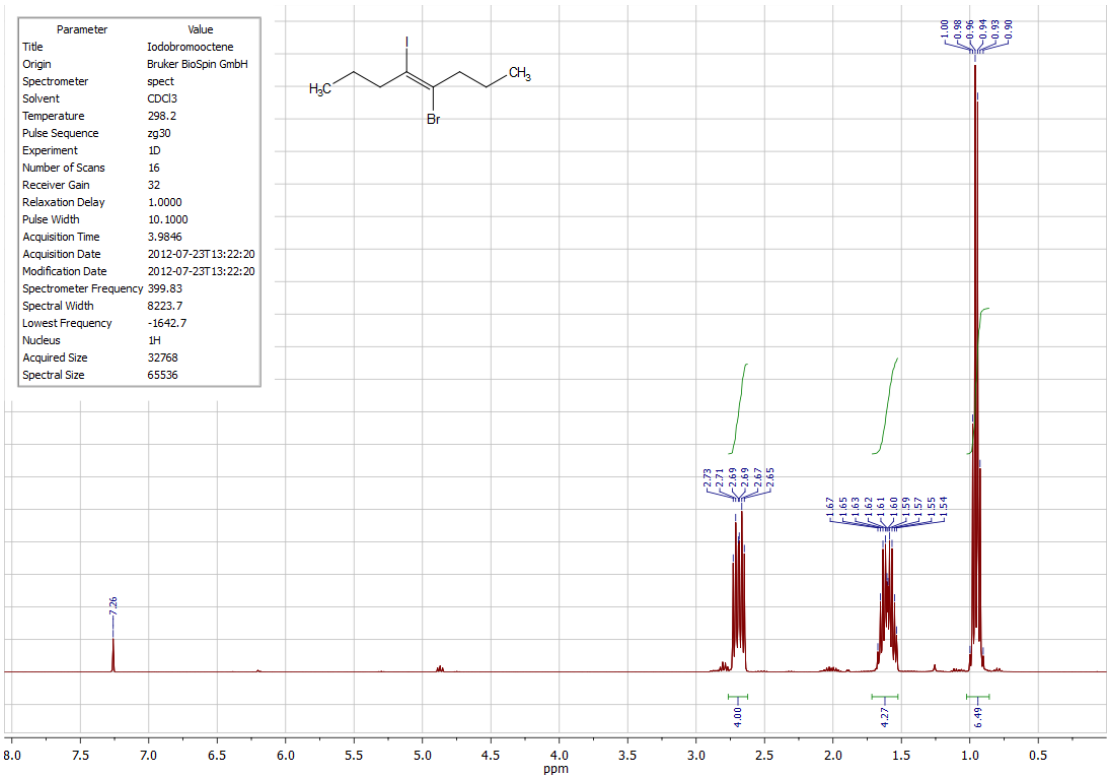

^{1}H-NMR of compound **25**

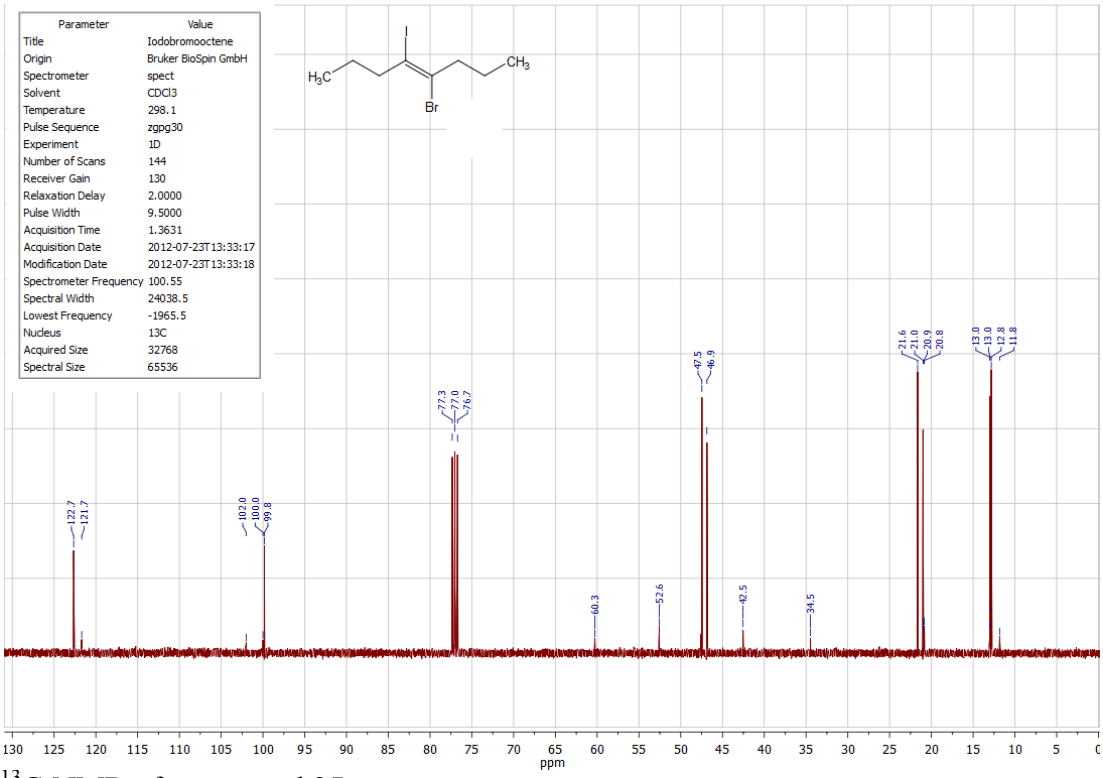

^{13}C-NMR of compound **25**

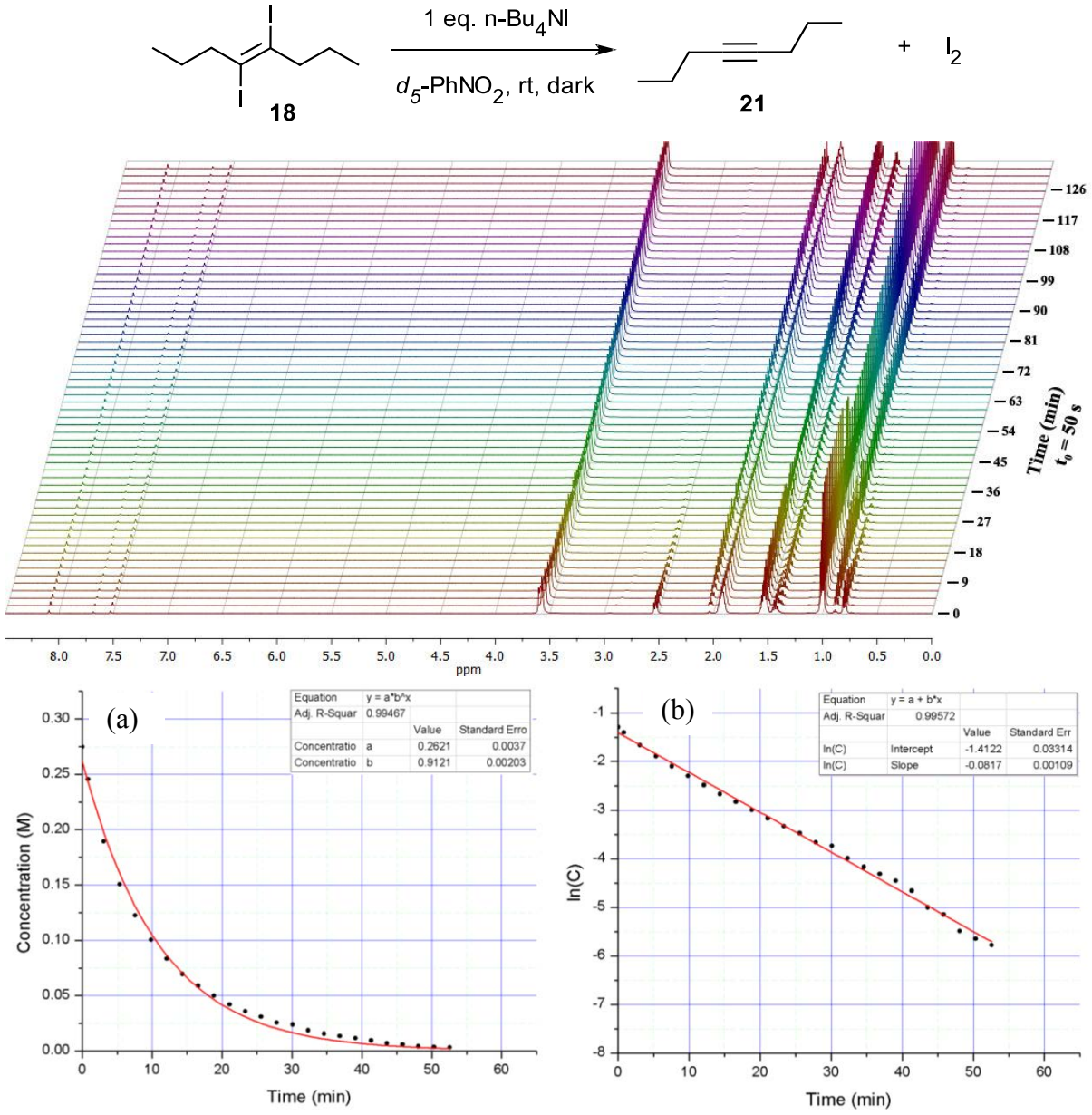

Kinetic analysis of 0.275 M alkene **18** reacting with 0.275 M n-Bu_4NI in d_5-$PhNO_2$. The protons alpha to the diiodoalkene of **18** were integrated from 2.51–2.58 ppm and the protons alpha to the alkyne of **21** were integrated between 2.12–2.05 ppm. Plot (a) shows concentration of compound **18** (C) as a function of time. Plot (b) shows ln(C) as a function of time.

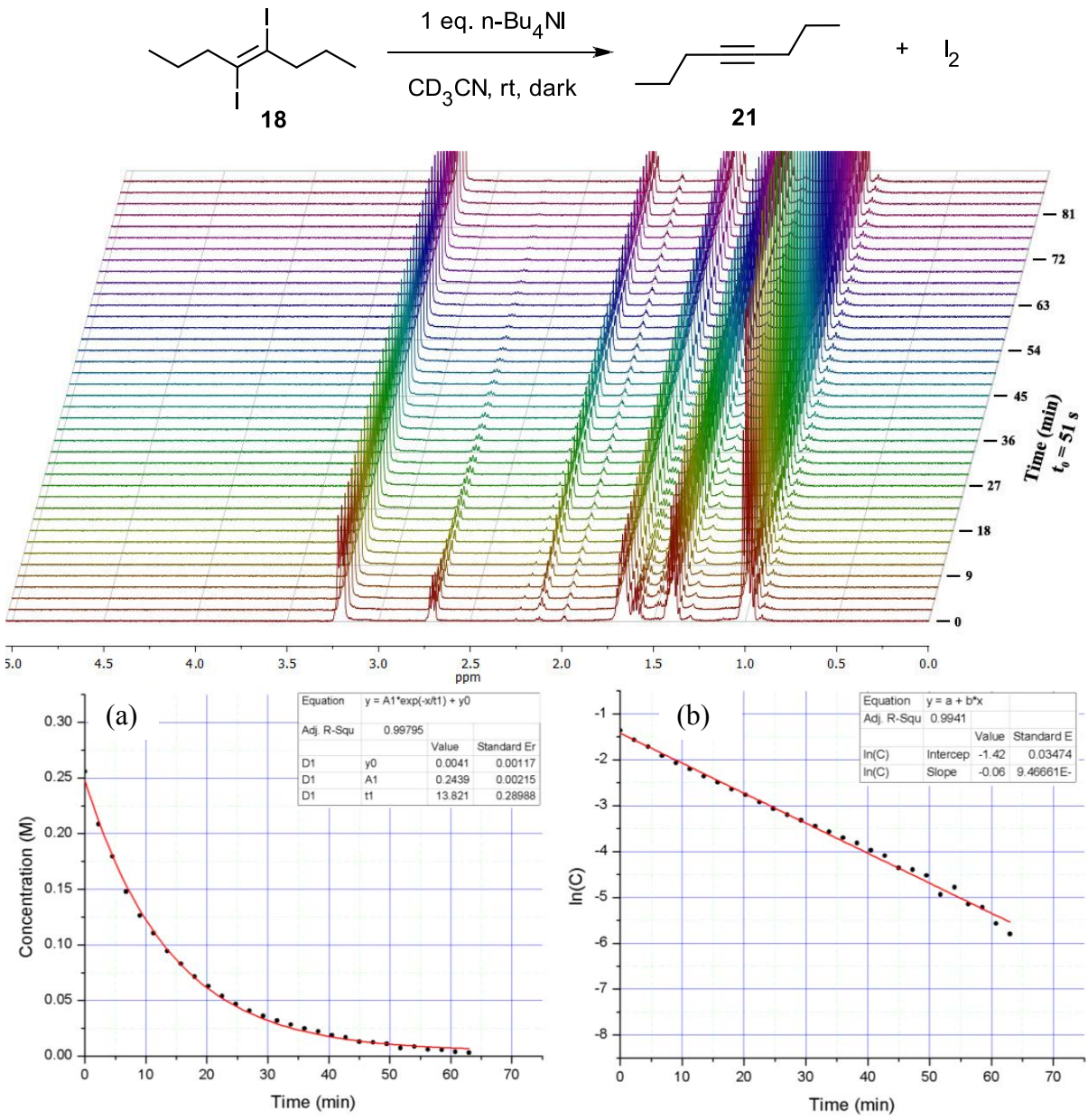

Kinetic analysis of 0.275 M alkene **18** reacting with 0.275 M n-Bu_4NI in CD_3CN. The protons alpha to the diiodoalkene of **18** were integrated from 2.51–2.58 ppm and the protons alpha to the alkyne of **21** were integrated between 2.12–2.05 ppm. Plot (a) shows concentration of compound **18** (C) as a function of time. Plot (b) shows the natural log of concentration plotted as a function of time.

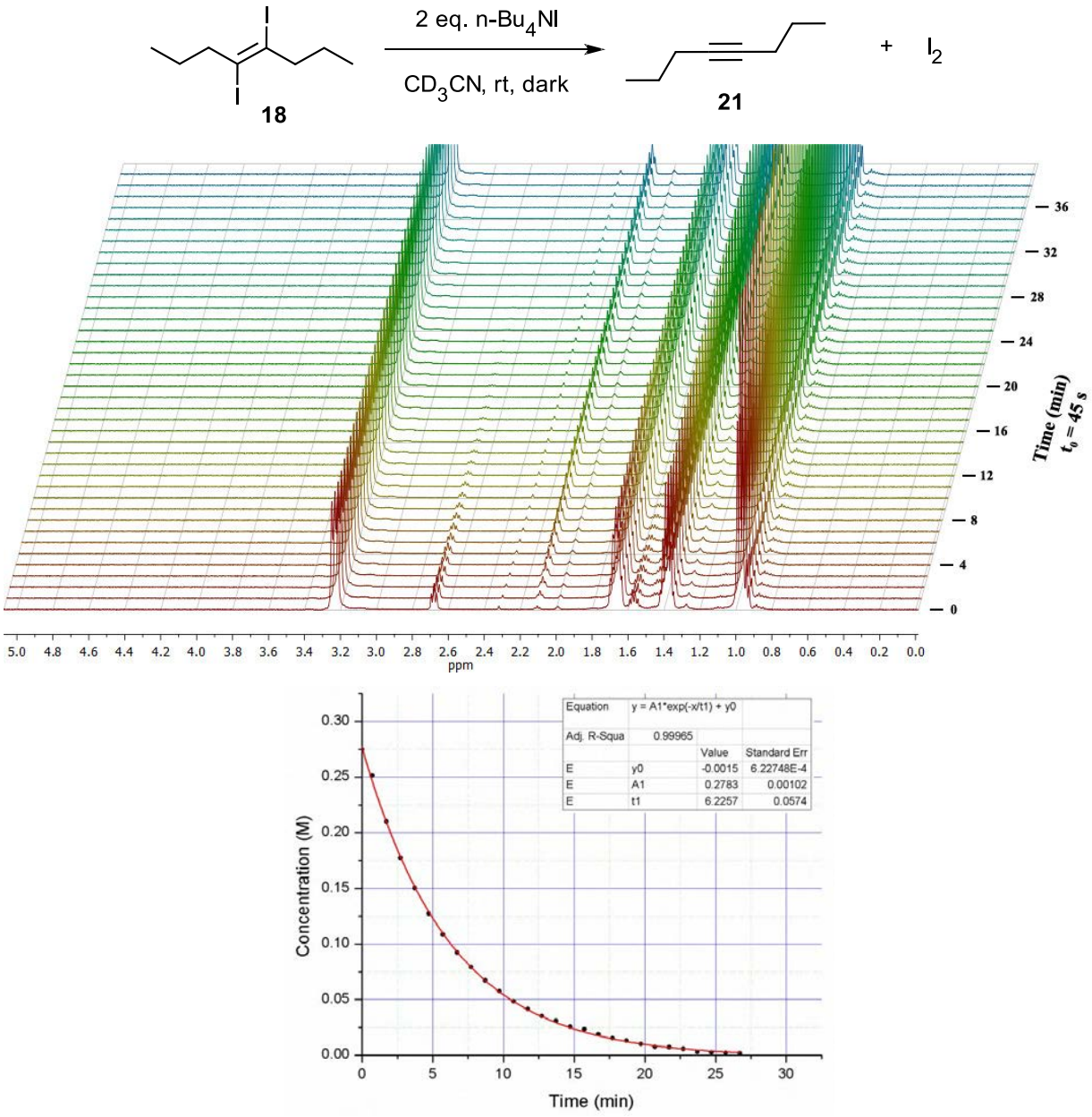

Kinetic analysis of 0.275 M Alkene **18** reacting with 0.550 M n-Bu_4NI in CD_3CN. The protons alpha to the diiodoalkene of **18** were integrated from 2.51–2.58 ppm and the protons alpha to the alkyne of **21** were integrated between 2.12–2.05 ppm. The plot shows concentration of compound **18** (C) as a function of time.

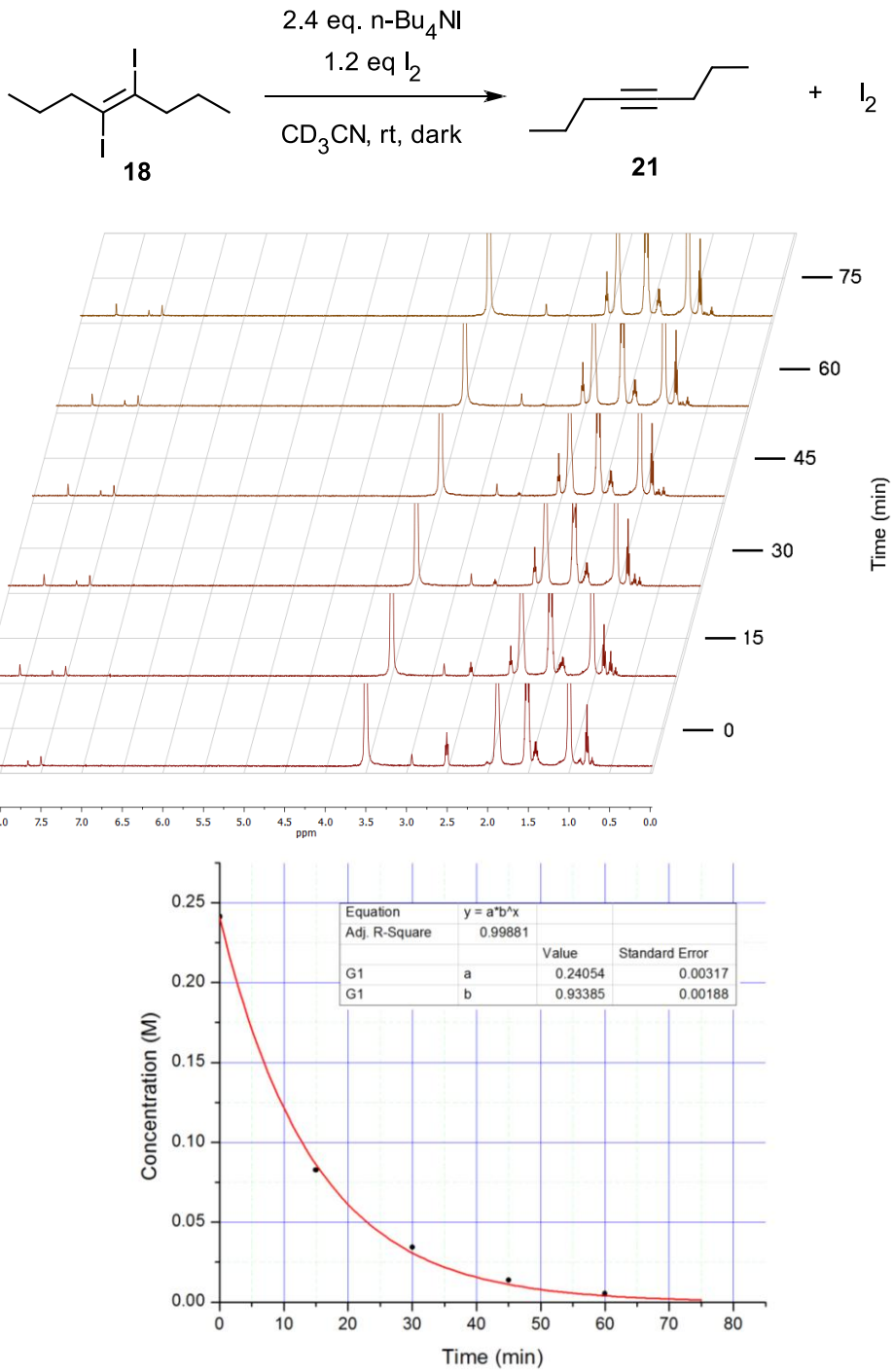

Kinetic analysis of 0.275 M alkene 1, 0.330 M I_2, and 0.660 n-Bu_4NI. Time delay from injection of alkene **18** and collection of first data point is estimated to be about 1 minute. The plot shows concentration as a function of time.

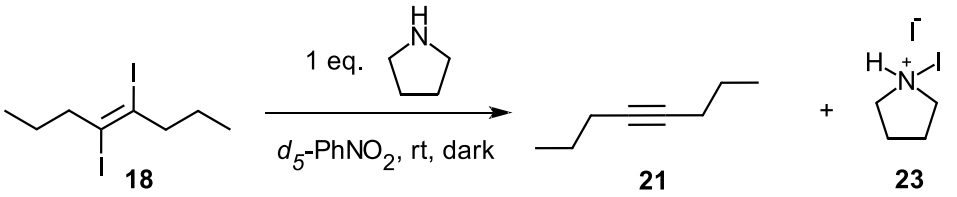
1 eq.
d_5-PhNO$_2$, rt, dark
18
21
23

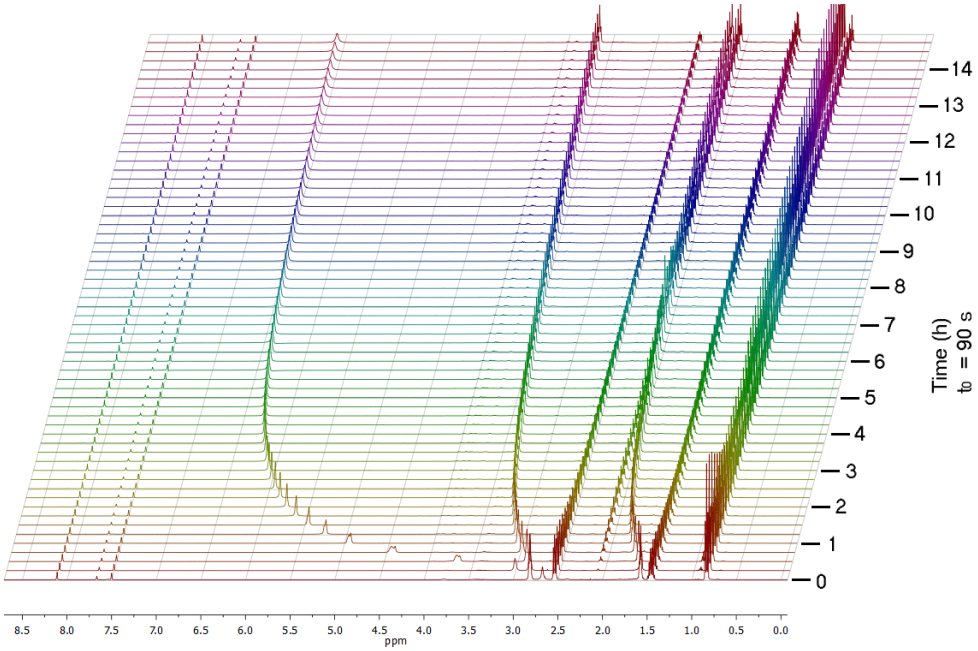
14
13
12
11
10
9
8
7
6
5
4
3
2
1
0
Time (h)
t_0 = 90 s
8.5 8.0 7.5 7.0 6.5 6.0 5.5 5.0 4.5 4.0 3.5 3.0 2.5 2.0 1.5 1.0 0.5 0.0
ppm

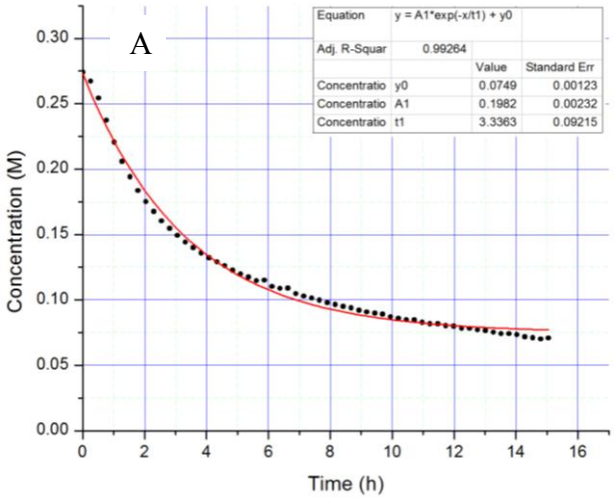
A
Equation y = A1*exp(-x/t1) + y0
Adj. R-Squar 0.99264
Value Standard Err
Concentratio y0 0.0749 0.00123
Concentratio A1 0.1982 0.00232
Concentratio t1 3.3363 0.09215
Concentration (M)
Time (h)

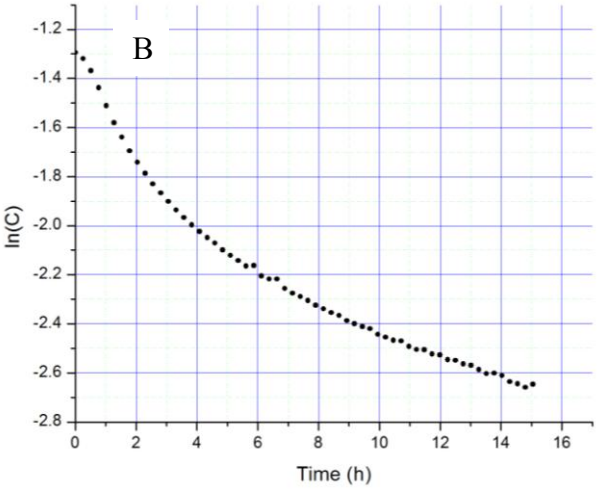
B
ln(C)
Time (h)

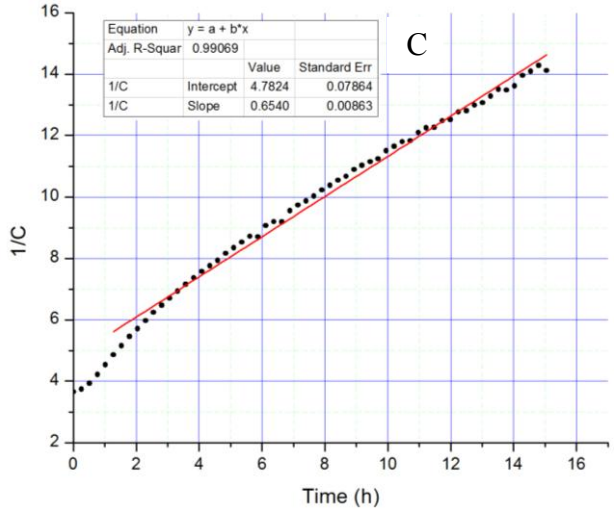

Kinetic analysis of 0.275 M Alkene **18** reacting with 0.275 M Pyrrolidine in d_5-$PhNO_2$. The methyl group of **18** was integrated from 0.87–0.81 ppm and the methyl group of **21** was integrated between 0.89–0.95 ppm. Plot A shows concentration of compound **18** (C) as a function of time. Plot B shows ln(C) as a function of time. Plot C shows C^{-1} as a function of time.

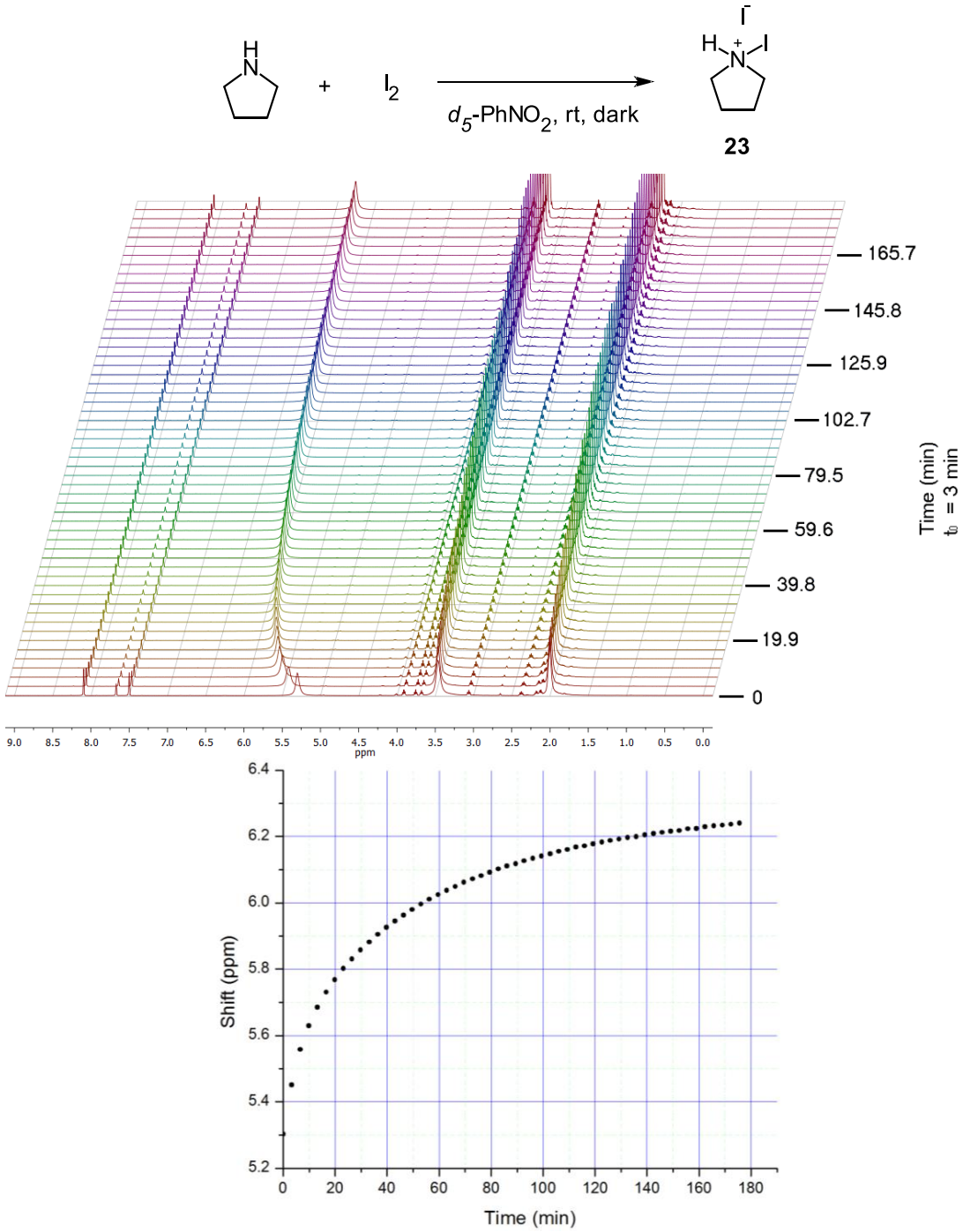

Kinetic analysis of 0.275 M iodine reacting with 0.275 M pyrrolidine in d_5-nitrobenzene. The pyrrolidinium proton shift is plotted as a function of time.

Tetrabutylammonium fluoride induced deiodination

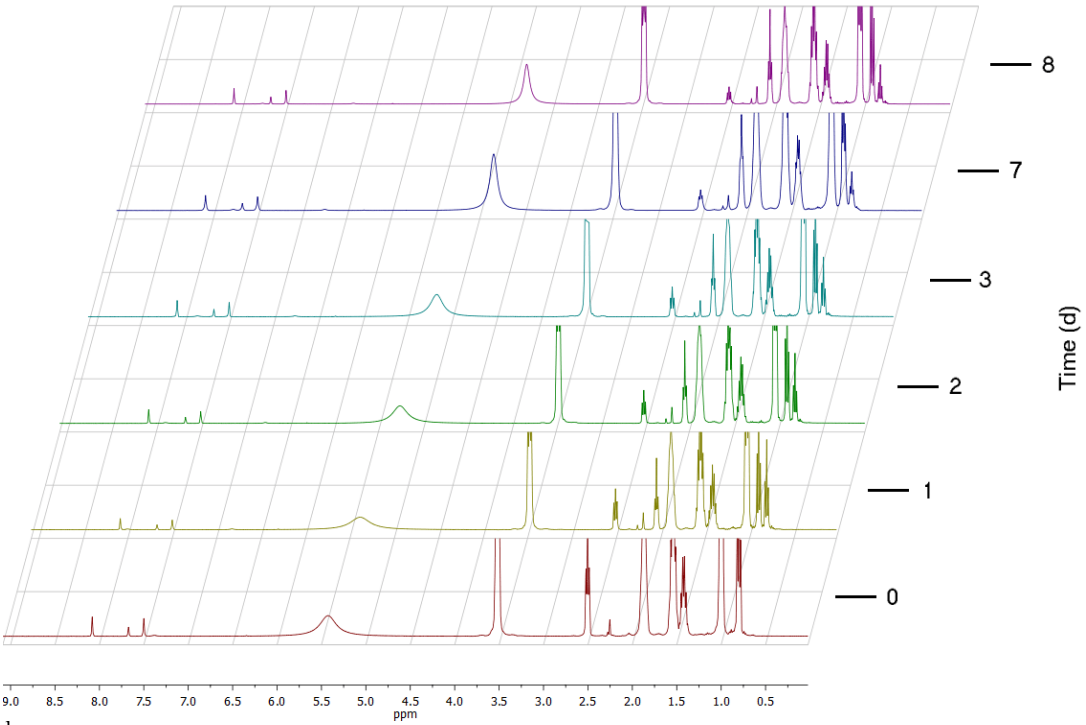

^{1}H NMR (400 MHz, d_5-PhNO$_2$)

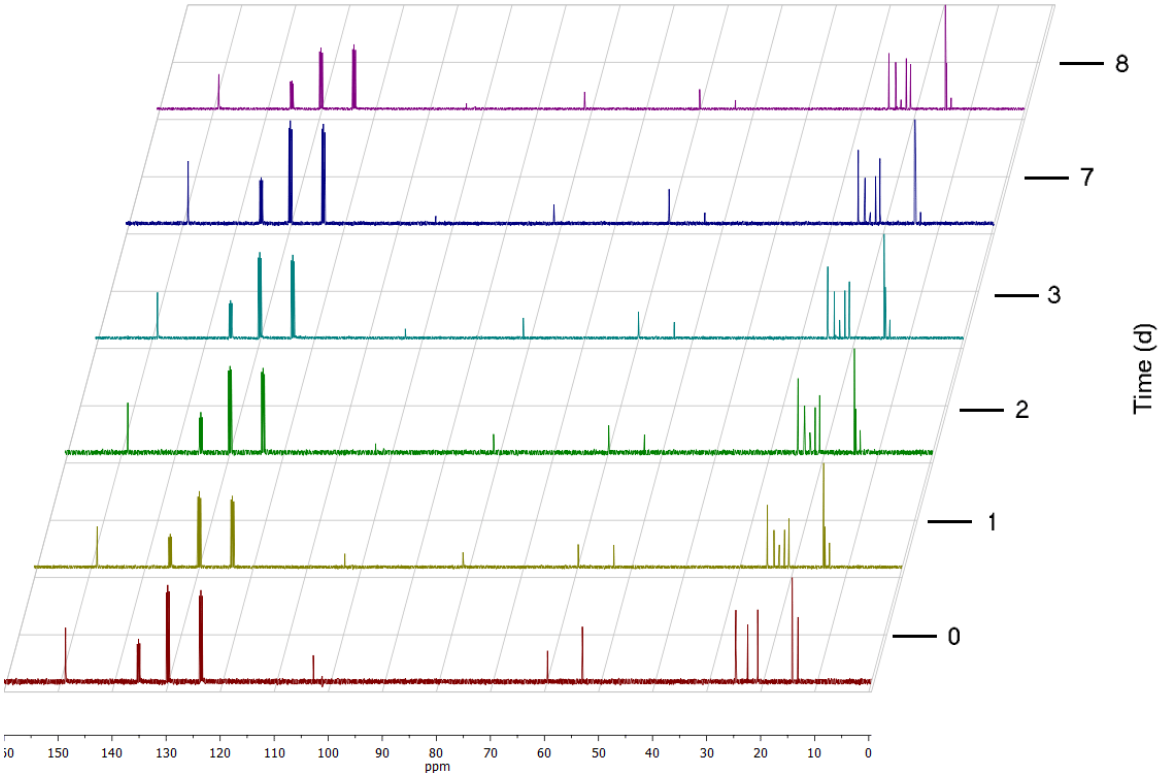

^{13}C NMR (100 MHz, d_5-PhNO$_2$)

Tetrabutylammonium chloride induced deiodination

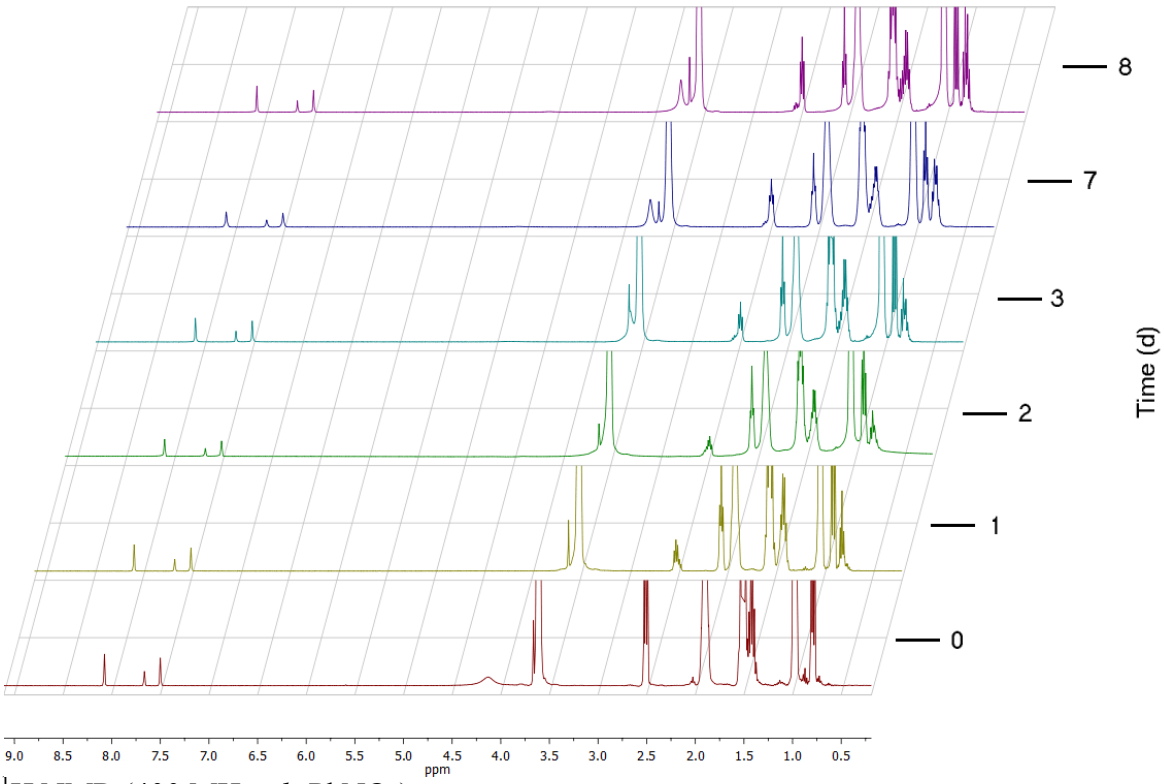

^{1}H NMR (400 MHz, d_5-$PhNO_2$)

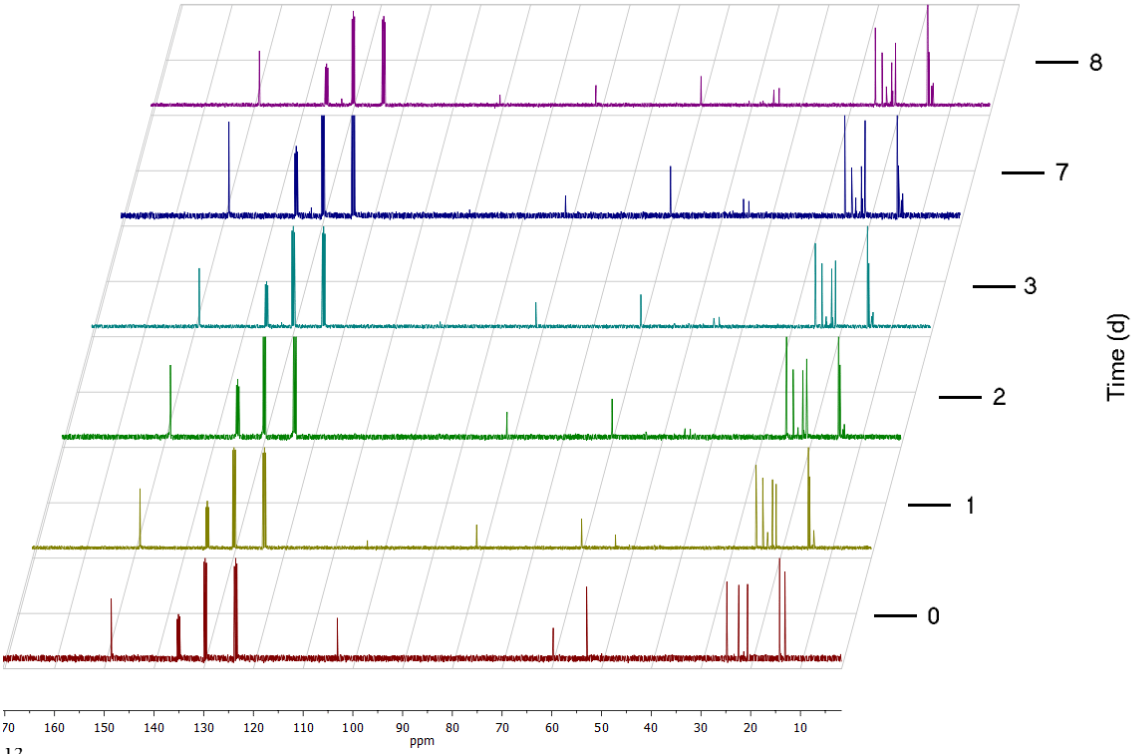

^{13}C NMR (100 MHz, d_5-$PhNO_2$)

Tetrabutylammonium bromide induced deiodination

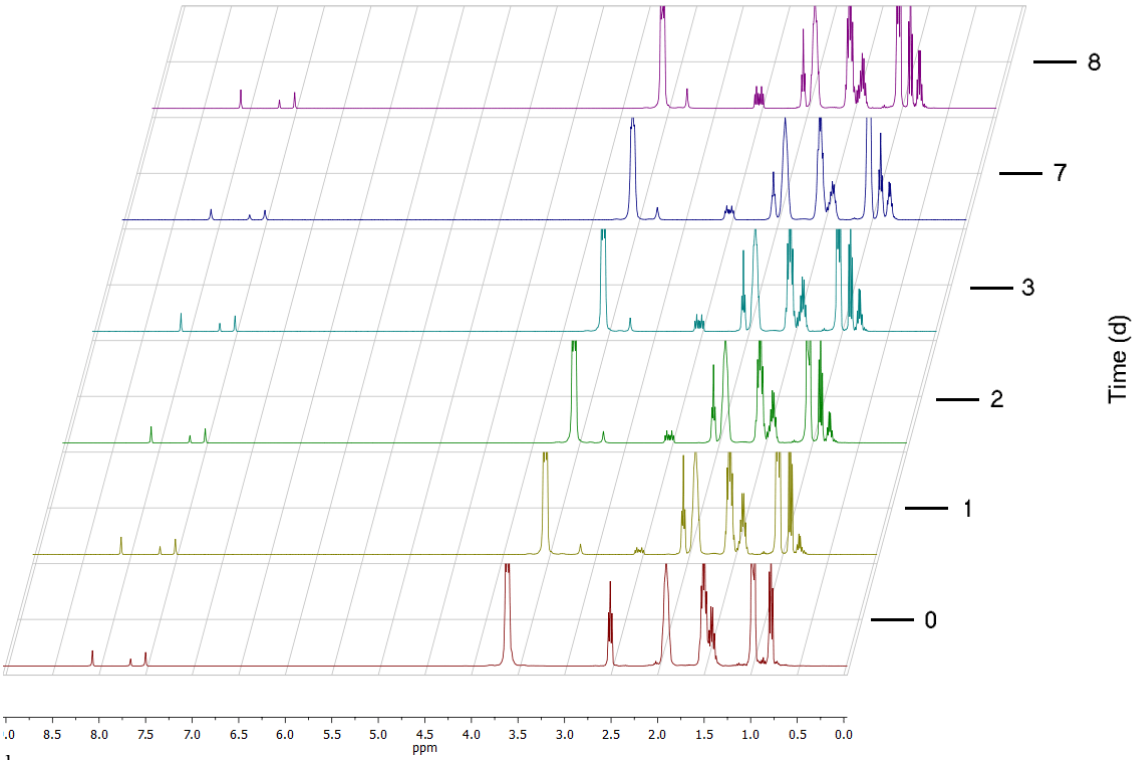

^{1}H NMR (400 MHz, d_5-$PhNO_2$)

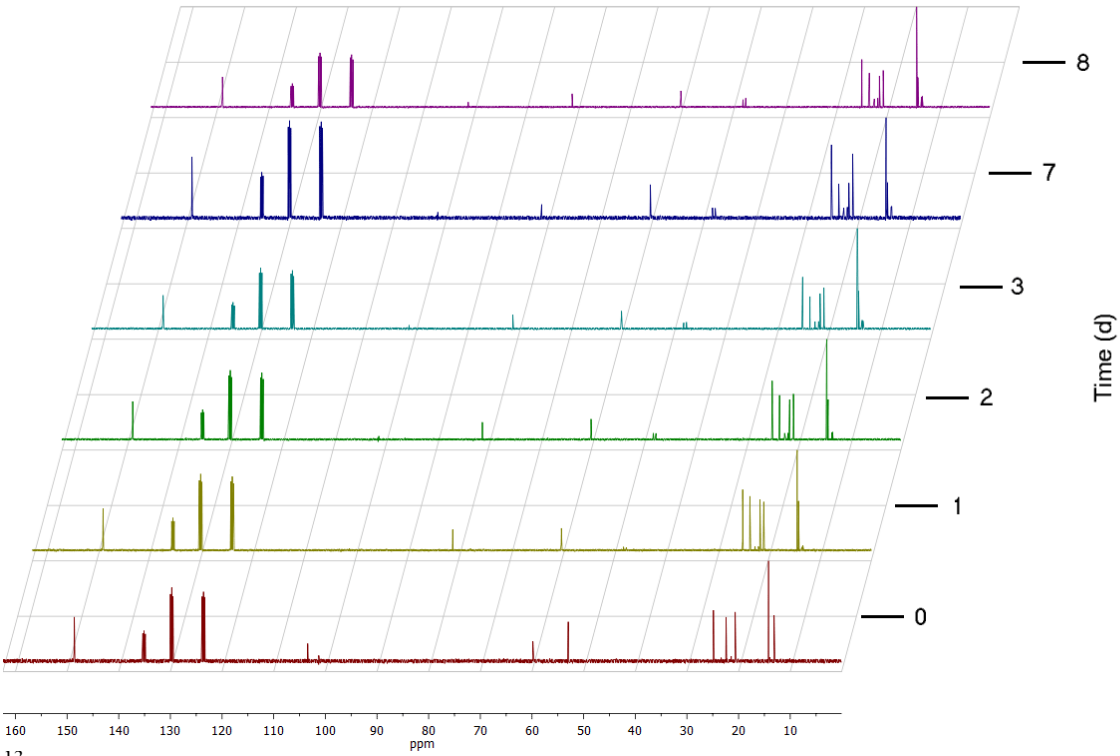

^{13}C NMR (100 MHz, d_5-$PhNO_2$)